Title: APLN/APLNR-targeting improves anti-angiogenic efficiency and blunts pro-invasive side effects of VEGFA/VEGFR2-blockade in glioblastoma

Running title: APLNR/VEGFA co-targeting inhibits glioblastoma angiogenesis and invasion

Giorgia Mastrella[1*], Mengzhuo Hou[1*], Min Li[1*], Veit Stöcklein[2], Nina Zdouc[1], Marie N. M. Volmar[1], Hrvoje Miletic[3,4], Sören Reinhard[5], Christel Herold-Mende[6], Susanne Kleber[7], Katharina Eisenhut[1], Gaetano Gargiulo[8], Michael Synowitz[9], Angelo L. Vescovi[10], Patrick Harter[11], Josef M. Penninger[12], Ernst Wagner[5], Michel Mittelbronn[13], Rolf Bjerkvig[3], Dolores Hambardzumyan[14], Ulrich Schüller[15], Jörg-Christian Tonn[2], Josefine Radke[16] , Rainer Glass[1,17,18] and Roland E. Kälin[18,1,+]

Affiliations

[1]Neurosurgical Research, Department of Neurosurgery, University Hospital, LMU Munich, Germany;

[2]Department of Neurosurgery, University Hospital, LMU Munich, Germany;

[3]Department of Biomedicine, University of Bergen, Norway;

[4]Department of Pathology, Haukeland University Hospital, Bergen, Norway;

[5]Department of Pharmacy, LMU Munich, Germany;

[6]Division of Neurosurgical Research, Department of Neurosurgery, University of Heidelberg, Germany;

[7]Department of Molecular Neurobiology, German Cancer Research Center (DKFZ), Heidelberg, Germany;

[8]Max Delbrück Center for Molecular Medicine, Berlin, Germany;

[9]Department of Neurosurgery, University Hospital Center Schleswig Holstein, Kiel, Germany;

[10]IRCCS Casa Sollievo della Sofferenza, San Giovanni Rotondo, Italy;

[11]Edinger-Institute (Neurological Institute), Goethe-University Medical School, Frankfurt am Main, ; Germany;

[12]Institute of Molecular Biotechnology of the Austrian Academy of Sciences, Vienna, Austria;

[13]Department of Anatomic and Molecular Pathology, Luxembourg Centre of Neuropathology (LCNP), Luxembourg.

[14]Department of Pediatrics and Aflac Cancer Center of Children's Health Care of Atlanta, Emory University School of Medicine, Atlanta, USA;

[15]Institute of Neuropathology and Department of Pediatric Haematology and Oncology, University Medical Center, Hamburg-Eppendorf AND Research Institute Children's Cancer Center, Hamburg, Germany;

[16]Charité - Universitätsmedizin Berlin, corporate member of Freie Universität Berlin, Humboldt-Universität zu Berlin, and Berlin Institute of Health, Department of Neuropathology, Berlin, Germany, German Cancer Consortium (DKTK), partner site Charité Berlin, Berlin, Germany and Berlin Institute of Health (BIH), 10178 Berlin, Germany;

[17]German Cancer Consortium (DKTK), partner site Munich; and German Cancer Research Center (DKFZ), Heidelberg, Germany;

[18]Walter Brendel Center of Experimental Medicine, Faculty of Medicine, LMU Munich, Germany;

*equal contributions;

+corresponding author. Tel: +49 89 4400 731 48, Fax: +49 89 4400 777 89, roland.kaelin@med.lmu.de

Keywords: tumor angiogenesis, glioblastoma cell invasion, apelin, APLNR, bevacizumab

Precis: Pharmacological targeting of the apelin receptor (APLNR) has synergistic effects with and blunts resistance to established anti-angiogenic therapies in glioblastoma.

Financial support: R.G. and R.E.K. gratefully acknowledge funding by the DFG (GL691/2; SFB824), the „Wilhelm Sander-Stiftung“, the „Anni-Hofmann Stiftung“, the „Verein zur Förderung von Wissenschaft und Forschung an der Medizinischen Fakultät der LMU München“ (WiFoMed), the Curt Bohnewandt Fonds, the „Friedrich-Baur-Stiftung“ and the „Familie Mehdorn Stiftung“. M.L. was supported by a China scholarship council (CSC) graduate scholarship. J.R. is a participant in the BIH-Charité Clinical Scientist Program funded by the Charité - Universitätsmedizin Berlin and the Berlin Institute of Health. U.S. is supported by the “Fördergemeinschaft Kinderkrebs-Zentrum Hamburg”.

Conflict of interest statement: The authors declare no potential conflicts of interest.

Word count: abstract, 224 words; main text, 4298 words

7 figures

49 references

Abstract

Anti-angiogenic therapy of glioblastoma with bevacizumab, a vascular endothelial growth factor-A (VEGFA) blocking antibody, may accelerate tumor cell invasion and induce alternative angiogenic pathways. We investigated the roles of the proangiogenic receptor APLNR and its cognate ligand apelin in VEGFA/VEGFR2 antiangionic therapy against distinct subtypes of glioblastoma. In proneural glioblastoma, apelin levels were downregulated by VEGFA or VEGFR2 blockade. A central role for apelin/APLNR in controlling glioblastoma vascularization was corroborated in a serial implantation model of the angiogenic switch that occurs in human glioblastoma. Apelin and APLNR are broadly expressed in human glioblastoma, and knockdown or knockout of *APLN* in orthotopic models of proneural glioblastoma massively reduced glioblastoma vascularization as compared with controls. However, the reduction in apelin expression led to accelerated glioblastoma cell invasion. Analysis of stereotactic glioblastoma biopsies from patients as well as our data from *in vitro* and *in vivo* experiments revealed increased dissemination of APLNR-positive tumor cells when apelin levels were reduced. Application of apelin-F13A, a mutant APLNR ligand, blocked both tumor angiogenesis and glioblastoma cell invasion. Furthermore, co-targeting VEGFR2 and APLNR synergistically improved survival of mice bearing proneural glioblastoma. In summary, we show that apelin/APLNR signaling controls glioblastoma angiogenesis and invasion, and that both pathological features are blunted by apelin-F13A. We suggest that apelin-F13A can improve the efficiency and reduce the side effects of established anti-angiogenic treatments for proneural glioblastoma.

Introduction

Glioblastoma is the most common and most malignant primary brain tumor (1). Current standard treatment consists of maximal resection followed by radiotherapy with concomitant temozolomide chemotherapy if safe (2,3). A subgroup of glioblastoma is generated by epigenetic dysregulation (CpG-island methylator phenotype in isocitrate dehydrogenase mutant gliomas; IDH^{MUT}) but the majority of glioblastoma represents IDH wild-type (wt) glioblastoma (4), which can origin from neoplastic neural precursor cells (NPCs)(5,6) after ablation or somatic mutation of the tumour suppressor p53, deletion of neurofibromatosis-1 (NF1) or loss of cdkn2a. Such genetic aberrations can coincide with loss of the phosphatase and tensin homolog deleted on chromosome-10 (PTEN). The vast majority of primary glioblastoma is driven by genetic mutation in key tumour suppressor genes concomitant with accelerated activity of different proto-oncogenic signalling pathways (e.g. epidermal growth factor receptor, EGFR, or platelet derived growth factor receptor-A, PDGFRA) or through a mutant (ligand independent) form of EGFR (EGFR-variant-3, EGFRvIII) (5).

Hallmarks of glioblastoma include poorly-differentiated neoplastic astrocytes, increased cell proliferation, tumour necrosis, microvascular proliferation and formation of an aberrant vasculature (1). Thus, anti-angiogenic treatments appear to be a promising strategy for glioblastoma (7). However, clinical studies using bevacizumab (AVAglio, RTOG-0825) a humanized monoclonal antibody that blocks vascular endothelial growth factor-A (VEGFA) signaling did not improve overall survival in patients with glioblastoma (8,9). Glioblastoma often develops resistance to bevacizumab owing to upregulation of alternative proangiogenic pathways and the induction of tumor cell invasion (10). Moreover, differences in angiogenic responses could originate from inter-individual glioblastoma heterogeneity, as evidenced by the genetic stratification of glioblastoma (11). The Cancer Genome Atlas (TCGA) revealed three subtypes of glioblastoma, namely proneural, classical, and mesenchymal, which show differences in prognosis and response to treatment (4,12).The neural glioblastoma subtype, previously defined by these authors, was recently considered as a potential artefact (13). A retrospective analysis of the AVAglio trial indicated that patients with (isocitrate-dehydrogenase wild-type) proneural glioblastoma can benefit from bevacizumab by increased overall survival (14). Based on these findings, it seems that stratification of patients according to their glioblastoma subtype may represent a first measure to improve the outcome of anti-angiogenesis therapy. In addition, some subtypes might show improved responses to treatment with bevacizumab in combination with other treatments, providing a more robust gain in overall survival (14,15)

We previously hypothesized that the G-protein coupled receptor APJ (APLNR) and its cognate peptide-ligand apelin play some roles in tumor development based on a study in which we performed *in situ* hybridization using glioblastoma specimens obtained from

patients (16). Although apelin was undetectable in the healthy brain and APLNR mRNA expression was very low in normal brain vessels, we observed a dramatic upregulation of both apelin and APLNR in glioblastoma-associated microvascular proliferations, as well as in radially orientated neoplastic cells surrounding band-like foci ("pseudopalisading necroses"). In hypoxic regions, apelin was highly coexpressed with VEGFA (16,17). In this context, it was suggested that apelin levels indicate improved tumour hypoxia due to vascular normalization upon bevacizumab treatment (18). Moreover, apelin/APLNR signaling was shown to also lie downstream of VEGFA/VEGFR in vascular development (for a recent review see Kälin and Kälin, 2017 (19)).

In the present study using *in vitro* and *in vivo* models, we confirm that apelin/APLNR signaling has a strong pro-angiogenic role in proneural glioblastoma. We show for the first time that blocking VEGFA/VEGFR2 signaling in glioblastoma reduces apelin levels and accelerates the invasion of APLNR-expressing proneural glioblastoma cells. Importantly, administration of apelin-F13A, a mutant form of the natural apelin-13 peptide with avidity for APLNR (20), reduced tumor angiogenesis and cell invasion in glioblastoma models, and had synergistic effects with VEGFR2 blockade. Taken together, our findings suggest that blocking VEGFA/VEGFR2 signaling and administration of apelin-F13A may constitute an improved anti-angiogenic regimen for glioblastoma that suppresses the side effects of anti-angiogenic treatments, like increased tumor cell invasion, in patients treated with bevacizumab (10,21).

Results

Apelin is downregulated by VEGFA/VEGFR2 blockade

We explored the pathophysiological context of apelin signaling in a glioblastoma subtype-specific manner by searching the TCGA dataset of glioblastoma tumors for genes coexpressed with *APLN* via the GlioVis portal (22). Interestingly, gene ontology analysis revealed that high apelin expression was associated with angiogenesis and blood vessel morphogenesis (Supplementary Fig. S1A) in the proneural or classical subtypes, but not in the mesenchymal subtype of glioblastoma. Supplementary Table S1 shows that, in the classical and proneural subtypes, several known angiogenic marker genes (e.g. *ANGPTL4, CD34*, *COL4A*, *FLT1*, *SEMA3E*, *WNT7A*, and *VEGFA*) are co-expressed with the *APLN* gene*,* which corroborates previous observations that the particularly the proneural and classical glioblastoma subtypes may respond to established or new anti-angiogenic treatments (14,23). To investigate a functional link between the VEGFA/VEGFR2 and apelin/APLNR signaling pathways, we examined the effects of bevacizumab in a mouse model of proneural glioblastoma. First, we analyzed tumor samples from a murine platelet-derived growth factor B (PDGFB)-driven proneural-like glioblastoma model based on the RCAS/Tva system (24). In this model, nestin-positive neural precursor cells (NPCs) were specifically transduced with rcas-virus carrying PDGFB. In combination with *cdkn2a*-loss, PDGFB overexpression produces a proneural form of glioblastoma in mice. Tumor-bearing mice were then treated with a murine bevacizumab surrogate anti-VEGFA antibody (B20-4.1.1, Roche), which increased survival and decreased total vessel area, but also let to an increased tumor volume compared with mice treated with vehicle (25). *In situ* hybridization of control tumors revealed strong apelin mRNA expression in areas corresponding to glioblastoma pseudopalisades (Fig. 1A asterisks) and tumor vessels (Fig. 1A arrows). In the anti-VEGFA antibody treated samples pseudopalisades were less prominently stained by apelin *in situ* hybridization (Fig. 1A asterisks) and smaller and less numerous vascular proliferates were detectable (Fig. 1A arrows). qPCR confirmed that apelin expression was downregulated in the treated samples as compared with control samples (Fig. 1A).

In a second set of experiments, we orthotopically implanted mice with murine transgenic glioblastoma stem cells (GSC; *p53* knockout GSCs overexpressing PDGFB, *p53*^{KO}PDGFB GSCs) as a model of human proneural glioblastoma (26,27). After tumor establishment, the murine VEGFR2-blocking antibody DC101 (as a model of ramucirumab treatment in humans, Eli Lilly) was intracerebrally infused into the mice. As in the RCAS/Tva model, the control tumors showed strong apelin expression in tumor cells (Fig. 1B, asterisks, right panel) and in tumor vessels (Fig. 1B, arrows right panel). Apelin mRNA expression was greatly reduced in the DC101-treated tumors. In particular, we found that apelin-labeling was strongly and significantly reduced in pseudopallisades within DC101-treated (5,1%) compared to control

tumours (34,3%) while the extent of pseudopalisades (quantification of the total pseudopalisading area) was unchanged (Fig. 1C). Also apelin positive vascular staining was significantly reduced from 4,6% in DC101-compared to 3.0% aCSF treated tumours. Comparable observations we made in biopsies of glioblastoma from patients before and after bevacizumab treatment. While the total area of pseudopalisading necrosis did not significantly change (Fig. 1D) we found that apelin expression was significantly lower in the tumor samples obtained after anti-angiogenic treatment (Fig. 1E Supplementary Fig. S1D) than in the initial resected samples. As described for the murine glioblastoma (Fig. 1A,B) apelin mRNA expression was increased in vascular proliferates (Fig. 1E arrows) and in radially oriented necroses (1E asterisks) of tumor before bevacizumab treatment but greatly reduced in vessels (Fig. 1E arrows) and pseudopalisades after therapy (Fig. 1E asterisks and comparison with H&E staining in Fig. 1D). In agreement with previous studies (16) we observed that apelin expression was also much higher in glioblastoma (initial biopsy before anti-angiogenesis) than in tumor-free human brain tissue (Supplementary Fig. S1C).

These results indicate that the *APLN* and *VEGFA* genes are co-expressed in glioblastoma and that blocking VEGFA/VEGFR2 signaling using anti-VEGFR2 antibodies reduced apelin expression. Hence, we sought to elucidate whether APLNR targeting has synergistic effects with VEGFA/VEGFR2 blockade. We also investigated the potential adverse effects of reduced apelin expression in glioblastoma.

Apelin and APLNR upregulation is correlated with the angiogenic switch in glioblastoma

Multiple signaling molecules are induced during the angiogenic switch in glioblastoma (28,29) contributing to pathological angiogenesis. We previously established a rodent model of the angiogenic switch in glioblastoma that involved serial transplantation of a patient-derived xenograft (15,21,30). During the first implantation cycles, this model is characterized by highly infiltrative brain tumors without apparent signs of neoangiogenesis (Fig. 2A) (30). The tumors gradually transform into an angiogenesis-dependent phenotype (angiogenic switch) after more than four generations of *in vivo* passaging (21). An advantage of this patient-derived xenograft model is that it allowed us to determine the relative expression levels of individual genes derived from the glioblastoma cells or the host. In a separate model, we modulated EGFR signaling (by overexpression of a mutant EGFR variant; EGFRvIII) to induce the angiogenic switch providing another method to uncover signaling pathways controlling angiogenesis and invasiveness in glioblastoma (15).

In both models we compared the gene expression patterns in the initial generation of tumors against later-generation tumors (Fig. 2A). We found that the vascular expression levels of apelin and APLNR were dramatically increased in the tumor microenvironment of angiogenic

versus invasive glioblastoma (together with *KDR* levels, encoding VEGFR2; Fig. 2A). These findings were corroborated in the second angiogenic switch model in which we blocked EGFR signaling by overexpression of dominant negative EGFR (Supplementary Fig. S2A), highlighting a central role of the APLNR signaling pathway in promoting angiogenesis in glioblastoma.

Host-derived apelin controls glioblastoma angiogenesis

To study the role of APLNR signaling within the tumor microenvironment, we next orthotopically implanted murine GSCs into *APLN*-wildtype (*APLN*^{WT}) or *APLN*-knockout (*APLN*^{KO}) mice. In the first set of *in vivo* experiments, we used proneural-like *p53*^{KO}PDGFB GSCs expressing low levels of apelin (Supplementary Fig. S2B). The glioblastoma originating from these cells produced an invasive and well-vascularized tumor. The vessel length density (VLD) was quantified in the tumor area, allowing us to measure the extent of tumor vascularization independent of tumor size (31,32); the VLD was 1,327 mm/mm^3 (Fig. 2B). When *p53*^{KO}PDGFB GSCs were implanted into *APLN*^{KO} mice, the VLD was significantly reduced by 41% to 776 mm/mm^3. These values are similar to those of the tumor-free hippocampus (1100 mm/mm^3) of adult mice (32). The intratumoural vessel length (VL) was reduced by 47% from 1,520 mm in *APLN*^{WT} mice to 799 mm in *APLN*^{KO} mice (Fig. 2B).

In human glioblastoma, the apelin expression levels were related to angiogenic signaling pathways in proneural and classical, but not mesenchymal glioblastoma. Therefore, we also established a mouse GSC culture model of the classical glioblastoma subtype (*cdkn2a*^{KO}EGFRvIII GSCs; *cdkn2a*-knockout cells overexpressing EGFRvIII (23,27)). The glioblastoma originating from *cdkn2a*^{KO}EGFRvIII GSCs produced a high vascular density (Supplementary Fig. S2C). The VLD was 2746 mm/mm^3 in *APLN*^{WT} mice (Supplementary Fig. S2C) and was significantly reduced by 33% to 1,830 mm/mm^3 in *APLN*^{KO} mice. Overall VL was reduced by 75.4% from 82,726 mm in *APLN*^{WT} mice to 20,349 mm in *APLN*^{KO} mice. This set of experiments corroborated our working hypothesis that host-derived apelin plays a prominent role in controlling the extent of tumor vascularization.

Combined effects of glioblastoma cell- and host-derived apelin on tumor angiogenesis

Next, we investigated the contribution of glioblastoma cell-derived apelin on tumor angiogenesis *in vivo.* We selected two primary glioblastoma cultures of the proneural subtype that expressed relatively high levels of apelin (arrows in Supplementary Fig. S2D). First, we manipulated primary GBM14 cells (33) to express a shRNA construct to knockdown endogenous *APLN* (GBM14^{AKD}; Supplementary Fig. S2E) or a non-silencing control shRNA (GBM14^{NSC}). Genome-wide copy number analysis of all GSCs using a high-definition SNP array indicated a gain in *APLN* gene copy number in GBM14 cells (not shown), which might

explain the greater apelin expression levels in GBM14 cells than in other primary glioblastoma cells (Supplementary Fig. S2D). *APLN*-knockdown did not affect glioblastoma viability or expansion *in vitro* (Supplementary Fig. S2E). Six weeks after orthotopic injection of $GBM14^{NSC}$ cells into immunocompromised wildtype mice, we detected the formation of a vascularized brain tumor mass with a VLD of 1249 mm/mm^3 (Fig. 2C). The VLD of $GBM14^{AKD}$ orthotopic xenografts in wildtype mice was 930 mm/mm^3, a reduction of 25.5% versus $GBM14^{NSC}$, which suggests that glioblastoma-derived apelin is proangiogenic. The modulation of human glioblastoma-derived apelin is pathologically meaningful in mouse models because the amino acid sequences of the bioactive peptide apelin-13 of human or mouse origin are identical (16).

Implantation of $GBM14^{NSC}$ into immunodeficient $APLN^{KO}$ mice reduced the tumor vasculature by approximately 25% as compared with $GBM14^{NSC}$ gliomas grown in immunocompromised $APLN^{WT}$ mice (Fig. 2C). When $GBM14^{AKD}$ cells were implanted into immunodeficient $APLN^{KO}$ mice, we detected scant tumor angiogenesis with a VLD of 569 mm/mm^3, a 54% reduction relative to that in control mice (Fig. 2C). Furthermore, the overall VL was reduced from 1720 mm to 588 mm (by 66%), 460 mm (by 73%), and 161 mm (by 91%), respectively.

We also orthotopically implanted mice with a second well-established human primary GSC model (NCH644 cells (34)) corresponding to the proneural subtype (35). NCH644 cells showed moderate apelin expression levels (Supplementary Fig. S2D) together with a loss in *APLN* gene copy number. These cells produced a glioblastoma with a VLD of 1168 mm/mm^3 in $APLN^{WT}$ mice (Supplementary Fig. S2G). Stable knockdown of *APLN* in the tumor cells ($NCH644^{AKD}$; Supplementary Fig. S2G) and orthotopic injection into immunocompromised $APLN^{WT}$ mice reduced the VLD by 50% to 648 mm/mm^3 (Supplementary Fig. S2G).

This series of experiments consistently indicated that tumor cell-derived and/or host-derived *APLN* levels are directly correlated with the level of tumor angiogenesis. Glioblastoma vascularization was reduced by *APLN* knockdown in tumor cells or *APLN* knockout. Injection of $APLN^{KD}$ glioblastoma cells into $APLN^{KO}$ mice achieved an even greater reduction in glioblastoma angiogenesis.

Reduced apelin in APLNR-expressing glioblastoma is related to invasion

So far, we have shown that apelin levels are modulated by anti-angiogenic therapy and that apelin/APLNR expression is induced at the angiogenic switch in glioblastoma. The contribution of host- and glioblastoma-derived apelin to tumor vascularization was corroborated using knockdown and knockout models. When we searched the IVY Glioblastoma Atlas Project RNAseq database, we found regionally distinct expression levels of apelin and APLNR (Fig. 3A; Supplementary Fig. S3A). In particular, apelin was more abundantly expressed in tumor areas enriched with microvascular proliferation and

hyperplastic blood vessels (BV; with high levels of *KDR* expression). Angiogenic, hypoxic glioblastoma areas that were enriched with necrosis or contained pseudopallisades (a perinecrotic zone or pseudopalisading cells around necrosis) were characterized by high levels of VEGFA and apelin mRNA together with high angiogenin expression, a potent mediator of new blood vessel formation (36) (Supplementary Fig. S3A). However, apelin expression was very low in microdissected glioblastoma samples containing an infiltrating tumor or a leading edge (Fig. 3A) whereas APLNR mRNA expression remained high, especially in the infiltrating tumor zone (Fig. 3A). The elevated expression of APLNR was also associated with increased expression of genes involved in tumor cell invasion like *MMP2* (matrix metallopeptidase 2) and *BAI1*/*3* (brain-specific angiogenesis inhibitor 1/2) but the expression of tissue inhibitor of metalloproteinase-1 (TIMP1), an MMP2 inhibitor, was low (Supplementary Fig. S3A).

To further investigate a potential role of APLNR in invasive glioblastoma areas, we used glioblastoma biopsies obtained by neurosurgical resection using a neuronavigation system. Using this set of samples, we could specifically investigate glioblastoma tissue harvested from the tumor border (Supplementary Fig. S3B). *In situ* hybridization revealed that the tumor center expressed apelin in cellular (arrowheads) and vascular regions (arrows; also visible on consecutive H&E), whereas apelin was not detected at the tumor border. APLNR was also expressed in the cellular (arrowheads) and vascular (arrows) regions in the tumor center, but APLNR expression was more pronounced in some dispersed cells along the tumor border (Supplementary Fig. S3B, arrowheads). *In situ* hybridization revealed that apelin or APLNR was relatively scant in tumor-free brain tissue (compare to Fig. 3B, brain). To provide a greater resolution of local apelin/APLNR expression in glioblastoma WHO grade IV, we examined stereotactic glioblastoma biopsies with defined three-dimensional coordinates (Fig. 3B). In successive biopsies taken along the stereotactic trajectory (z-axis), a neuropathologist identified a cell-dense pleomorphic glial tumor expressing glial fibrillary acidic protein (GFAP) and microtubule-associated protein 2 (MAP2), wildtype *IDH1* (isocitrate dehydrogenase 1), 15% Ki67 positive tumor cell nuclei, and numerous vascular proliferates from coordinate z = 0 until 3 mm towards the tumor border. From 5 mm to 8 mm along the z-axis, the biopsies contained central nervous system tissue with a progressively decreasing number of infiltrating glial tumor cells. *In situ* hybridization revealed a progressive reduction in apelin expression (Fig. 3B; compare z = 6 and z = 8 mm to = 0), but APLNR expression was detectable in glioblastoma cells (arrowheads) over a larger distance from the cell-dense tumor (Fig. 3B; z = 6 and z = 8 mm). Taken together, these findings indicate that APLNR expression is maintained in scattered glioblastoma cells within the apelin-free invasive tumor margin.

To investigate a potential role for apelin/APLNR signaling in glioblastoma invasion *in vitro*, we embedded GBM14 cells (GBM14^{AKD} or GBM14^{NSC}) in a collagen matrix (23). We found that the GBM14^{AKD} cells were much more invasive than the control GBM14^{NSC} cells (Fig. 3C). To exclude that the increase in invasive area observed with GBM14^{AKD} cells compared to GBM14^{NSC} control cells was not a result of enhanced *in vitro* proliferation we analysed *in vitro* proliferation assays and compared their Ki67 status but did not detect any difference (Supplementary Fig. S2E, S4G,H).

In addition by performing two migration assays (Supplementary Fig. S3C, D), a wound healing and a Boyden chamber chemotaxis assay, we confirmed that the depletion of apelin in glioblastoma cells (GBM14 and U87MG) lead to significantly increased invasion *in vitro*. Thus, depletion of endogenous apelin led to an increased invasive behaviour. However, application of apelin-F13A, another APLNR ligand (37), to GBM14 spheres reduced their invasiveness (Fig. 3D). A similar inhibitory effect of apelin-F13A on glioma cell invasion was also observed in murine p53^{KO}PDGFB GSCs (Fig. 3E). In line with that, addition of apelin-F13A in the two migration assays also attenuated the increased invasiveness of APLN^{KD} cells again (Supplementary Fig. S3C, D).

Overall, we found that APLNR is expressed in the apelin-free invasive zone of patient-derived glioblastoma samples that the absence of endogenous apelin can increase glioblastoma cell invasion *in vitro*, and that application of the APLNR ligand apelin-F13A has an anti-invasive effect.

Anti-invasive role of apelin in glioblastoma *in vivo*

Next, we investigated whether apelin modulates tumor invasion in murine glioblastoma models *in vivo*. Within 6 weeks after orthotopic implantation, the GBM14^{NSC} GSCs had grown to a detectable brain tumor mass. Immunostaining for a green fluorescent protein (GFP) reporter in GBM14 cells revealed a tumor mass consistent with glioblastoma detected histologically (H&E staining; Fig. 4A; arrowheads indicate compact GFP volume). In addition, individual GFP-positive cells (arrows) have invaded the brain. When intratumoural apelin levels were gradually reduced by implanting GBM14^{AKD} cells into wildtype mice (as compared with GBM14^{NSC} in wildtype mice) or by inoculation of GBM14^{NSC} versus GBM14^{AKD} cells into *APLN*^{KO} mice, the overall tumor volume gradually decreased, but the invasiveness of glioblastoma cells increased significantly (Fig. 4A). The overall tumor volume was determined by measuring the total area including regions with single invasive tumor cells visible on GFP-stained sections. In addition, the compact tumor volume was determined by measuring the area of GFP-positive tumor cells that were in direct contact with neighbouring tumor cells (Supplementary Fig. S4B). The invasive tumor volume was determined as the difference between overall GFP and compact GFP tumor volume, and tumor invasiveness

was determined as the percentage of invasive tumor volume over overall GFP tumor volume (Fig. 4A). Moreover, the distance of single GFP-positive cells that had migrated from the compact tumor part increased significantly with decreasing apelin expression (Fig. 4A).

To confirm that the change in *in vivo* tumor volume was not a result of altered glioblastoma cell proliferation, we also checked the Ki67 status in all apelin knockdown GBM14 xenografts and did not find a difference to GBM14^{NSC}APLN^{WT} tumors (Supplementary Fig. S4I).

Orthotopic implantation of NCH644^{NSC} into wildtype mice generated tumors with few regions of accelerated invasiveness (Supplementary Fig. S4C; arrows), but implantation of NCH644^{AKD} xenografts into wildtype mice resulted in the development of glioblastoma with a reduced central tumor mass but a much more pronounced invasive pattern (Supplementary Fig. S4C; arrows).

Similar observations were made using an immunocompetent model of proneural glioblastoma, in which we implanted *p53*^{KO}PDGFB GSCs into apelin-deficient hosts. Again, the resulting tumors were much more invasive than glioblastomas grown in *APLN*^{WT} hosts (Fig. 4B). In *p53*^{KO}PDGFB glioblastoma, the distance of tumor cell migration away from the dense tumor mass increased from 1.1 in *APLN*^{WT} to 2.6 mm in *APLN*^{KO} mice. In addition, the invasive ratio increased from 1.6 to 2.6 (Supplementary Fig. S4E) and the percentage of invasive versus overall volume increased from 59% to 72% (Fig. 4B). Using *cdkn2a*^{KO}EGFRvIII glioblastoma as a model of the classical subtype, we found that the compact and overall volumes were decreased by 53% in *APLN*^{KO} mice compared to *APLN*^{WT} mice, but tumor invasiveness was significantly increased (Supplementary Fig. S4F). In another approach to investigate apelin-modulated glioblastoma cell-invasion we implanted human primary glioblastoma cells into murine orthotopic brain slice culture. Here apelin knockdown increased the invasiveness of proneural NCH644 as well as classical GBM5av cells (Supplementary Fig. S4J, K).

In summary, we found that apelin derived from the host and tumor cells is an essential mediator of neoangiogenesis in glioblastoma and that apelin also contributes to suppressing glioblastoma cell invasion. This was demonstrated by an inverse correlation between apelin expression levels with glioblastoma invasiveness in our *in vitro, ex vivo* and *in vivo* models and by the direct anti-invasive effect of APLNR stimulation in our collagen-based invasion as well as two migration assays. In glioblastoma cells, APLNR stimulation can apparently suppress invasion while a low levels of APLNR-ligands (in the tumor margin or after VEGFA/VEGFR2 blockade) permit glioblastoma invasion.

Apelin-F13A inhibits glioblastoma angiogenesis and invasion

To investigate the potential of APLNR as a therapeutic target for glioblastoma, we tested the *in vivo* application of apelin-F13A (37) in an invasive, immunocompetent model

(*p53*^{KO}PDGFB). Apelin-F13A with the C-terminal phenylalanine mutated to alanine can antagonize the APLNR *in vivo* (38), but was also found to act as an agonist on different functional assays, such as adenyl cyclase inhibition or APLNR internalisation (39,40). To investigate if invasive tumor cells are potentially responsive for apelin peptides (which is a prerequisite for using apelin-F13A as an anti-invasive agent) we performed immunofluorescence labeling for APLNR in scattered, infiltrative glioblastoma cells in our models (Supplementary Fig. S5A,B). We found that about 90% of invasive human GBM14 or *p53*^{KO}PDGFB GSCs abundantly expressed APLNR. Then we explored the therapeutic properties of apelin-F13A in our *in vivo* models and therefore induced gliomas, which were intracerebrally infused for 2 weeks with apelin-F13A (subsequently mice were sacrificed and brains inspected). The vascular density of these murine gliomas was reduced from a VLD of 1069 mm/mm^3 in control mice to 629 mm/mm^3 in apelin-F13A-treated mice (Fig. 5A). The total VL decreased from 1146 mm to 352 mm (not shown) and overall tumor volume was decreased by 56% from 104 mm^3 in control mice to 46 mm^3 in apelin-F13A-treated mice. While the compact tumor volume did not change significantly, the invasive tumor volume decreased by 53% from 72 mm^3 in control mice treated with artificial cerebrospinal fluid (aCSF) to 34 mm^3 in apelin-F13A-treated mice (Fig. 5A). We then repeated this experiment using proneural GBM14 GSCs. As these glioblastoma grew significantly slower, the APLNR synthetic ligand apelin-F13A was infused for 4 weeks. We observed a reduction in VLD for these human-derived glioblastoma, from 1333 mm/mm^3 in control mice to 749 mm/mm^3 in apelin-F13A-treated mice (Fig. 5B). Additionally, total VL was decreased from 1252 mm to 810 mm (not shown) and overall tumor volume decreased by 68% from 69 mm^3 in control mice to 22 mm^3 in apelin-F13A-treated mice. As in the *p53*^{KO}PDGFB model, the compact tumor volume did not change significantly in the human glioblastoma model, but the invasive tumor volume decreased by 59% from 31 mm^3 in control mice to 13 mm^3 in apelin-F13A-treated mice (Fig. 5B).

To test the binding specificity of the apelin peptides to as well as the functional response of the glioblastoma APLNR, we performed two *in vitro* internalisation assays (16,40-43); since internalization-rates of G-protein coupled receptors (GPCR) give valuable insight in signaling activity by native (non-recombinant) GPCR (44). By detecting APLNR immunofluorescence we found that the addition of apelin-13 and apelin-F13A caused the internalisation of the APLNR to cytoplasmic and perinuclear regions (Supplementary Fig. S5C). Most interestingly, we detected a difference in the APLNR redistribution in response to the two peptides. While apelin-13 lead to a massive decrease of APLNR localization in the nucleus, apelin-F13A caused exactly the opposite outcome (Supplementary Fig. S5C). In a second internalisation assay we administered GFP-linked apelin peptides to GBM14 cells. We found that both, apelin-13 and apelin-F13 were internalised by the cells, while a scrambled apelin-13scr

peptide was not (Supplementary Fig. S5D). In addition confirmed the specificity of peptide uptake by performing a dose escalation with unlabelled peptide showing that uptake of both GFP-labelled peptides was specifically blocked by its unlabelled counterpart (Supplementary Fig. S5E).

These findings imply that the synthetic APLNR ligand apelin-F13A efficiently suppressed angiogenesis and invasiveness in two models of glioblastoma. Apelin-F13A can bind and activate the APLNR, functions as a competitive agonist for other APLNR ligands and has only partial APLNR-activating properties (20). Our receptor internalization assay revealed that apelin-13 or apelin-F13A induce distinct patterns of intracellular APLNR localization which can point-out differences in signaling cues initiated by these two peptides. This may explain why only apelin-F13A (but not apelin-13) was able to block the proangiogenic effects of intratumoural apelin.

Co-targeting VEGFR2 and APLNR synergistically improved survival of murine models of glioblastoma

One of the major adverse effects of bevacizumab for the treatment of glioblastoma is an increase in tumor cell invasiveness or upregulation of alternative angiogenic factors (10). Hence, we asked if blocking the pro-angiogenic and -invasive properties of APLNR could overcome the pathological side effects of established anti-angiogenic regimen like anti-VEGFR2 therapy, and hence improve overall survival. Orthotopically implanted *p53*^{KO}PDGFB glioblastoma were allowed to expand for 1 week in mice. These mice were then treated intracerebrally with apelin-F13A, anti-VEGFR2 antibody (DC101), apelin-F13A and anti-VEGFR2 antibody, or with vehicle (aCSF) alone as a control (Fig. 6A). The median survival of aCSF treated mice was 52 days. Administration of DC101 increased survival by 28% compared with control mice, with a median survival of 67 days. Administration of apelin-F13A alone achieved a similar increase in survival (63 days; 19% increase) compared with control mice. Notably, coadministration of DC101 and apelin-F13A had synergistic effects, with a 65% increase in the survival rate (86 days). Median survival of the co-treated mice was significantly elevated compared to administration of DC101 ($p = 0{,}0385$) or apelin-F13A ($p=0{,}0327$) alone. Immunohistological analysis of tumors with comparable overall tumor volume showed that administration of DC101 alone had a pro-invasive effect with a 77% increase in the invasive volume relative to control mice (Fig. 6B). Interestingly the anti-invasive effect of apelin-F13A reduced the invasive volume to 26% compared with control mice and combined treatment to 33% compared with DC101 treatment alone. DC101 decreased VLD to 72% and apelin-F13A decreased VLD to 58% relative to control mice, while coadministration of apelin-F13A and DC101 decreased VLD to 40% compared to control.

In summary, we observed that co-targeting of the APLNR and VEGFR2 signalling pathways exerted synergistic anti-angiogenic effects and strongly reduced the pro-invasive side effects of established anti-angiogenic strategies. We suggest that inhibition of VEGFR2 inhibition may be beneficial for the treatment of patients with the proneural subtype of glioblastoma, if apelin-F13A is administered to stimulate APLNR.

Discussion

In this study, we revealed a central role of the apelin/APLNR signaling pathway in anti-angiogenic treatment of glioblastoma and in countering resistance to bevacizumab. We showed that apelin is required for tumor angiogenesis and we uncovered a previously unknown function of the apelin/APLNR signaling pathway in glioblastoma cell invasion (Fig. 7). Furthermore, we investigated for the first time the pathological roles of host- or tumor cell-derived apelin separately, and examined their specific effects on glioblastoma expansion, invasion, and angiogenesis. Our data indicate that the apelin/APLNR signaling pathway has dichotomous roles in angiogenesis and invasion in glioblastoma, and we established that stimulation of APLNR using apelin-F13A is a promising strategy to treat the proneural subtype of glioblastoma. A clinical perspective for the co-application of apelin-F13A together with VEGFA/VEGFR2 inhibitors is also suggested because coadministration of apelin-F13A and DC101 synergistically blunted glioblastoma vascularization and diminished the pro-invasive side-effects associated with VEGFA/VEGFR2 inhibition. In addition, the reduce vascularization might be accompanied with apelin vascular normalization that could be supportive for combined chemotherapy (18).

In previous studies, the pathological function of apelin was largely associated with tumor vascularization (45-47) and consequently we observed that tumor cell- and host-derived apelin has additive effects on tumor angiogenesis. We found that apelin expression levels were positively correlated with vascular density in murine and human glioblastoma models of the proneural glioblastoma subtype as well as in classical glioblastoma. The vascular upregulation of apelin was further confirmed by co-localisation of apelin peptide in tumor vessels by immunofluorescence (Supplementary Fig. S2H). We focused on the proneural and classical subtypes of glioblastoma because TCGA data suggested that the apelin/APLNR signaling pathway mediates vascularization in these two subtypes but not in the mesenchymal subtype of glioblastoma.

In the present study, we used GSC cultures that were previously extensively characterized for their stem-like capacity (48,49). A recent publication proposed a critical role of the apelin/APLNR signaling pathway in GSC maintenance (50). However, in our GSC models, we did not find any alterations in cell viability, proliferation, or sphere formation capability following attenuation of apelin expression or APLNR blockade.

Knockdown of *APLN* in glioblastoma cells or knockout of *APLN* in the host both enhanced tumor cell invasion, and implantation of $APLN^{KD}$ cells into $APLN^{KO}$ mice further accelerated the dissemination of glioblastoma cells. This was particularly apparent in glioblastoma cells with elevated APLNR expression levels. Application of apelin-F13A blunted glioblastoma invasion and neoangiogenesis. These findings support the view that autocrine and paracrine

apelin signaling has proangiogenic effects on vascular cells and blunts invasion of glioblastoma cells. This observation is clinically relevant because bevacizumab lowers intratumoural apelin levels, which may explain why bevacizumab-treated patients often suffer from increased glioblastoma cell invasion (10). We propose that bevacizumab directly (via blockade of VEGFA activity) and indirectly (by lowering apelin expression) exerts powerful anti-angiogenic effects. However, we have shown that a reduction in apelin disinhibits glioblastoma cell invasion, which may result in treatment resistance. Our data suggest that the synthetic APLNR ligand apelin-F13A can support anti-angiogenic therapies by blocking vascularization (synergistically with VEGFA/VEGFR2 inhibitors) and preventing invasion. In this study, we exploited the pharmacological properties of apelin-F13A, which acts a partial agonist for APLNR (20,51) and as a competitive agonist for natural apelin isoforms, like apelin-13 (37). We hypothesize that apelin-F13A cannot sufficiently activate APLNR expressed on the endothelium to induce vascular sprouting but sufficiently stimulates APLNR on glioblastoma cells to blunt invasion and prolong survival. This can be explained by a lower receptor binding capacity (39) and alternative activation of intracellular signaling pathways (52) by apelin-F13A as compared with natural APLNR ligands. We acknowledge that the experimental therapeutic agent apelin-F13A can potentially have further effects on the tumor microenvironment (like e.g. on intratumoural immune cell populations), which may support the anti-angiogenic and anti-invasive traits reported in this study. However, when quantifying tumor associated myeloid cells in experimental gliomas treated with control substances or apelin-F13A we did not observe a statistically significant change in myeloid cell numbers (not shown).

Clinical trials of glioblastoma therapies in the last two decades have highlighted the need to identify predictive markers to improve the clinical outcomes of new compounds (2,53). One approach for patient stratification according to molecular and pathological criteria involves clustering of glioblastoma into genetic subtypes (12), which may be particularly relevant to anti-angiogenic treatments using bevacizumab (14) and apelin-F13A (as in this study) because both agents have beneficial effects on the proneural subtype of glioblastoma. In addition, the high expression of APLNR in glioblastoma may qualify as a marker for an increased propensity of glioblastoma cells to invade during bevacizumab treatment, a process that can be blocked by apelin-F13A.

In conclusion, the results of this study introduce a new strategy to reduce therapeutic resistance during anti-angiogenic therapy and identify glioblastoma subtypes that may show better therapeutic responses by co-targeting the apelin/APLNR and VEGFA/VEGFR2 signaling pathways.

Materials and methods

Cell culture

GSCs were derived from human glioblastoma biopsies (as previously reported for NCH644 and NCH588J (34); GBM10, GBM13 and GBM14 (33); and GBM5av to 10av (48)) and were maintained under stem cell cultivation conditions in DMEM-F12 (Cat. 11320-074) supplemented with 1× B27 (Cat. 17504-044), 5% penicillin-streptomycin (Cat. 151140-122; all ThermoFisher Scientific, Waltham, MA, USA), 10 ng/ml epidermal growth factor (EGF; Cat. 236-EG; Biotechne; Minneapolis, MN, USA) and 10 ng/ml fibroblast growth factor (FGF; Cat. 100-18B PeproTech, Hamburg, Germany). For all cultures, gene copy number analysis was performed and the *TP53*, *EGFR*, *PDGFRA*, *PIK3CA*, *PIK3R1*, *PIK3CG*, *PTEN*, *NF1*, *RB1*, *IDH1*, and *ATRX* loci were sequenced. We confirmed that all cultures were tumorigenic upon orthotopic implantation in immunodeficient mice. All of the GSCs, except for GBM10 cells, corresponded to the glioblastoma subtype of the parental tumor.

Neural-precursor cells (NPCs) were isolated from the subventricular zone (SVZ) of 5-day-old Bl6/J or FVB mice with homozygous deletion of *TP53* or *CDKN2A*. Isolated cells were cultured in spheroid conditions with DMEM-F12 medium supplemented with 1× B27, 1% penicillin-streptomycin, 10 ng/ml EGF (Cat. 236-EG; Biotechne) and 10 ng/ml FGF (Cat. 100-18B; PeproTech). U87MG (HTB14) cells were obtained from the American Type Culture Collection (ATCC) and cultured under adherent conditions in DMEM containing 1× MEM non-essential amino acids (Cat. 11140-035), 5% penicillin-streptomycin, and 10% fetal bovine serum (Cat. 102270-106; all ThermoFisher Scientific). GL261 cells were obtained from the National Cancer Institute, NCI-Frederick (Tumor Cell Repository) and maintained under neurosphere cell culture conditions as described above. All cells were maintained at 37°C in a humidified atmosphere of 95% O_2 and 5% CO_2.

Cell transduction

Mouse transgenic glioma cells as a model of the proneural glioblastoma subtype (*p53*^{KO}*PDGFB* GSCs) were generated by transduction of a single cell suspension of *p53*^{KO} NPCs for 1 h with a multiplicity of infection (MOI) of 80 of VSV-G pseudotyped GFP-PDGFB retroviral particles (kindly provided by F.Calzolari/M.Götz, Department of Physiological Genomics, LMU Munich, Germany). Human *PDGFB* cDNA was derived from the RCAS-pBIG plasmid (kindly provided by E. Holland, Fred Hutchinson Cancer Research Center Seattle, WA; USA). Transduction efficiency was verified by GFP immunofluorescence and was >99%. To study the influence of p53 status in the generated *p53*^{KO}*PDGFB* mouse GSCs, cells were transfected with lipofectamine (Cat. 18324020; ThermoFisher Scientific) and 3 µg of empty vector containing ampicillin-neomycin resistance, hotspot *p53* mutant (R172H, R175H, R248W, R249S, R270H, R273H, V143A) or wildtype *p53* plasmid DNA.

Transfected GSCs were first selected for 4 weeks with 3 mg/ml of G418 antibiotics and selection was maintained using 1 mg/ml of G418.

As a model of the classical glioblastoma subtype, *cdkn2a*^{KO} NPCs were transfected with EGFRvIII-blasticidin/GFP plasmids to obtain *cdkn2a*^{KO}EGFRvIII GSCs. To obtain EGFRvIII-EGFR overexpressing cells, cells were then transfected with 3 µg of neomycin-EGFR plasmid, and the cells were selected for 2 weeks with 1 mg/ml of Geneticin (Cat. 10131027; ThermoFisher Scientific). For proneural-like *p53*^{KO}EGFR GSCs, *p53*^{KO}NPCs were transfected with 3 µg of neomycin-EGFR plasmid and selected for 2 weeks with 1 mg/ml of Geneticin.

For gene silencing in GBM14 and NCH644, we used three different lentiviral shRNAmir constructs for apelin (AKD; Cat. RHS4430: V3LHS_401190) or non-silencing control (NSC; Cat. RHS4346) to produce viral particles in HEK293T cells with the TransLenti Viral GIPZ Packaging System (Cat. TPLP4614, all Dharmacon GE Life Sciences, Lafayette, CO, USA) according to the manufacturer´s instructions. Virus particle-containing supernatant was harvested 2 days after transfection, filtered with a 0.22 µm filter to avoid cellular contamination and stored at −80°C. Primary GSC spheroids were dissociated with Accutase (Cat. A6964; Sigma Aldrich, Taufkirchen, Germany), while U87MG cells were detached with trypsin/EDTA (Cat. L2153; Merck Millipore; Darmstadt; Germany). Then, 8×10^4 cells were incubated with 500 µl of virus particles at an MOI of 0.6–0.7 for 6 h in a 24-well plate. Next, 1 ml of medium was added and the cells were left overnight at 37°C. The next day, the cells were centrifuged and resuspended in fresh medium. After cell recovery, cells were selection using puromycin (Cat. P8833; Sigma Aldrich) for up to 3 weeks. The concentration of antibiotics was determined beforehand using a lethal dose curve. The efficiency of transduction/selection was >99%, as confirmed by fluorescence-activated cell sorting and immunofluorescence.

Animals

All experiments were performed in compliance with the National Guidelines for Animal Protection, Germany, with approval of the local animal care committee of the Government of Oberbayern (Regierung von Oberbayern). All experiments were conducted in accordance with the UK Coordinating Committee on Cancer Research guidelines (54). *APLN*^{KO} mice were obtained from J.M. Penninger (55) and crossed with *Rag2*^{KO} mice (B6.129S6-Rag2^{tm1Fwa}) (56) kindly provided by G. Willimsky (Charité – Universitätsmedizin Berlin) and previously purchased from Taconic. All mice had a C57Bl/6J background and genotyping was performed as previously described (55,56). *Foxn1*$^{nu/nu}$ mice were ordered from Envigo. All mice were kept in a 12-h light/dark cycle with *ad libitum* access to food and water. Mice

were sacrificed at defined presymptomatic time points or at a humane endpoint in survival studies.

Tumor implantation

Mice were anesthetized with 7 µl/g of body weight of a mixture of xylazine (Rompun 2%; Bayer, Leverkusen Germany) and ketamin (Ketavet; Zoetis, Berlin Germany) in 0.9% NaCl. They were immobilized on a stereotactic frame (David Kopf Instruments, Tujunga, CA, USA) in flat-skull position and kept warm. A midline incision was made on the skull with a scalpel. To prevent the cornea from drying out, the eyes of the mice were covered with a moisturizing cream (Bepanthen; Bayer). Then, 1×10^5 (human) or 1×10^4 (mouse) cells/µl in supplement-free medium were implanted by stereotactic injection 1 mm anterior and 1.5 mm right to the bregma using a 22G Hamilton syringe (Hamilton, Bonaduz, Switzerland) after drilling a hole into the skull with a 23G needle. At a depth of 4 mm, the cells were slowly injected within 2 min. After a settling period of another minute, the needle was removed at 1-mm-steps/minute. The incision was sutured and patched with Opsite spray dressing (Smith & Nephew, Hamburg, Germany). Analgesia was achieved by administering a dose of 4 mg/kg before surgery and 2 × 2 mg/kg doses of intraperitoneal carprofen (Rymadil, Zoetis) for 3 days after surgery.

Intracerebral drug application

One day before implantation, mini-osmotic pumps were filled with 30 µg of apelin-F13A (Bachem) or 0.8 mg of DC101 (Eli Lilly) for sustained delivery over 14 days (Model 1002; Alzet; Cupertino, CA, USA) or 60 µg of apelin-F13A for sustained delivery over 28 days (Model 2004, Alzet) in aCSF (as described by Alzet) or with aCSF alone following priming overnight in aCSF at 37°C. The mini-osmotic pumps were implanted under anesthesia as previously described (57). The needle of the brain infusion kit 3 (Alzet) was inserted into the hole originally prepared for orthotopic tumor implantation. The mice were sacrificed at the end of the pump's life (14 or 28 days) or at humane endpoints in survival studies.

Quantitative PCR

RNA was extracted using Trizol (Cat. 15596-026; ThermoFisher Scientific) according to the manufacturer's instructions. Total RNA (1 µg) was reverse-transcribed into cDNA using a QuantiTect Reverse Transcription Kit (Cat. 205313; Qiagen, Hilden, Germany) and the cDNA was analyzed by quantitative PCR using TaqMan Gene Expression Assays for apelin (Hs00936329_m1; Mm00443562_m1; Rn00581093_m1), APLNR (Hs00945496_s1; Mm00442191_s1; Rn00580252_s1), KDR (Hs009117_m1; Rn00564986_m1), VEGFA (Hs00900054_m1), EG5 (Hs00189698_m1), and GAPDH (Hs99999905_m1;

Mm99999915_g1; Rn01775763_g1) with TaqMan Gene Expression Master Mix (Cat. 4369016) in a StepOnePlus Instrument (all ThermoFisher Scientific). Samples were amplified using the standard running method within StepOne Software v2.2.2 by increasing the cycle number to 45. In each run, the expression levels of the target gene were normalized to those of *GAPDH* as a housekeeping gene.

Copy number analysis

Copy number analysis of all primary glioblastoma was performed on a using Affymetrix Cytoscan® HD Microarray at IMGM Laboratories (Martiensried, Germany).

Viability andproliferationassays

For viability and proliferation assays, 6000 cells/well were plated in 96-well plates in DMEM-F12 medium on day 0. Cell viability was measured after 24, 48, 72, and 96 h using a MTT assay (CellTiter 96 Non-Radioactive Cell Proliferation Assay, Cat. G4000; Promega; Madison, WI, USA) to assess cell metabolic activity. Cells were incubated for 1 h with the Stop Mix solution. Absorbance was measured on a Versa Max microplate reader with SoftMax Pro software (Molecular Devices; Sunnyvale, CA, USA) at a reference wavelength of 630 nm. The background absorbance of wells containing cell-free supernatant was subtracted from all measurements. Six replicate samples were used in each experiment. Three experiments were performed for each cell type.

Invasion assays

For this assay, we used U87MG cells which had been maintained in spheroid conditions in DMEM-F12 medium. Spheroids were picked under an Axiovert25 microscope (Carl Zeiss, Oberkochen, Germany). Spheroids were plated onto 24-well plates in 50 µl containing 1 mg/ml Rat Tail Collagen I (Cat. A10483-01; ThermoFisher Scientific), 10× PBS, 1 N NaOH, and diluted in bi-distilled water according to the manufacturer's instructions. As a chemoattractant source, the U87MG spheroids were added to the collagen mix. Apelin-F13A was added at to the collagen mix at a concentration of 1 µM. The collagen matrix was left to gell for 50 min at 37°C and then covered with 600 µl DMEM-F12 medium. Cell invasion was monitored for 7 days by taking photographs every day under an Axiovert25 microscope with Axiocam MRm and Axiovision Rel. 4.8 software (Carl Zeiss). The images were analyzed with ImageJ distribution Fiji (58) and the invasive area (mm^2) was calculated as: ΔA = (area covered on day n) − (sphere area on day 0).

Human glioblastoma specimens

Glioblastoma samples were obtained from the Neurosurgery Department of the University Hospital, LMU Munich (under the ethical project number 599-16, 18-304). Samples were classified according to whether they were taken from the center or border of the original tumor mass at the time of surgical resection. Necrotic tumor tissue, as evaluated by H&E staining, was excluded from the analysis. Paraffin-embedded glioblastoma samples were obtained by stereotactic biopsy at the Center for Neuropathology and Prion Research (ZNP), LMU Munich. The surgical depth (the distance in mm from the target point 0 defined by the neurosurgeon) and the histopathological description was recorded for each section obtained per specimen. Sections of patients pre- and post-bevacizumab treatment were obtained from the Edinger Instiute, Frankfurt am Main (ethical project number UCT Frankfurt GS 4/09 SNO-6-2018)

***In situ* hybridization**

The work bench and instruments were carefully cleaned with RNAse-Zap (Cat. R2020; Sigma Aldrich). Solutions were prepared using RNAse free water and sterilized. Sections on slides were deparaffinised by serial passages into Roti-Histol and graded alcohol (100%–25%). Tissue was permeabilized by incubation for 10 min in 10 µg/ml proteinase K (Cat. 04-1070; PeqLab, VWR, Darmstadt, Germany). Slides were fixed for 10 min in 4% paraformaldehyde (PFA) and blocked for 10 min with acetic anhydride (0.25%; Cat. 320102; Sigma Aldrich) in triethanolamine (1.5%; Cat. 09278; Sigma Aldrich). Sections were dried for 2 h at room temperature, incubated overnight at 65°C in a humidified chamber with digoxigenin (DIG)-labelled (DIG RNA labelling, cat. 11277073910; Roche Diagnostics) antisense or sense probes at a final concentration of 7 µg/ml, and diluted in a hybridization solution containing 100 µg/ml salmon sperm DNA (Cat AM9680; Ambion, ThermoFisher Scientific) to mask unspecific binding, and 100 µg/ml of co-precipitant RNA (yeast RNA; Cat. AM7118; Ambion). RNA probes were generated from human and mouse *APLN* and *APLNR* cDNA as previously described (16). The probe-containing hybridization solution was boiled at 95°C for 10 min before application. On day 2, non-specific signals were removed by stringency washing in graded saline sodium citrate (from 20× to 0.1×) and incubated with alkaline phosphatase-conjugated anti-DIG antibody (Cat. 11093274910; Roche Diagnostics) overnight at 4°C. On day 3, the slides were washed in PBS-T (0.1% Tween in 1× PBS) and incubated with 5-bromo-4-chloro-3-indolyl phosphate (BCIP)/nitro blue tetrazolium (NBT)

substrate (Cat. SK-5400; Vector Laboratories, Burlingame, CA, USA) in 0.1 M Tris-HCl (pH 9.5) at 37°C for up to 4 days. For counterstaining with eosin, the slides underwent serial passages in graded alcohol (70%–100%) followed by application of Roti-Histol, and were then mounted with Entellan (Cat. 107960, Merck Millipore). Pictures were taken under an Axioskop2 microscope with Axiocam 105 Color and Axiovision SE64 Rel. 4.9 software (Carl Zeiss).

Immunofluorescence and vessel density quantification

Under pentobarbital (Narcoren®; Merial, Halbergmoos, Germany) anesthesia, mice were transcardially perfused with 1× PBS followed by 4% phosphate-buffered PFA. The brain was post-fixed for 2 days in 4% PFA and then left in 30% sucrose for ≥24 h at 4°C. The brain was then embedded in Cryomatrix® (Cat. 6769006; ThermoFisher Scientific) and frozen at −20°C. Tissue samples were prepared as horizontal sections (40-µm-thick) using a microtome. Floating sections were blocked for 1 h at room temperature in 1× PBS containing 5% normal donkey serum (NDS; Cat. 017-000-121; Jackson Immuno-Research, Westgrove, PA, USA), and 0.3% Triton-X (Cat. 93418; Fluka). The sections were then incubated overnight at 4°C with the following primary antibodies: rabbit anti-MKi67 (1:200, Cat. ab16667), rabbit anti-APLNR (1:100, Cat. ab66218), rabbit anti-APLN 1:100, Cat. ab59469 (all Abcam, Cambridge, UK), rat anti-CD31 (1:50, cat. 550274; BD Biosciences, Franklin Lakes, NJ, USA), rabbit anti-von Willebrand factor (vWF; 1:400, Cat. A0082; Dako, Agilent Technologies, Santa Clara, CA, USA), or rabbit anti-GFP (1:500, Cat. A11122; ThermoFisher Scientific). The next day, the sections were incubated for 3 h at room temperature with the following secondary antibodies: biotin-labelled donkey anti-rabbit or anti-rat antibody (1:250, Cat. 711-065-152; 712-065-150) and/or 2 h at room temperature with streptavidin-AF488 or -AF594 (1:500, Cat. 016-540-084; 016-580-084, all Jackson Immuno-Research). Alternatively, sections were directly incubated for 2 h at room temperature with the secondary antibodies donkey anti-rabbit AF488 or AF594 (1:500, Cat. A-21206; A-21207, ThermoFisher Scientific). All antibodies were diluted in blocking solution. For nuclear DAPI 1:1000 was used. After staining, tissue was mounted in Fluorescent Mounting Medium (Cat. S3023; Dako) and photographs were taken using an Axiovert25 microscope with Axiocam MRm and Axiovision Rel 4.8 software (Carl Zeiss). Image analysis and quantification were performed using ImageJ distribution Fiji (58). Stereological analysis of vessel length density (31,32) was performed for the GFP-positive tumor area of CD31- or vWF-positive red fluorescent vessels on every 12th section using the space ball method of StereoInvestigator Software 10.21.1 (MicroBrightField Bioscience, Williston, VT, USA) connected to an Olympus-BX53-microscope (Olympus Europe; Hamburg, Germany) and a motorized object table (MicroBrightField Bioscience).

Immunohistochemistry and tumor volume

Free-floating sections were immersed in 0.3% peroxide for 10 min to block endogenous peroxidase, washed in PBS, and incubated for 1 h at room temperature in PBS containing 0.3% Triton X-100 and 5% normal donkey serum (NDS). Sections were then incubated with the primary antibodies rabbit anti-MKi67, , rabbit anti-GFP (1:1000, Cat. A-11122, ThermoFisher Scientific), or mouse anti-VIM (1:200, Cat. sc-6260, Santa Cruz Biotechnology, Dallas, TX, USA) overnight at 4°C in PBS containing 5% NDS. The next day, after three washes in PBS to remove unbound antibodies, the sections were incubated with secondary biotin donkey anti-rabbit, anti-rat, or anti-mouse antibodies (1:250, Cat. 711-065-152; 712-065-150; 115-065-166, Jackson Immuno-Research) for 3 h and then for 1 h at room temperature with streptavidin-conjugated horseradish peroxidase (1:200, Cat. SA-5004, Vector Laboratories). After washing in PBS, the sections were stained with DAB substrate according to manufacturer's instructions (Cat. DC137C100DCS, Innovative Diagnostik-Systeme, Hamburg, Germany). Finally, sections were mounted on glass slides (SuperfrostTM Plus, R.Langenbrinck GmbH, Emmendingen, Germany) and air dried for 10 min, followed by counterstaining with hematoxylin for 1 min. The slides were then rinsed with tap water, dehydrated with a graded series of ethanol (70%, 80%, 96%, 100%), cleared two times with xylene, and coverslipped with Roti®Histokit II mounting medium (Cat. 6640.1, Carl Roth GmbH, Karlsruhe, Germany). Tumor volumes were obtained from H&E or GFP-stained tumor sections by measuring the area of every 12th section and calculated using the Cavalieri Method (59).

Authors' Contributions

Designed the experiments: R.G., R.E.K.

Conducted experiments and analyzed data: G.M., M.H., M.L., V.S., N.Z., M.N.M.V., H.M., S.R., K. E., D.H., J.R., R.G., and R.E.K.

Obtained and characterized the experimental materials (patient tissues and cells), generated the mouse model (J.M.P.) or provided scientific support: H.M., D.H., C.H.-M., A. M.-V., P.H. G.G., M.S., J.M.P., A.L.V., E.W., M.M., R.B., U.S., and J.-C.T.

Writing the manuscript: R.G. and R.E.K.

Discussed results and revised manuscript: all authors

Acknowledgments

We are thankful to Stefanie Lange, Eva Sušnik, (Neurosurgical Research, LMU Munich), Eskil Eskilsson, Per Øystein Sakariassen (University of Bergen) and for general technical assistance, Steffen Dietzel and Andreas Thomae (Core Facility Bioimaging, Biomedical Center, LMU München) for the support with confocal microscopy, Günter Höglinger and Sigrid Schwarz (DZNE Munich site) for help with the StereoInvestigator and to Nicholas D. Smith http://www.scientific-writing.net/ for providing excellent Englisch language editing service. R.G. and R.E.K. gratefully acknowledge funding support from the DFG (GL691/2; SFB824), Wilhelm Sander-Stiftung, Anni-Hofmann Stiftung, Verein zur Förderung von Wissenschaft und Forschung an der Medizinischen Fakultät der LMU München (WiFoMed), Curt Bohnewandt Fonds, Friedrich-Baur-Stiftung, and Familie Mehdorn Stiftung. M.L. was supported by a China Scholarship Council (CSC) graduate scholarship. J.R. is a participant in the BIH-Charité Clinical Scientist Program funded by the Charité - Universitätsmedizin Berlin and the Berlin Institute of Health. Support for studies at the Charité by Frank L. Heppner is gratefully acknowledged. U.S. is supported by the Fördergemeinschaft Kinderkrebs-Zentrum Hamburg.

References

1. Louis DN, Perry A, Reifenberger G, von Deimling A, Figarella-Branger D, Cavenee WK, *et al.* The 2016 World Health Organization Classification of Tumors of the Central Nervous System: a summary. Acta Neuropathol **2016**;131:803-20
2. Stupp R, Mason WP, van den Bent MJ, Weller M, Fisher B, Taphoorn MJ, *et al.* Radiotherapy plus concomitant and adjuvant temozolomide for glioblastoma. N Engl J Med **2005**;352:987-96
3. Weller M, van den Bent M, Tonn JC, Stupp R, Preusser M, Cohen-Jonathan-Moyal E, *et al.* European Association for Neuro-Oncology (EANO) guideline on the diagnosis and treatment of adult astrocytic and oligodendroglial gliomas. Lancet Oncol **2017**;18:e315-e29
4. Brennan CW, Verhaak RG, McKenna A, Campos B, Noushmehr H, Salama SR, *et al.* The somatic genomic landscape of glioblastoma. Cell **2013**;155:462-77
5. Chen J, McKay RM, Parada LF. Malignant glioma: lessons from genomics, mouse models, and stem cells. Cell **2012**;149:36-47
6. Westphal M, Lamszus K. The neurobiology of gliomas: from cell biology to the development of therapeutic approaches. Nat Rev Neurosci **2011**;12:495-508
7. Jain RK, di Tomaso E, Duda DG, Loeffler JS, Sorensen AG, Batchelor TT. Angiogenesis in brain tumours. Nat Rev Neurosci **2007**;8:610-22
8. Chinot OL, Wick W, Mason W, Henriksson R, Saran F, Nishikawa R, *et al.* Bevacizumab plus radiotherapy-temozolomide for newly diagnosed glioblastoma. N Engl J Med **2014**;370:709-22
9. Gilbert MR, Dignam JJ, Armstrong TS, Wefel JS, Blumenthal DT, Vogelbaum MA, *et al.* A randomized trial of bevacizumab for newly diagnosed glioblastoma. N Engl J Med **2014**;370:699-708
10. Lu KV, Bergers G. Mechanisms of evasive resistance to anti-VEGF therapy in glioblastoma. CNS Oncol **2013**;2:49-65
11. Aldape K, Zadeh G, Mansouri S, Reifenberger G, von Deimling A. Glioblastoma: pathology, molecular mechanisms and markers. Acta Neuropathol **2015**;129:829-48
12. Verhaak RG, Hoadley KA, Purdom E, Wang V, Qi Y, Wilkerson MD, *et al.* Integrated genomic analysis identifies clinically relevant subtypes of glioblastoma characterized by abnormalities in PDGFRA, IDH1, EGFR, and NF1. Cancer Cell **2010**;17:98-110
13. Wang Q, Hu B, Hu X, Kim H, Squatrito M, Scarpace L, *et al.* Tumor Evolution of Glioma-Intrinsic Gene Expression Subtypes Associates with Immunological Changes in the Microenvironment. Cancer Cell **2017**;32:42-56 e6
14. Sandmann T, Bourgon R, Garcia J, Li C, Cloughesy T, Chinot OL, *et al.* Patients With Proneural Glioblastoma May Derive Overall Survival Benefit From the Addition of Bevacizumab to First-Line Radiotherapy and Temozolomide: Retrospective Analysis of the AVAglio Trial. J Clin Oncol **2015**
15. Talasila KM, Soentgerath A, Euskirchen P, Rosland GV, Wang J, Huszthy PC, *et al.* EGFR wild-type amplification and activation promote invasion and development of glioblastoma independent of angiogenesis. Acta Neuropathol **2013**;125:683-98
16. Kalin RE, Kretz MP, Meyer AM, Kispert A, Heppner FL, Brandli AW. Paracrine and autocrine mechanisms of apelin signaling govern embryonic and tumor angiogenesis. Dev Biol **2007**;305:599-614
17. Plate KH, Breier G, Weich HA, Risau W. Vascular endothelial growth factor is a potential tumour angiogenesis factor in human gliomas *in vivo*. Nature **1992**;359:845-8

18. Zhang L, Takara K, Yamakawa D, Kidoya H, Takakura N. Apelin as a marker for monitoring the tumor vessel normalization window during antiangiogenic therapy. Cancer Sci **2016**;107:36-44
19. Kälin S, Kälin RE. Apelin and Cancer. In: O. R, N.A. B, editors. Adipocitokines, Energy Balance and Cancer: Springer International Publishing Switzerland 2017. p 137-66.
20. O'Carroll AM, Lolait SJ, Harris LE, Pope GR. The apelin receptor APJ: journey from an orphan to a multifaceted regulator of homeostasis. J Endocrinol **2013**;219:R13-35
21. Keunen O, Johansson M, Oudin A, Sanzey M, Rahim SA, Fack F, *et al.* Anti-VEGF treatment reduces blood supply and increases tumor cell invasion in glioblastoma. Proc Natl Acad Sci U S A **2011**;108:3749-54
22. Bowman RL, Wang Q, Carro A, Verhaak RG, Squatrito M. GlioVis data portal for visualization and analysis of brain tumor expression datasets. Neuro Oncol **2017**;19:139-41
23. Eskilsson E, Rosland GV, Talasila KM, Knappskog S, Keunen O, Sottoriva A, *et al.* EGFRvIII mutations can emerge as late and heterogenous events in glioblastoma development and promote angiogenesis through Src activation. Neuro Oncol **2016**
24. Hambardzumyan D, Amankulor NM, Helmy KY, Becher OJ, Holland EC. Modeling Adult Gliomas Using RCAS/t-va Technology. Transl Oncol **2009**;2:89-95
25. Pitter KL, Tamagno I, Alikhanyan K, Hosni-Ahmed A, Pattwell SS, Donnola S, *et al.* Corticosteroids compromise survival in glioblastoma. Brain **2016**;139:1458-71
26. Sonabend AM, Yun J, Lei L, Leung R, Soderquist C, Crisman C, *et al.* Murine cell line model of proneural glioma for evaluation of anti-tumor therapies. J Neurooncol **2013**;112:375-82
27. Jones TS, Holland EC. Animal models for glioma drug discovery. Expert Opin Drug Discov **2011**;6:1271-83
28. Hanahan D, Folkman J. Patterns and emerging mechanisms of the angiogenic switch during tumorigenesis. Cell **1996**;86:353-64
29. Bergers G, Benjamin LE. Tumorigenesis and the angiogenic switch. Nat Rev Cancer **2003**;3:401-10
30. Sakariassen PO, Prestegarden L, Wang J, Skaftnesmo KO, Mahesparan R, Molthoff C, *et al.* Angiogenesis-independent tumor growth mediated by stem-like cancer cells. Proc Natl Acad Sci U S A **2006**;103:16466-71
31. Dockery P, Fraher J. The quantification of vascular beds: a stereological approach. Exp Mol Pathol **2007**;82:110-20
32. Franciosi S, Gama Sosa MA, English DF, Oler E, Oung T, Janssen WG, *et al.* Novel cerebrovascular pathology in mice fed a high cholesterol diet. Mol Neurodegener **2009**;4:42
33. Drachsler M, Kleber S, Mateos A, Volk K, Mohr N, Chen S, *et al.* CD95 maintains stem cell-like and non-classical EMT programs in primary human glioblastoma cells. Cell Death Dis **2016**;7:e2209
34. Campos B, Wan F, Farhadi M, Ernst A, Zeppernick F, Tagscherer KE, *et al.* Differentiation therapy exerts antitumor effects on stem-like glioma cells. Clin Cancer Res **2010**;16:2715-28
35. Podergajs N, Brekka N, Radlwimmer B, Herold-Mende C, Talasila KM, Tiemann K, *et al.* Expansive growth of two glioblastoma stem-like cell lines is mediated by bFGF and not by EGF. Radiol Oncol **2013**;47:330-7
36. Miyake M, Goodison S, Lawton A, Gomes-Giacoia E, Rosser CJ. Angiogenin promotes tumoral growth and angiogenesis by regulating matrix metallopeptidase-2 expression via the ERK1/2 pathway. Oncogene **2015**;34:890-901

37. Lee DK, George SR, O'Dowd BF. Unravelling the roles of the apelin system: prospective therapeutic applications in heart failure and obesity. Trends Pharmacol Sci **2006**;27:190-4
38. Lee DK, Saldivia VR, Nguyen T, Cheng R, George SR, O'Dowd BF. Modification of the terminal residue of apelin-13 antagonizes its hypotensive action. Endocrinology **2005**;146:231-6
39. Medhurst AD, Jennings CA, Robbins MJ, Davis RP, Ellis C, Winborn KY, *et al.* Pharmacological and immunohistochemical characterization of the APJ receptor and its endogenous ligand apelin. J Neurochem **2003**;84:1162-72
40. Fan X, Zhou N, Zhang X, Mukhtar M, Lu Z, Fang J, *et al.* Structural and functional study of the apelin-13 peptide, an endogenous ligand of the HIV-1 coreceptor, APJ. Biochemistry **2003**;42:10163-8
41. Pope GR, Tilve S, McArdle CA, Lolait SJ, O'Carroll AM. Agonist-induced internalization and desensitization of the apelin receptor. Mol Cell Endocrinol **2016**;437:108-19
42. Reaux A, De Mota N, Skultetyova I, Lenkei Z, El Messari S, Gallatz K, *et al.* Physiological role of a novel neuropeptide, apelin, and its receptor in the rat brain. J Neurochem **2001**;77:1085-96.
43. Zou MX, Liu HY, Haraguchi Y, Soda Y, Tatemoto K, Hoshino H. Apelin peptides block the entry of human immunodeficiency virus (HIV). FEBS Lett **2000**;473:15-8.
44. Calebiro D, Godbole A. Internalization of G-protein-coupled receptors: Implication in receptor function, physiology and diseases. Best Pract Res Clin Endocrinol Metab **2018**;32:83-91
45. Berta J, Hoda MA, Laszlo V, Rozsas A, Garay T, Torok S, *et al.* Apelin promotes lymphangiogenesis and lymph node metastasis. Oncotarget **2014**;5:4426-37
46. Berta J, Kenessey I, Dobos J, Tovari J, Klepetko W, Jan Ankersmit H, *et al.* Apelin expression in human non-small cell lung cancer: role in angiogenesis and prognosis. J Thorac Oncol **2010**;5:1120-9
47. Sorli SC, Le Gonidec S, Knibiehler B, Audigier Y. Apelin is a potent activator of tumour neoangiogenesis. Oncogene **2007**;26:7692-9
48. Binda E, Visioli A, Giani F, Trivieri N, Palumbo O, Restelli S, *et al.* Wnt5a Drives an Invasive Phenotype in Human Glioblastoma Stem-like Cells. Cancer Res **2017**;77:996-1007
49. Podergajs N, Motaln H, Rajcevic U, Verbovsek U, Korsic M, Obad N, *et al.* Transmembrane protein CD9 is glioblastoma biomarker, relevant for maintenance of glioblastoma stem cells. Oncotarget **2016**;7:593-609
50. Harford-Wright E, Andre-Gregoire G, Jacobs KA, Treps L, Le Gonidec S, Leclair HM, *et al.* Pharmacological targeting of apelin impairs glioblastoma growth. Brain **2017**;140:2939-54
51. Pitkin SL, Maguire JJ, Kuc RE, Davenport AP. Modulation of the apelin/APJ system in heart failure and atherosclerosis in man. Br J Pharmacol **2010**;160:1785-95
52. De Mota N, Lenkei Z, Llorens-Cortes C. Cloning, pharmacological characterization and brain distribution of the rat apelin receptor. Neuroendocrinology **2000**;72:400-7
53. Haynes HR, Camelo-Piragua S, Kurian KM. Prognostic and predictive biomarkers in adult and pediatric gliomas: toward personalized treatment. Front Oncol **2014**;4:47
54. UKCCCR guidelines for the welfare of animals in experimental neoplasia. Cancer Metastasis Rev **1989**;8:82-8
55. Kuba K, Zhang L, Imai Y, Arab S, Chen M, Maekawa Y, *et al.* Impaired heart contractility in Apelin gene-deficient mice associated with aging and pressure overload. Circ Res **2007**;101:e32-42

56. Shinkai Y, Rathbun G, Lam KP, Oltz EM, Stewart V, Mendelsohn M, *et al.* RAG-2-deficient mice lack mature lymphocytes owing to inability to initiate V(D)J rearrangement. Cell **1992**;68:855-67
57. Grathwohl SA, Kälin RE, Bolmont T, Prokop S, Winkelmann G, Kaeser SA, *et al.* Formation and maintenance of Alzheimer's disease beta-amyloid plaques in the absence of microglia. Nat Neurosci **2009**;12:1361-3
58. Schindelin J, Arganda-Carreras I, Frise E, Kaynig V, Longair M, Pietzsch T, *et al.* Fiji: an open-source platform for biological-image analysis. Nat Methods **2012**;9:676-82
59. Mayhew TM, Mwamengele GL, Dantzer V. Stereological and allometric studies on mammalian cerebral cortex with implications for medical brain imaging. J Anat **1996**;189 (Pt 1):177-84

Figures

Figure 1.

Apelin is downregulated by anti-VEGFA or anti-VEGFR2 treatment. **A,** Apelin expression was analyzed in a murine PDGFB-driven glioblastoma model, based on the RCAS/Tva system (24). Apelin expression in paraffin-embedded sections from glioblastoma-bearing control mice treated with vehicle or anti-VEGFA antibody (B20-4.1.1; Roche) was analyzed by *in situ* hybridization. In control samples, apelin is strongly expressed in pseudopalisading structures (asterisk) and in tumor vessels (arrows). By contrast, the expression of apelin is nearly lost in anti-VEGFA antibody-treated samples, with few apelin-positive vessels. Apelin qPCR also showed downregulation of apelin in anti-VEGFA antibody-treated samples. 4 versus 4 samples were analyzed. Values are reported as the mean ± SEM and Student's *t* test was used to determine statistical significance. *p<0.05, **p<0.005, and ***p<0.0005. **B,** Mice implanted with *p53*^{KO}PDGFB GSCs were intracerebrally infused with anti-VEGFR2 antibody (DC101; Ely Lilly) or aCSF. Both groups (n= 7 or 10) grew large proneural gliobastomas (shown in the H&E overview in Supplementary Fig. S1B) with variable cell density (asterisks indicate high cell density on higher-magnification H&E images), invasiveness (arrowheads indicate more invasive tumor border), and areas of vascular proliferates (arrows). *In situ* hybridization of consecutive sections from control tumors revealed apelin expression on pseudopalisades (asterisk) and tumor vessels (arrows); the treated tumors are largely devoid of tumor apelin with few apelin-positive vessels (arrows). **C**, Quantfiication of pseudopalisading or apelin positive areas was performed in ImageJ using the threshold function on 6 representative pictures (5x magnficiation) per animal on H&E or consecutive sections stained for apelin mRNA. **D**, H&E sections obtained from 7 patients pre and post bevacizumab treatment were quantified for cell dense pseudopalisading area. As pseudopallisades were more numerous and narrow before treatment, they were less but broader after treatment resulting in no significant difference. Values are reported as the mean ± SEM and Student's *t* test was used to determine statistical significance. *p<0.05, **p<0.005, ***p<0.0005. **E**, Apelin expression in paraffin-embedded sections from the same glioblastoma patients pre and post bevacizumab therapy were analyzed by *in situ* hybridization. Apelin is strongly expressed in vascular proliferates (arrows) and visible in pseudopalisading structures (asterisk) pre bevacizumab but much less prominent in vessels and pseudopalisading areas post treatment.

Figure 2.

Glioma cell- and host-derived apelin control glioblastoma angiogenesis. **A,** Apelin and APLNR were upregulated in the tumor microenvironment following the angiogenic switch in a serial implantation model. Patient-derived glioblastoma cells were serially passaged in immunodeficient rats for more than four generations. The vascular marker KDR together with apelin and APLNR were strongly upregulated in the rat tumor microenvironment in the angiogenic samples as compared with the invasive tumor samples, while tumor-derived human apelin and APLNR expression was low in both samples. In comparison, VEGFA expression was constantly high in angiogenic and invasive xenografts. Expression levels were quantified by species-specific qPCR in 8 invasive versus 5 angiogenic tumors originating from 7 different patients (30). **B,** Murine GSCs with low endogenous levels of apelin were implanted into wildtype or *APLN*^{KO} mice to assess the contribution of microenvironmental apelin on glioma angiogenesis. Glioblastoma *p53*^{KO}PDGFB GSCs were grown in wildtype or *APLN*^{KO} mice and subjected to H&E and anti-GFP immunostaining. To measure vessel density, immunostaining for vWF was performed and the microvasculature was analyzed by stereomorphology throughout the tumor marked by GFP expression. The vascular structure of the tumor was characterized in terms of VLD and total VL. VLD and VL were greater in wildtype mice (n = 7) and were significantly reduced in APLN^{KO} mice (n = 8). **C,** Tumor cell-derived apelin contributes to glioblastoma angiogenesis. Patient-derived GBM14 GSCs were implanted into immunodeficient mice. Immunostaining for CD31 was performed and the microvasculature in the GFP-positive tumor area was analyzed by stereomorphology. The numbers of mice per group were 7, 7, 4, and 4 for GBM14^{NSC} into wildtype mice, GBM14^{AKD} into wildtype mice, GBM14^{NSC} into *APLN*^{KO} mice, and GBM14^{AKD} into *APLN*^{KO} mice, respectively. VLD and total VL were greatly reduced in the glioblastomas with modulated apelin levels relative to controls. Values are reported as the mean ± SEM and Student's *t* test was used to determine statistical significance. *p<0.05, **p<0.005, ***p<0.0005.

Figure 3.

APLNR is expressed in the tumor margin and attenuation of apelin/APLNR signaling *in vitro* uncovers a role of APLNR in glioblastoma cell invasion. **A,** IVY Glioblastoma Atlas Project dataset depicting increased (red) or decreased (green) expression of apelin, APLNR, VEGFA, and KDR relative to the background (black), as analyzed by RNAseq of laser-dissected cells from glioblastoma tissue sections. Apelin expression is increased in the pseudopallisading cells around regions of necrosis, while apelin and APLNR are both upregulated in microvascular proliferations. In contrast to apelin, VEGF and KDR, the expression of APLNR is also upregulated in the infiltrating tumor area. **B,** Stereotactic biopsies were taken from patients with glioblastoma, and the levels are labelled in millimetres along a trajectory from the cell dense tumor (z = 0 mm) to the infiltrative tumor in the tumor periphery (z = 6 and 8 mm). Apelin is expressed in tumor vessels (arrows) and individual cells (arrowheads) in the cell dense tumor (z = 0), but it undetectable in the periphery (z = 6 and 8 mm). APLNR is expressed in tumor vessels (arrows) and in individual cells at z = 0, and in peripheral cells at z = 6 and 8 mm. The magnified inserts show the cellular staining. Apelin and APLNR mRNA was undetectable on tumor-free brain tissue. **C**–**E**, *In vitro* cell invasion was investigated using a rat tail collagen invasion assay. **C**, Invasion of $GBM14^{NSC}$ and $GBM14^{AKD}$ cells was quantified following the addition of U87MG spheres as an external migratory stimulus. $GBM14^{AKD}$ cells showed significantly greater invasion compared with the control $GBM14^{NSC}$ cells. **D** and **E,** Application of 1 μM of apelin-F13A attenuated *in vitro* cell invasion of $GBM14^{NSC}$ (**D**) and $p53^{KO}$PDGFB (**E**) GSCs. Data are obtained from at least 5 different spheres per condition and reported as the mean ± SEM. Two-way ANOVA was used to determine statistical significance. *p<0.05, **p<0.005, ***p<0.0005.

Figure 4.

Anti-invasive role of apelin in orthotopic models of proneural glioblastoma. **A** and **B,** All glioblastoma were analyzed by H&E and GFP immunostaining to assess overall, compact and invasive tumor volumes, as well as the migration distance of single cells from the tumor mass. In all panels, the compact tumor border is indicated by arrowheads, and arrows show examples of single invading cells. **A**, GBM14^{NSC} or GBM14^{AKD} GSCs were grown in immunodeficient wildtype or *APLN*^{KO} mice. Although there is no difference in overall tumor volume, the invasive tumor volume (% invasive volume) is significantly greater for GBM14^{AKD} cells implanted into wildtype mice (n = 7), GBM14^{NSC} cells implanted into *APLN*^{KO} mice (n = 4), and GBM14^{AKD} cells implanted into *APLN*^{KO} mice (n = 4) as compared with GBM14^{NSC} cells implanted into wildtype mice (n = 7). The distance of single invading cells to the tumor center is significantly greater in the *APLN*^{KO} mouse xenografts. **B,** *p53*^{KO}PDGFB cells as a model of the proneural glioblastoma subtype were grown in immunocompetent wildtype or *APLN*^{KO} mice. Although the overall tumor volume is unchanged in *APLN*^{KO} mice (n = 8) compared with wildtype mice (n = 7), the invasiveness, as assessed by percent invasive volume and distance of migration, is substantially increased in *APLN*^{KO} mice. Values are reported as the mean ± SEM and Student's *t* test was used to determine statistical significance. *p<0.05, **p<0.005, ***p<0.0005.

Figure 5.

The APLNR ligand apelin-F13A inhibits glioblastoma angiogenesis and invasion. **A** and B, murine *p53*^{KO}PDGFB (**A**) or human GBM14 (**B**) GSCs were implanted and glioblastoma established for 1 or 2 weeks, respectively. Then, aCSF or 30 µg of apelin-F13A were administered for 2 weeks (**A**) or 60 µg was administered for 4 weeks (**B**) via intracerebral infusion. The vessel density and growth of tumors were measured. The mouse- and patient-derived human glioblastoma showed a significant reduction in tumor vasculature, measured by VLD and VL, as well as significant reductions in invasive and overall tumor volume. The arrows indicate single invasive tumor cells in GFP- or H&E-stained sections while the arrowheads point to the compact tumor border. aCSF or apelin-F13A were infused into 8 and 6 mice with murine glioblastoma and 6 and 5 mice with human glioblastoma, respectively. Values are reported as the mean ± SEM and Student's *t* test was used to determine statistical significance. *$p<0.05$, **$p<0.005$, ***$p<0.0005$.

Figure 6.

Co-targeting of VEGFR2 and APLNR synergistically improves survival of mice bearing glioblastoma. **A,** Intracerebral infusion of 30 µg of apelin-F13A and/or 0.8 mg of the anti-VEGFR2 antibody DC101 significantly increased survival compared with the infusion of aCSF in mice bearing *p53*^{KO}PDGFB glioblastoma. Median survival was 52 days in aCSF-treated mice and was increased similarly by the administration of DC101 (67 days) or apelin-F13A (63 days; $p<0.05$) alone, administration of both DC101 and apelin-F13A significantly increased survival to 86 days ($p<0.005$). Thus, co-treatment with apelin-F13A and DC101 increased survival by 28% ($p<0.05$). Ten, 7, 9, and 6 mice were treated with aCSF, DC101, apelin-F13A, and DC101 plus apelin-F13A, respectively. Log-rank (Mantel-Cox) test was used to determine statistical significance. *$p<0.05$, **$p<0.005$, ***$p<0.0005$. **B,** Glioblastoma invasiveness was analyzed in GFP-stained sections. In the composite images, the compact border is indicated by a blue line and the invasive tumor border is indicated with a red line. In the close-up images, massive invasion of single cells is visible in DC101-treated tumors. While the invasive glioblastoma volume increased in DC101-treated tumors to 55% compared with 30% in control tumors, the invasive glioblastoma volume was decreased to 8% in apelin-F13A-treated tumors. Invasiveness was reduced to 18% in mice treated with DC101 and apelin-F13A. Data are shown for 4 tumors in the treated groups and 5 tumors in the control group. **C,** vWF-immunostained vessels were quantified by stereomorphology. DC101 and apelin-F13 treatment significantly decreased VLD to 440 and 357 mm/mm^3, respectively, versus 613 mm/mm^3 in control mice. Coadministration of DC101 and apelin-F13 decreased VLD to 243 mm/mm^3, which was significantly lower than that in DC101-treated tumors. Four tumors were analyzed per group. Values are reported as the mean ± SEM and Student's *t* test was used to determine statistical significance. *$p<0.05$, **$p<0.005$, ***$p<0.0005$.

Figure 7.

Model of the dichotomous role of apelin/APLNR signaling in resistance to bevacizumab treatment. A neoplastic glioblastoma cell is shown in the vicinity of a brain capillary. The glioblastoma cell expresses both apelin (green) and the APLNR. By autocrine signaling, apelin ligands will induce APLNR to inhibit glioblastoma cell invasion. A paracrine apelin signal from glioblastoma cells also act on APLNR-expressing brain capillaries to activate tumor angiogenesis. The newly forming angiogenic sprouts start expressing apelin, which further propels neovascularization leading to direct (through APLNR) and indirect (rich vascular bed) containment of glioblastoma cells, resulting in the formation of weakly invasive but highly angiogenic glioblastoma. Glioblastoma cells with low apelin expression (or if apelin levels are artificially depleted) are characterized by low tumor neovascularization but the APLNR-expressing glioblastoma cells are highly invasive. Administration of ectopic apelin-F13A peptide (red), for example, reduces neoangiogenesis and glioblastoma cell invasiveness, resulting in attenuated glioblastoma growth. The blood vessels also express VEGFR2, and vasculogenesis is stimulated following VEGFA administration. Anti-angiogenic therapies that target the VEGFA/VEGFR2 signaling axis, like bevacizumab, reduce apelin expression and suppress tumor angiogenesis, but the anti-invasive effects of apelin are also reduced. However, co-targeting of APLNR- and VEGFR-signaling reduces angiogenesis further and also reverts the proinvasive response towards VEGFR-targeted therapy (caused by depleting tumor apelin) following alternative stimulation of APLNR.

Table 1: Abbreviations

Abbreviations	Full name
aCSF	artificial Cerebrospinal Fluid
$APLN^{KD}$	APLN-knockdown
$APLN^{KO}$	APLN-knockout
$APLN^{WT}$	APLN-wildtype
BV	Blood Vessels
GFP	Green Fluorescent Protein
GPCR	G-Protein Coupled Receptor
GSCs	Glioblastoma Stem Cells
NSC	non-silencing control
VL	Vessel Length
VLD	Vessel Length Density

Fig. 1

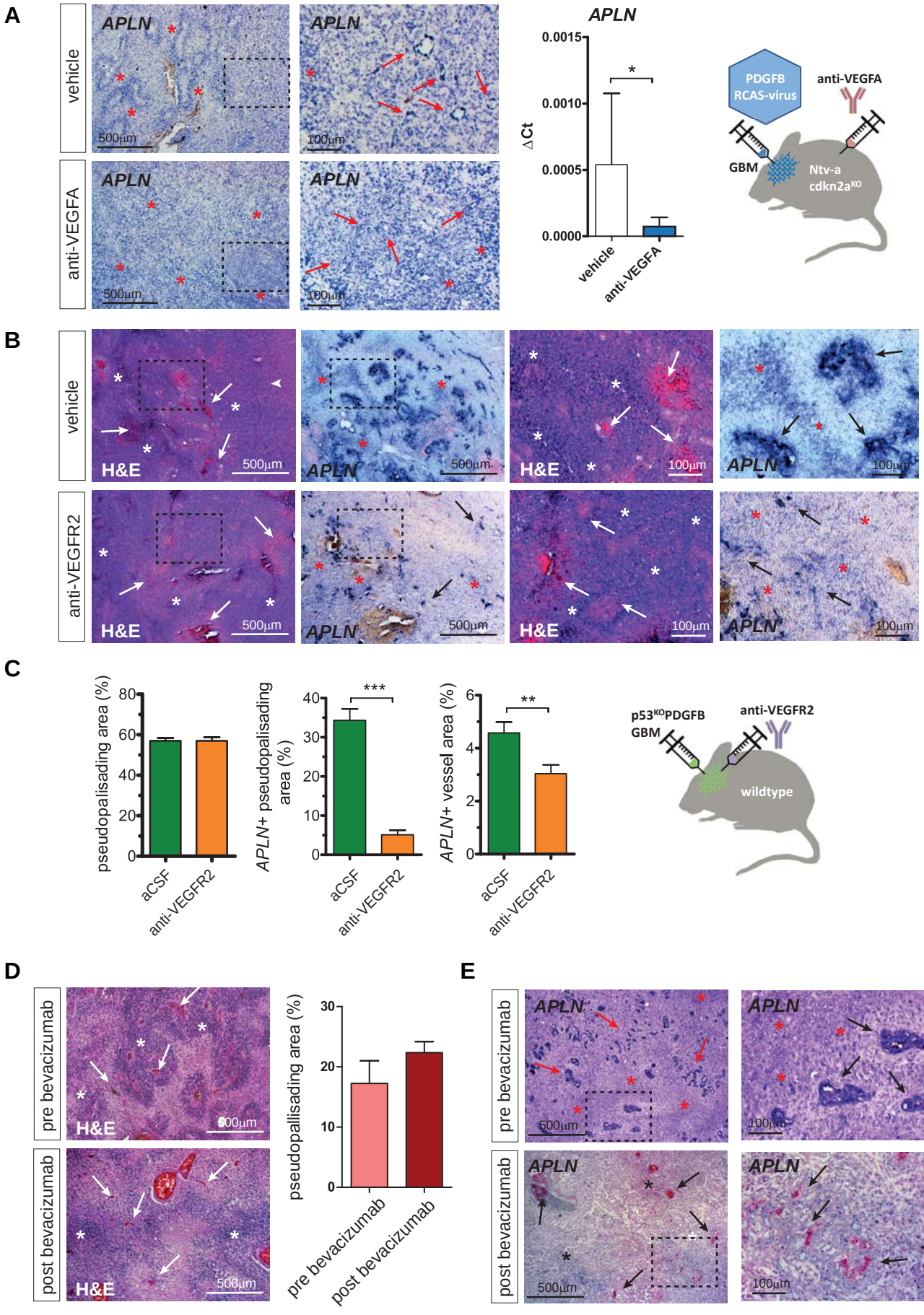
A
vehicle
anti-VEGFA
APLN
500µm
100µm
ΔCt
0.0015
0.0010
0.0005
0.0000
*
vehicle
anti-VEGFA
PDGFB
RCAS-virus
anti-VEGFA
GBM
Ntv-a
cdkn2a^KO
B
vehicle
anti-VEGFR2
H&E
500µm
100µm
C
pseudopalisading area (%)
80
60
40
20
0
aCSF
anti-VEGFR2
APLN+ pseudopalisading area (%)
***
40
30
20
10
0
APLN+ vessel area (%)
**
6
4
2
0
p53^KOPDGFB
GBM
anti-VEGFR2
wildtype
D
pre bevacizumab
post bevacizumab
H&E
500µm
pseudopallisading area (%)
30
20
10
0
E
APLN
500µm
100µm

Fig 2.

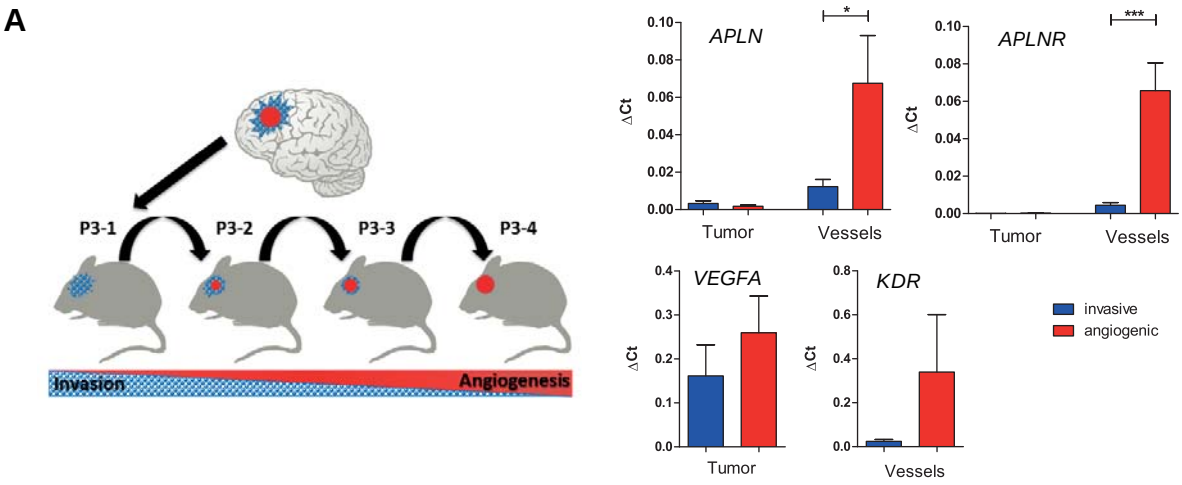
A
P3-1
P3-2
P3-3
P3-4
Invasion
Angiogenesis
APLN
APLNR
VEGFA
KDR
ΔCt
Tumor
Vessels
invasive
angiogenic

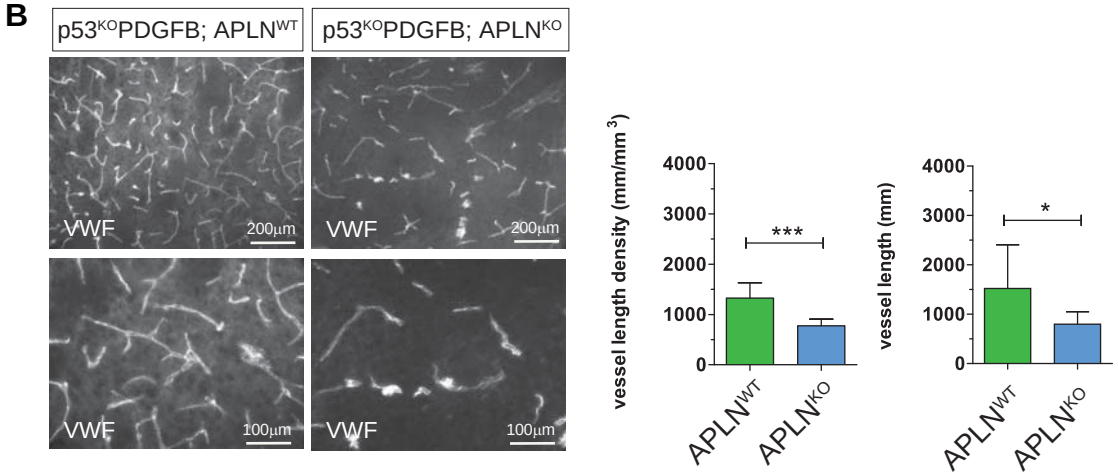
B
p53KOPDGFB; APLNWT
p53KOPDGFB; APLNKO
VWF
200μm
100μm
vessel length density (mm/mm3)
vessel length (mm)
APLNWT
APLNKO

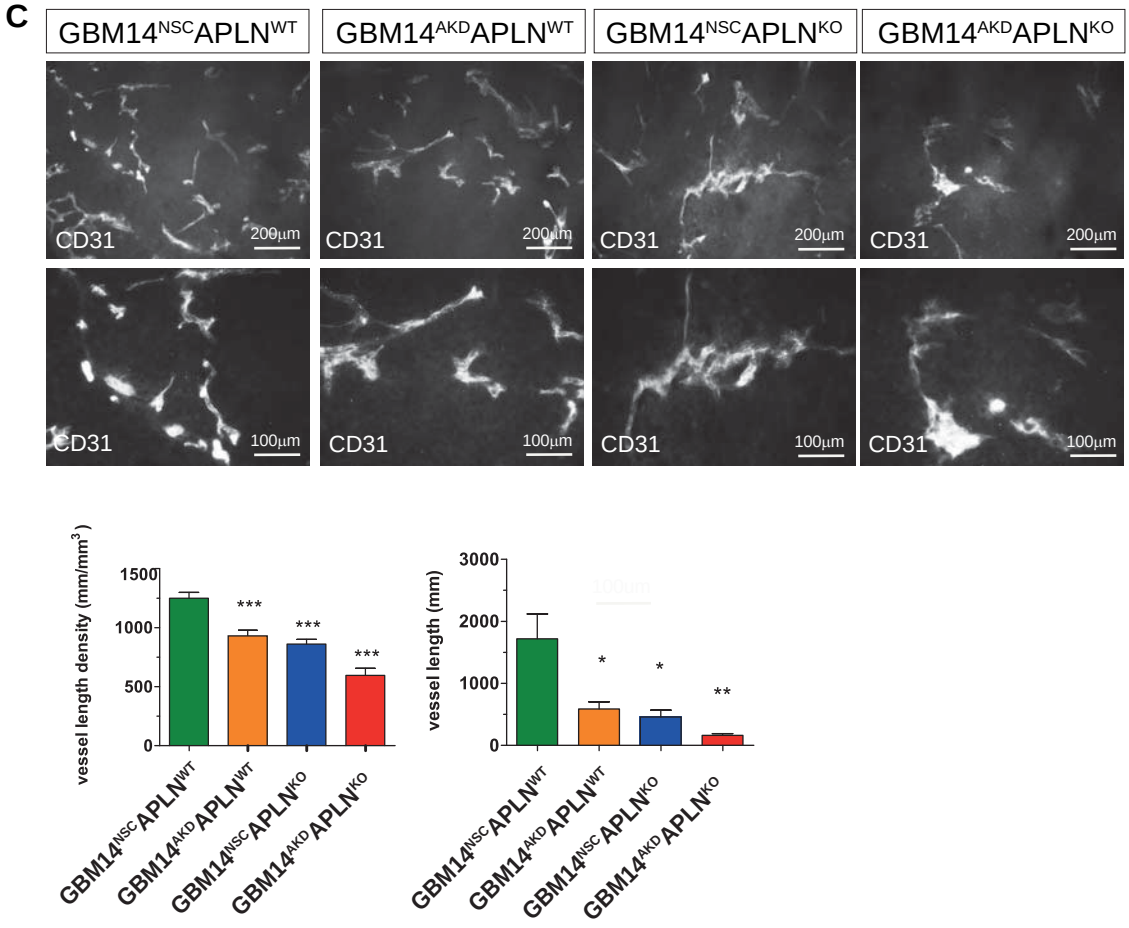
C
GBM14NSCAPLNWT
GBM14AKDAPLNWT
GBM14NSCAPLNKO
GBM14AKDAPLNKO
CD31
200μm
100μm
vessel length density (mm/mm3)
vessel length (mm)

Fig. 3

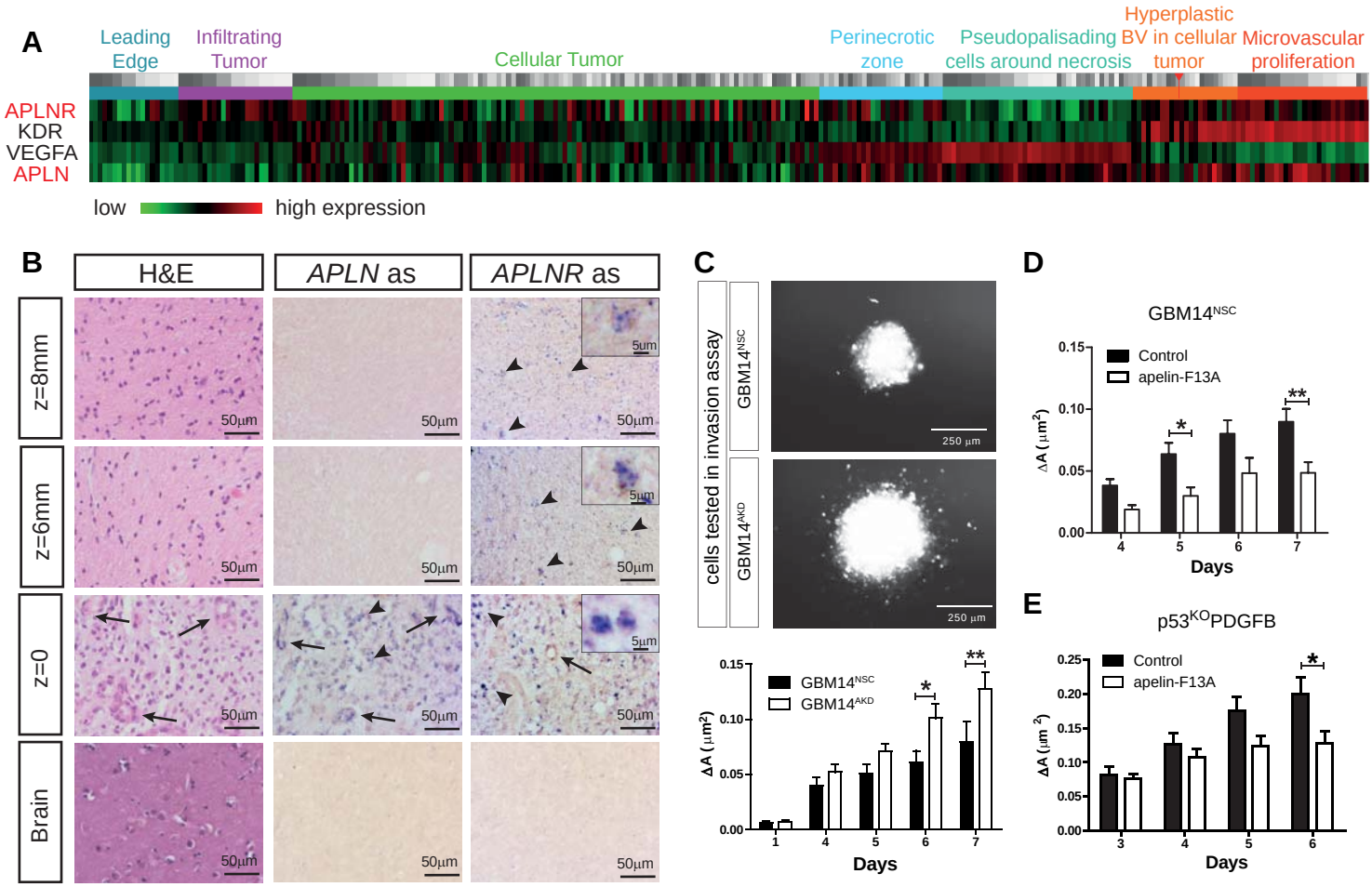
A
Leading Edge
Infiltrating Tumor
Cellular Tumor
Perinecrotic zone
Pseudopalisading cells around necrosis
Hyperplastic BV in cellular tumor
Microvascular proliferation
APLNR
KDR
VEGFA
APLN
low
high expression
B
H&E
APLN as
APLNR as
z=8mm
z=6mm
z=0
Brain
50µm
5µm
C
cells tested in invasion assay
GBM14NSC
GBM14AKD
250 µm
ΔA (µm2)
Days
D
GBM14NSC
Control
apelin-F13A
E
p53KOPDGFB

Fig. 4

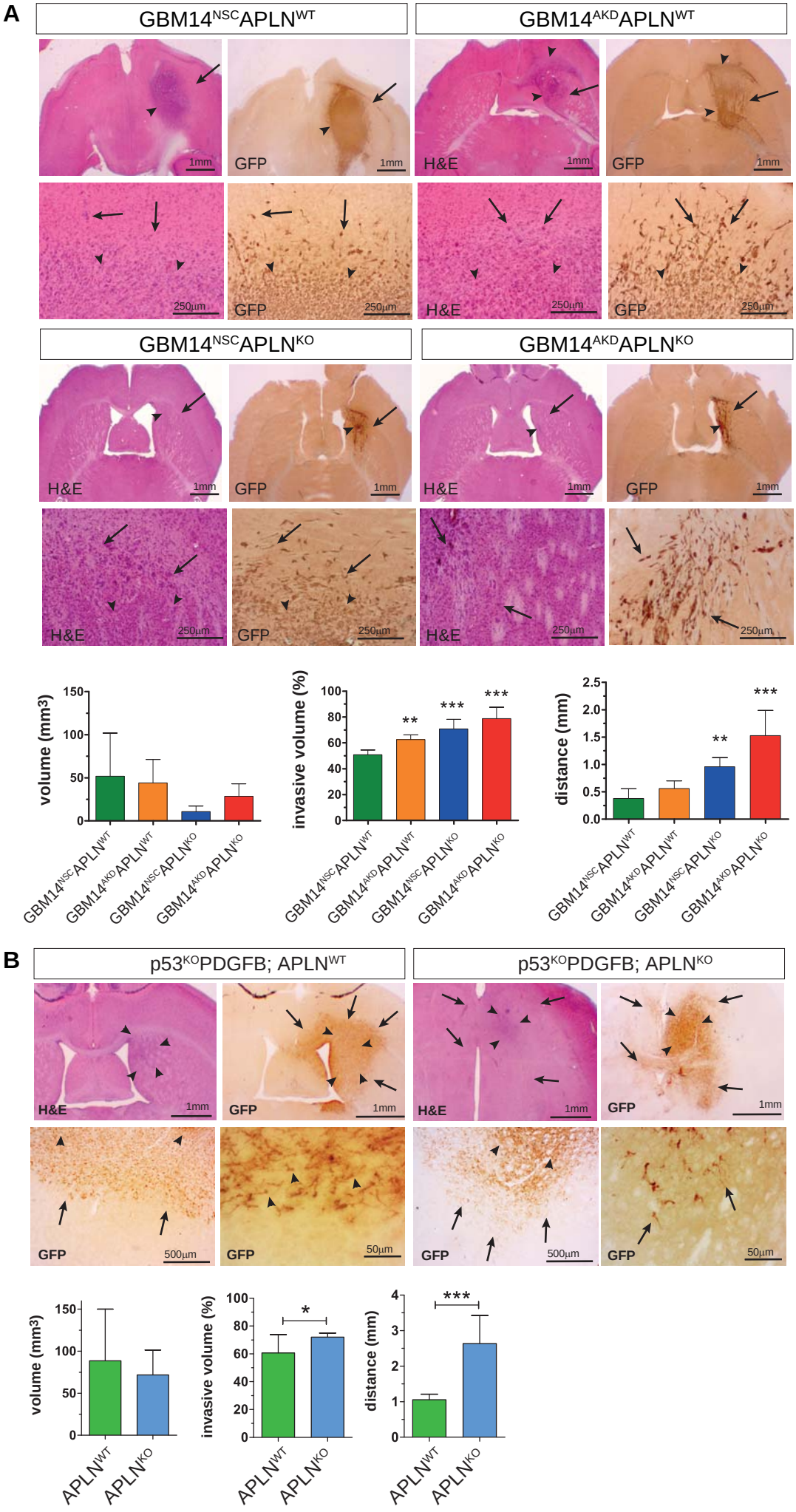
A
GBM14NSCAPLNWT
GBM14AKDAPLNWT
GBM14NSCAPLNKO
GBM14AKDAPLNKO
H&E
GFP
1mm
250μm
volume (mm3)
invasive volume (%)
distance (mm)
B
p53KOPDGFB; APLNWT
p53KOPDGFB; APLNKO
500μm
50μm
APLNWT
APLNKO

Fig. 5

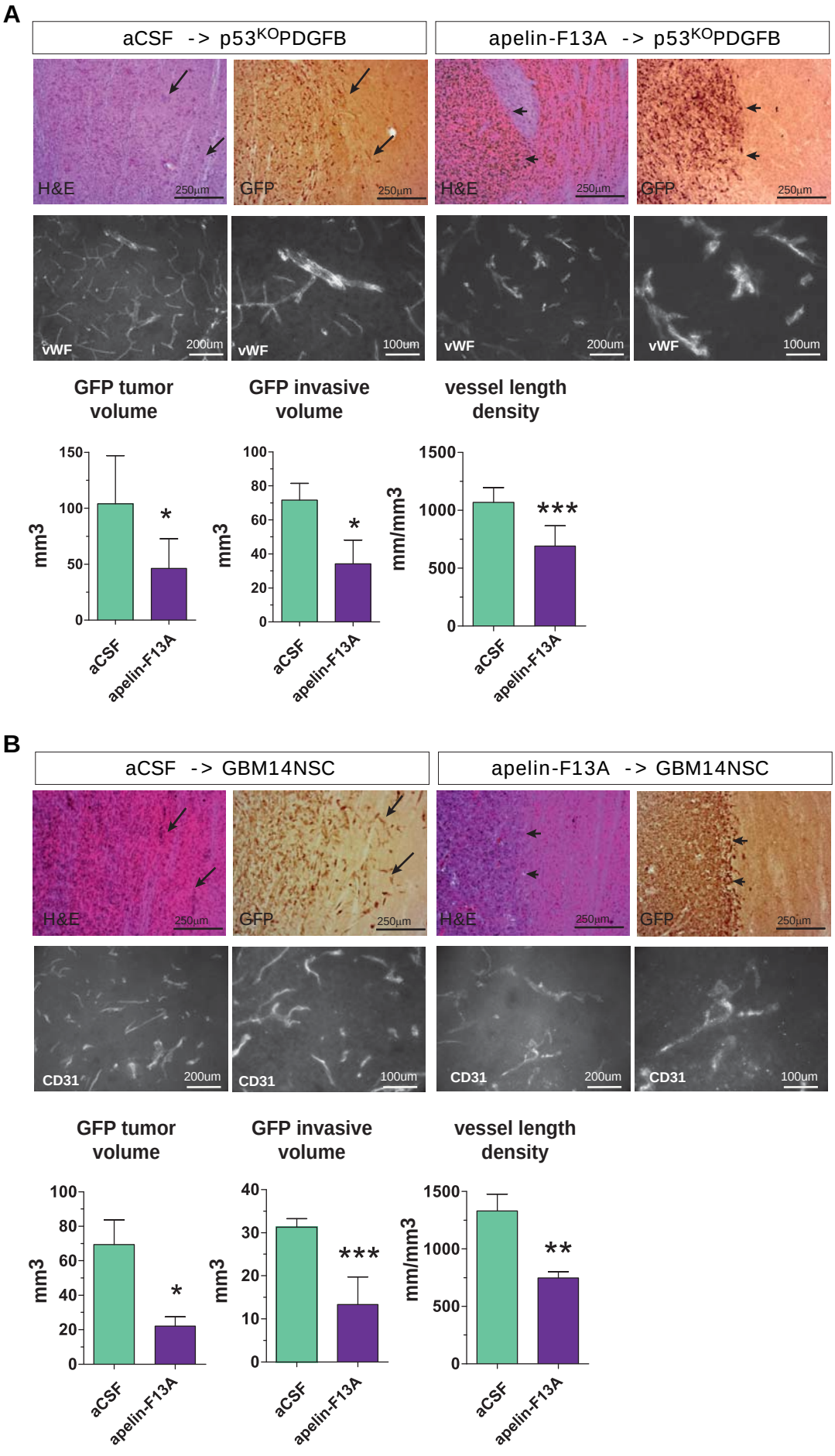
A
aCSF -> p53KOPDGFB
apelin-F13A -> p53KOPDGFB
H&E
GFP
vWF
250µm
200um
100um
GFP tumor volume
GFP invasive volume
vessel length density
mm3
mm/mm3
aCSF
apelin-F13A
B
aCSF -> GBM14NSC
apelin-F13A -> GBM14NSC
CD31

Fig 6.

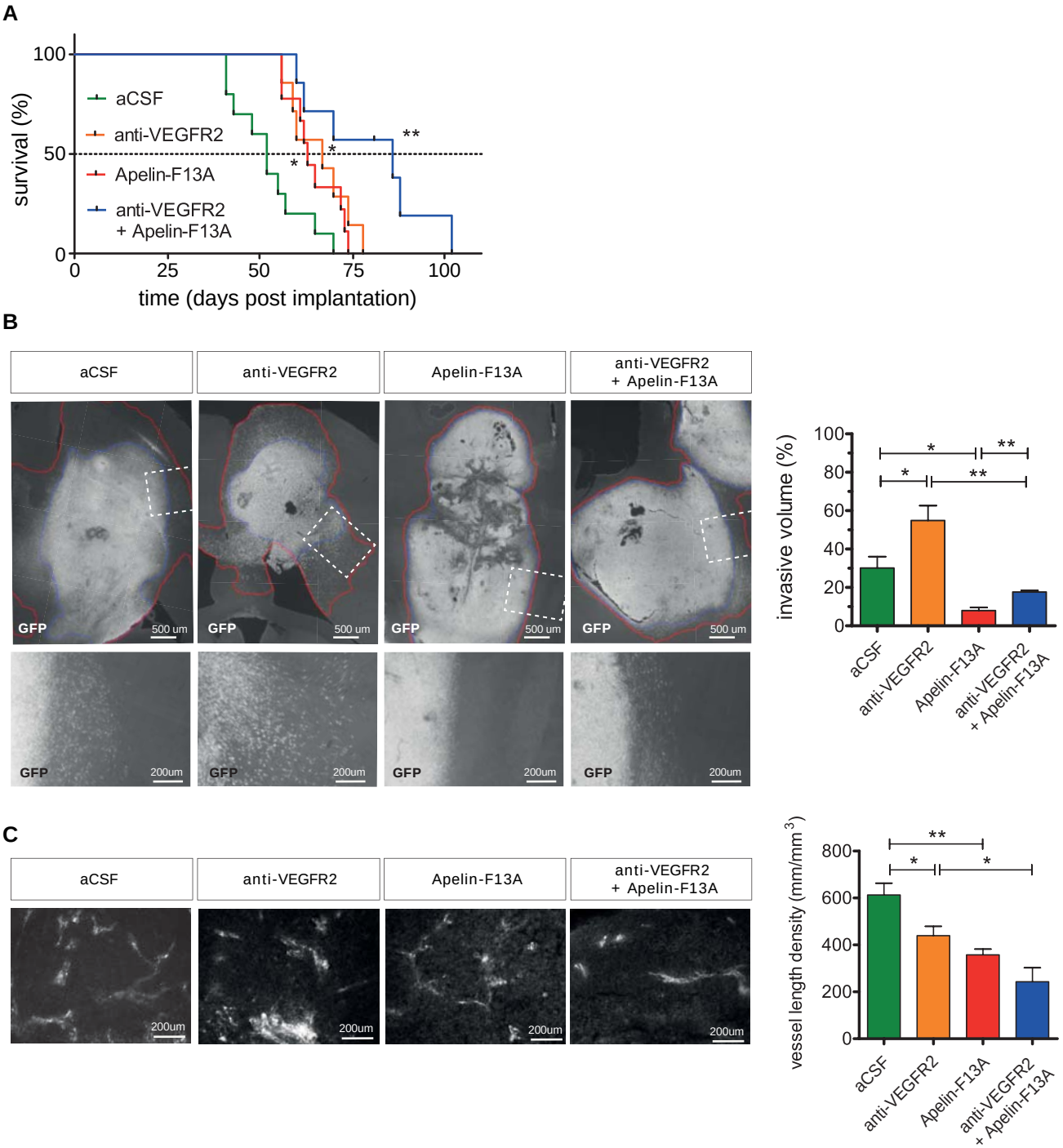
A
100
50
0
survival (%)
aCSF
anti-VEGFR2
Apelin-F13A
anti-VEGFR2
+ Apelin-F13A
*
*
**
0
25
50
75
100
time (days post implantation)
B
aCSF
anti-VEGFR2
Apelin-F13A
anti-VEGFR2
+ Apelin-F13A
GFP
500 um
200um
invasive volume (%)
100
80
60
40
20
0
*
**
*
**
aCSF
anti-VEGFR2
Apelin-F13A
anti-VEGFR2
+ Apelin-F13A
C
aCSF
anti-VEGFR2
Apelin-F13A
anti-VEGFR2
+ Apelin-F13A
200um
vessel length density (mm/mm3)
800
600
400
200
0
**
*
*
aCSF
anti-VEGFR2
Apelin-F13A
anti-VEGFR2
+ Apelin-F13A

Figure 7.

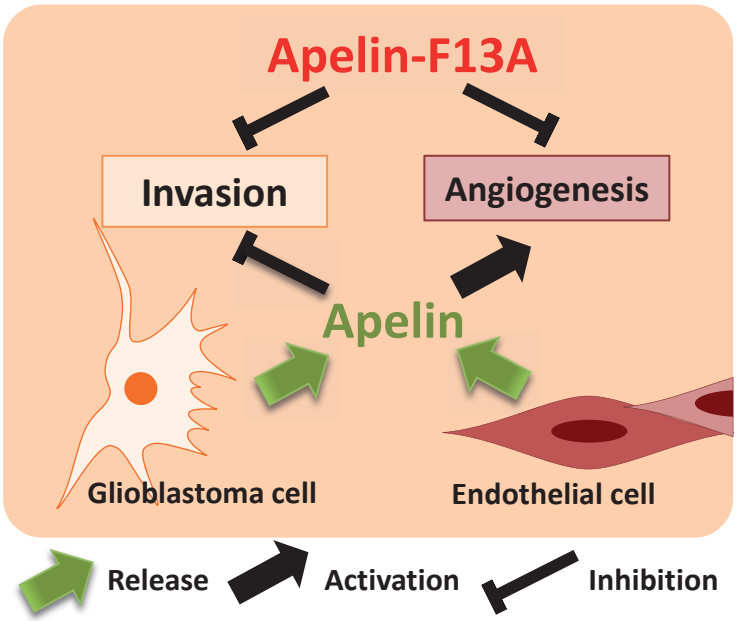
Apelin-F13A
Invasion
Angiogenesis
Apelin
Glioblastoma cell
Endothelial cell
Release
Activation
Inhibition

Table S1: ***APLN*** **co-expressed genes are enriched for angiogenesis in human GBM of the proneural and classical subtype**

Enriched in GBMs of proneural subtype

Gene Ontology Group ID	Description	GeneRatio	BgRatio	pvalue	p.adjust	qvalue	geneID	Count
GO:0001525	angiogenesis	34/310	411/16536	3,67E-13	1,26E-09	1E-09	ADAM8/ADM/ANGPTL4/APOH/AQP1/CAV1/CCL2/CHI3L1/COL4A1/COL4A2/CYR61/ENPEP/F3/HAND2/HMOX1/HOXA5/HOXA7/IL1A/IL1B/MEOX2/MMP19/NR2E1/NRCAM/PLAU/PLXDC1/RAMP1/SCG2/SEMA3E/SPINK5/SRPX2/TGFBI/UTS2/**VEGFA**/WNT7A	34
GO:0050900	leukocyte migration	30/310	342/16536	2,19E-12	3,75E-09	3E-09	ADAM8/BMP5/CAV1/CCL18/CCL2/CCR5/CD44/CXCL14/HCK/HMOX1/HOXA7/HRH1/IL1B/IL33/LGALS3/MMP9/P2RY12/PADI2/PTPRO/S100A8/S100A9/SAA1/SCG2/SLC16A3/SLC7A7/SPP1/TLR2/TREM1/VCAM1/**VEGFA**	30
GO:0048514	blood vessel morphogenesis	35/310	489/16536	1,04E-11	1,19E-08	9,6E-09	ADAM8/ADM/ANGPTL4/APOH/AQP1/CAV1/CCL2/CHI3L1/COL4A1/COL4A2/CYR61/ENPEP/F3/HAND2/HMOX1/HOXA5/HOXA7/IL1A/IL1B/MEOX2/MMP19/NR2E1/NRCAM/NTRK2/PLAU/PLXDC1/RAMP1/SCG2/SEMA3E/SPINK5/SRPX2/TGFBI/UTS2/**VEGFA**/WNT7A	35
GO:0097305	response to alcohol	28/310	324/16536	1,76E-11	1,51E-08	1,2E-08	ANXA1/AQP1/CA3/CA9/CCL2/CCR5/CD14/CDKN1A/CNR1/EGFR/F3/FOXA1/GJB2/IL1B/MAOB/MLC1/MSTN/NEFL/S100A8/S100A9/SERPINA7/SLC6A4/SOCS3/SPP1/SSTR1/TYR/UTS2/WNT7A	28
GO:0031099	regeneration	19/310	170/16536	4,76E-10	3,26E-07	2,6E-07	ADM/AFP/ANXA1/APOH/CAV1/CCL2/CDKN1A/CHL1/GATM/HOPX/MATN2/MSTN/NEFL/NNMT/OMG/PLAU/SOCS3/SPP1/WNT7A	19
GO:0048545	response to steroid hormone	27/310	406/16536	1,32E-08	7,53E-06	6,1E-06	ADM/ANXA1/AQP1/CA9/CAV1/CCL2/CDKN1A/EGFR/F3/FOXA1/GJB2/HMOX1/IL1B/LOX/MAOB/MSTN/NCF2/NEFL/NR0B1/NR2E1/SERPINA7/SLC6A4/SOCS3/SPP1/SSTR1/UTS2/WNT7A	27
GO:0045765	regulation of angiogenesis	18/310	196/16536	3,14E-08	1,27E-05	1E-05	ADM/ANGPTL4/APOH/AQP1/CCL2/CHI3L1/COL4A2/F3/HMOX1/HOXA5/IL1A/IL1B/NR2E1/SEMA3E/SPINK5/SRPX2/UTS2/**VEGFA**	18
GO:0050663	cytokine secretion	16/310	154/16536	3,29E-08	1,27E-05	1E-05	ANXA1/CAMP/CD14/CHI3L1/CLEC4E/CLEC5A/GBP1/GBP5/IL1A/IL33/NLRC4/SAA1/SRGN/TLR2/TNFRSF4/TREM1	16
GO:0030595	leukocyte chemotaxis	17/310	175/16536	3,33E-08	1,27E-05	1E-05	ADAM8/CCL18/CCL2/CCR5/CXCL14/HRH1/IL1B/LGALS3/PADI2/PTPRO/S100A8/S100A9/SAA1/SCG2/SPP1/TREM1/**VEGFA**	17
GO:0097530	granulocyte migration	13/310	103/16536	6,49E-08	2,07E-05	1,7E-05	ADAM8/CCL18/CCL2/HRH1/IL1B/LGALS3/S100A8/S100A9/SAA1/SCG2/SPP1/TREM1/**VEGFA**	13

Enriched in GBMs of classical subtype

Gene Ontology Group ID	Description	GeneRatio	BgRatio	pvalue	p.adjust	qvalue	geneID	Count
GO:0001525	angiogenesis	16/113	411/16536	1,94E-08	3,68E-05	3,2E-05	ADM/ANGPTL4/APOH/CD34/COL4A1/COL4A2/ENPEP/F3/**FLT1**/PF4/PITX2/PLXDC1/SPINK5/UTS2/**VEGFA**/WNT7A	16
GO:0048514	blood vessel morphogenesis	17/113	489/16536	3,54E-08	3,68E-05	3,2E-05	ADM/ANGPTL4/APOH/CD34/COL4A1/COL4A2/ENPEP/F3/**FLT1**/NTRK2/PF4/PITX2/PLXDC1/SPINK5/UTS2/**VEGFA**/WNT7A	17
GO:0045765	regulation of angiogenesis	11/113	196/16536	9,94E-08	6,89E-05	6E-05	ADM/ANGPTL4/APOH/CD34/COL4A2/F3/**FLT1**/PF4/SPINK5/UTS2/**VEGFA**	11
GO:1901342	regulation of vasculature development	11/113	212/16536	2,2E-07	0,000114	9,9E-05	ADM/ANGPTL4/APOH/CD34/COL4A2/F3/**FLT1**/PF4/SPINK5/UTS2/**VEGFA**	11
GO:0030198	extracellular matrix organization	13/113	385/16536	2,26E-06	0,000806	0,0007	COL4A1/COL4A2/FGB/HAPLN1/IBSP/ITGA1/LAMA2/LOX/MMP9/NCAN/NID2/SPINK5/VIT	13
GO:0043062	extracellular structure organization	13/113	386/16536	2,33E-06	0,000806	0,0007	COL4A1/COL4A2/FGB/HAPLN1/IBSP/ITGA1/LAMA2/LOX/MMP9/NCAN/NID2/SPINK5/VIT	13
GO:0010951	negative regulation of endopeptidase activity	10/113	237/16536	5,17E-06	0,001536	0,00133	DPEP1/LXN/MMP9/SERPINA6/SERPINA7/SERPINB3/SPINK5/SPOCK1/TFPI2/**VEGFA**	10
GO:0010466	negative regulation of peptidase activity	10/113	248/16536	7,71E-06	0,002004	0,00174	DPEP1/LXN/MMP9/SERPINA6/SERPINA7/SERPINB3/SPINK5/SPOCK1/TFPI2/**VEGFA**	10

Enriched in GBMs of mesenchymal subtype

Gene Ontology Group ID	Description	GeneRatio	BgRatio	pvalue	p.adjust	qvalue	geneID	Count
GO:1903531	negative regulation of secretion by cell	14/165	165/16536	1,09E-09	2,96E-06	2,4E-06	ABCC8/CD34/GBP1/IL11/IL1B/IL33/MAOB/NMB/NPY1R/P2RY1/P2RY12/TRH/UTS2/VSNL1	14
GO:0051048	negative regulation of secretion	14/165	188/16536	5,98E-09	8,1E-06	6,6E-06	ABCC8/CD34/GBP1/IL11/IL1B/IL33/MAOB/NMB/NPY1R/P2RY1/P2RY12/TRH/UTS2/VSNL1	14
GO:0010721	negative regulation of cell development	15/165	260/16536	5,26E-08	4,35E-05	3,6E-05	BDNF/BMP5/FOXA1/FOXA2/FRZB/GBP1/ID4/IL1B/KLK8/LTF/OLIG2/OMG/PI16/PTPRO/SEMA3A	15
GO:0010817	regulation of hormone levels	20/165	478/16536	6,43E-08	4,35E-05	3,6E-05	ABCC8/ADH4/ALDH1A3/APLN/BMP5/CHST9/CYP26A1/FOXA1/FOXA2/GALR1/IL11/IL1B/NMB/NPY1R/P2RY1/RDH10/TRH/UGT2B11/UTS2/VSNL1	20
GO:0048592	eye morphogenesis	11/165	145/16536	2,23E-07	0,000121	9,9E-05	ALDH1A3/BDNF/CALB1/CNGA3/CRB1/EFEMP1/EPHB1/MEGF11/NTRK2/PITX2/**VEGFA**	11
GO:0051051	negative regulation of transport	18/165	444/16536	4,87E-07	0,00022	0,00018	ABCC8/ACTN2/CD34/GBP1/IL11/IL1B/IL33/MAOB/NMB/NPY1R/P2RY1/P2RY12/SFRP4/SLN/SPINK1/TRH/UTS2/VSNL1	18
GO:0090596	sensory organ morphogenesis	13/165	254/16536	1,63E-06	0,000632	0,00052	ALDH1A3/BDNF/CALB1/CNGA3/CRB1/EFEMP1/EPHB1/FRZB/MEGF11/NTRK2/PITX2/TMIE/**VEGFA**	13
GO:0046689	response to mercury ion	4/165	12/16536	4,45E-06	0,001371	0,00112	AQP1/AQP9/GATM/PGAM2	4
GO:0007193	adenylate cyclase-inhibiting G-protein coupled receptor signaling pathway	7/165	67/16536	4,56E-06	0,001371	0,00112	ADCY8/GRM3/MCHR1/NPY1R/P2RY1/P2RY12/RGS1	7
GO:0046888	negative regulation of hormone secretion	7/165	71/16536	6,74E-06	0,001748	0,00143	ABCC8/IL11/IL1B/NMB/NPY1R/UTS2/VSNL1	7

APLN co-regulated genes from the adult TCGA-GBM dataset seperated by GBM genetic subtype (proneural, classical and mesenchymal) were obtained on GlioVis based on data of the Agilent-4502A platform and expressed as gene ontology enrichment groups (10 most significant biologcial process subgroups are shown). p and q value cut off are 0,05. The vascular endothelial growth factor receptor- 1 (VEGFR1: FLT1) and its ligand VEGFA are marked in bold.

Fig. S1

A

proneural

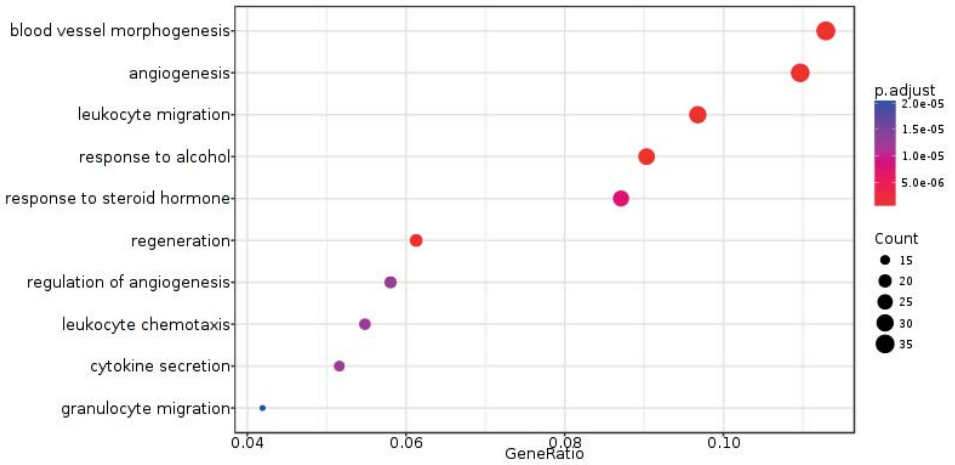

classical

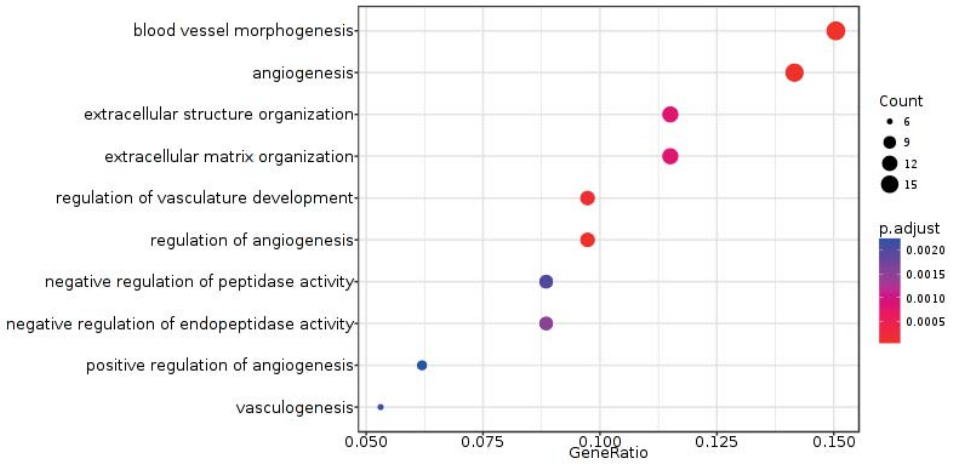

mesenchymal

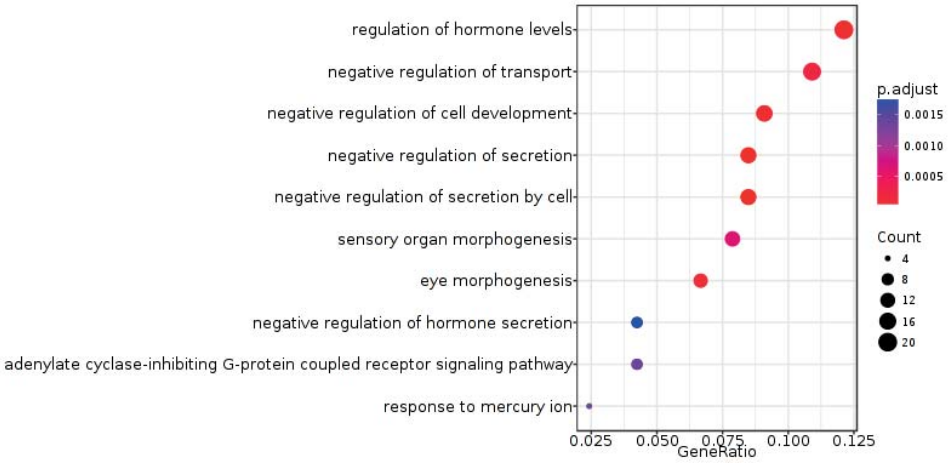

Fig. S1

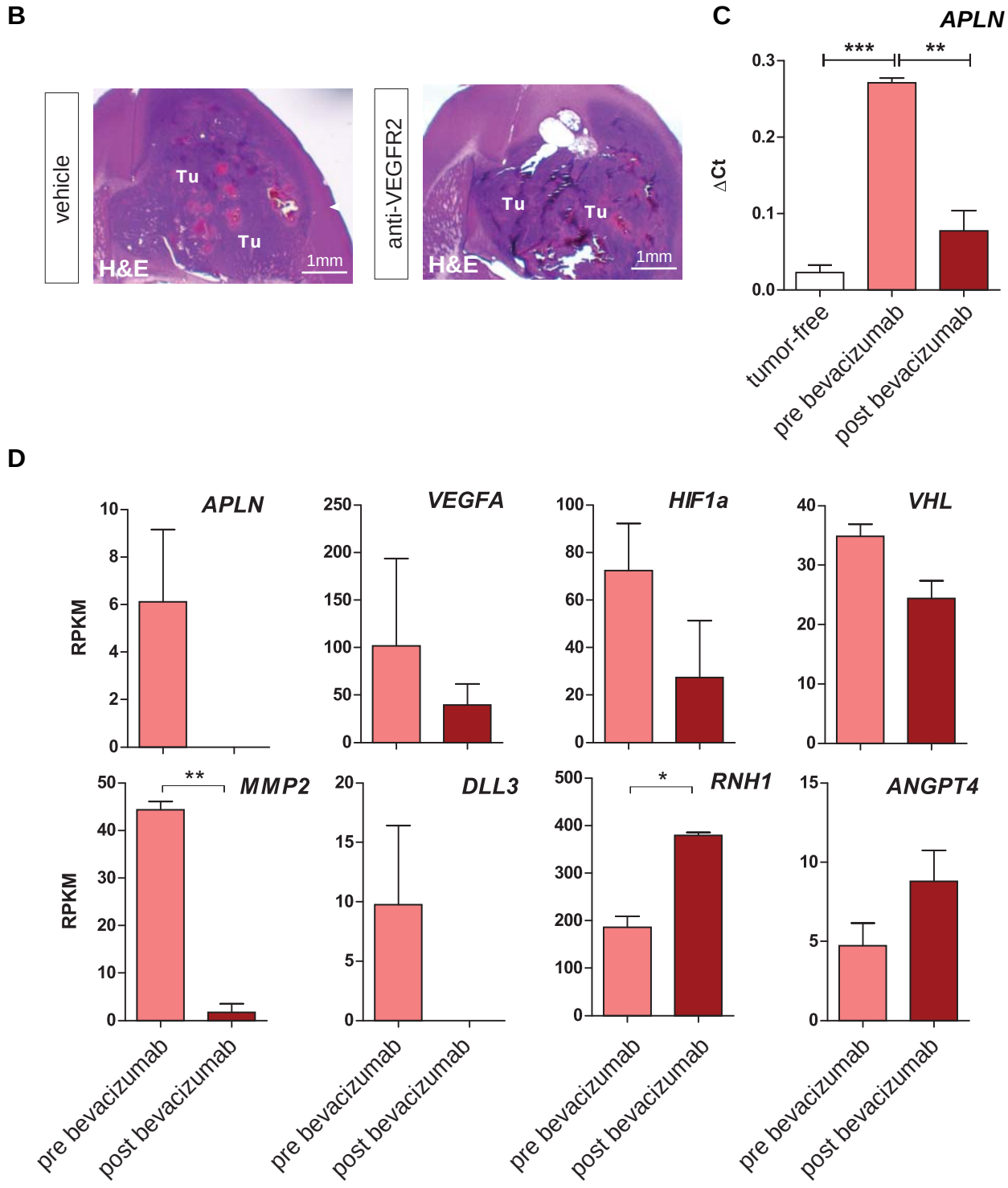
B
vehicle
Tu
Tu
H&E
1mm
anti-VEGFR2
Tu
Tu
H&E
1mm
C
APLN
***
**
ΔCt
0.3
0.2
0.1
0.0
tumor-free
pre bevacizumab
post bevacizumab
D
APLN
VEGFA
HIF1a
VHL
RPKM
MMP2
DLL3
RNH1
ANGPT4
**
*
pre bevacizumab
post bevacizumab

Fig S2.

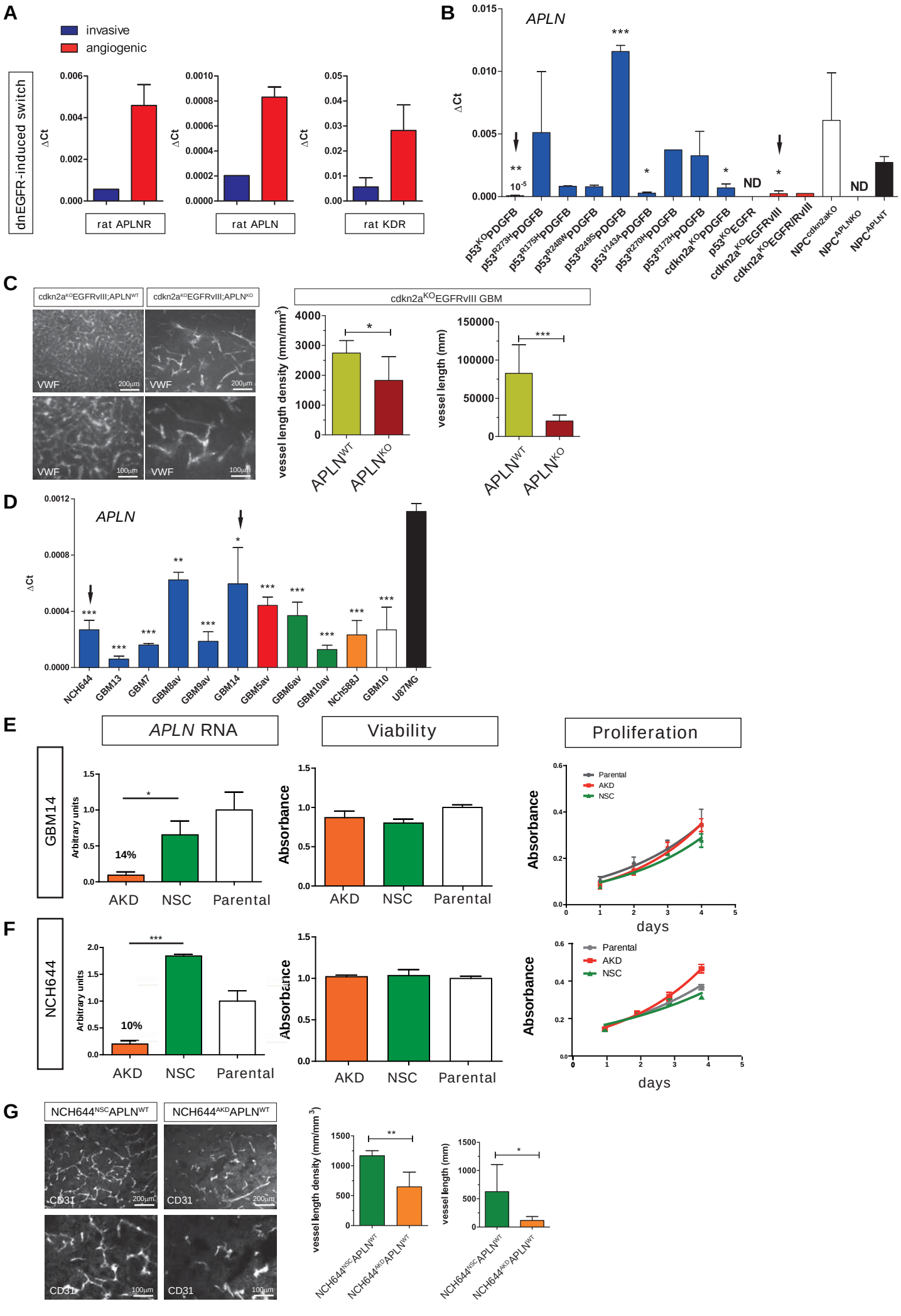
A
invasive
angiogenic
dnEGFR-induced switch
ΔCt
rat APLNR
rat APLN
rat KDR
B
APLN
ΔCt
p53KOPDGFB
p53R273HPDGFB
p53R175HPDGFB
p53R248WPDGFB
p53R249SPDGFB
p53V143APDGFB
p53R270HPDGFB
p53R172HPDGFB
cdkn2aKOPDGFB
p53KOEGFR
cdkn2aKOEGFRvIII
cdkn2aKOEGFR/RvIII
NPCcdkn2aKO
NPCAPLNKO
NPCAPLNT
ND
C
cdkn2aKOEGFRvIII;APLNWT
cdkn2aKOEGFRvIII;APLNKO
cdkn2aKOEGFRvIII GBM
VWF
vessel length density (mm/mm3)
vessel length (mm)
APLNWT
APLNKO
D
APLN
ΔCt
NCH644
GBM13
GBM7
GBM8av
GBM9av
GBM14
GBM5av
GBM6av
GBM10av
NCh588J
GBM10
U87MG
E
APLN RNA
Viability
Proliferation
GBM14
Arbitrary units
14%
AKD
NSC
Parental
Absorbance
days
F
NCH644
10%
G
NCH644NSCAPLNWT
NCH644AKDAPLNWT
CD31
vessel length density (mm/mm 3)
vessel length (mm)

Fig S2

H

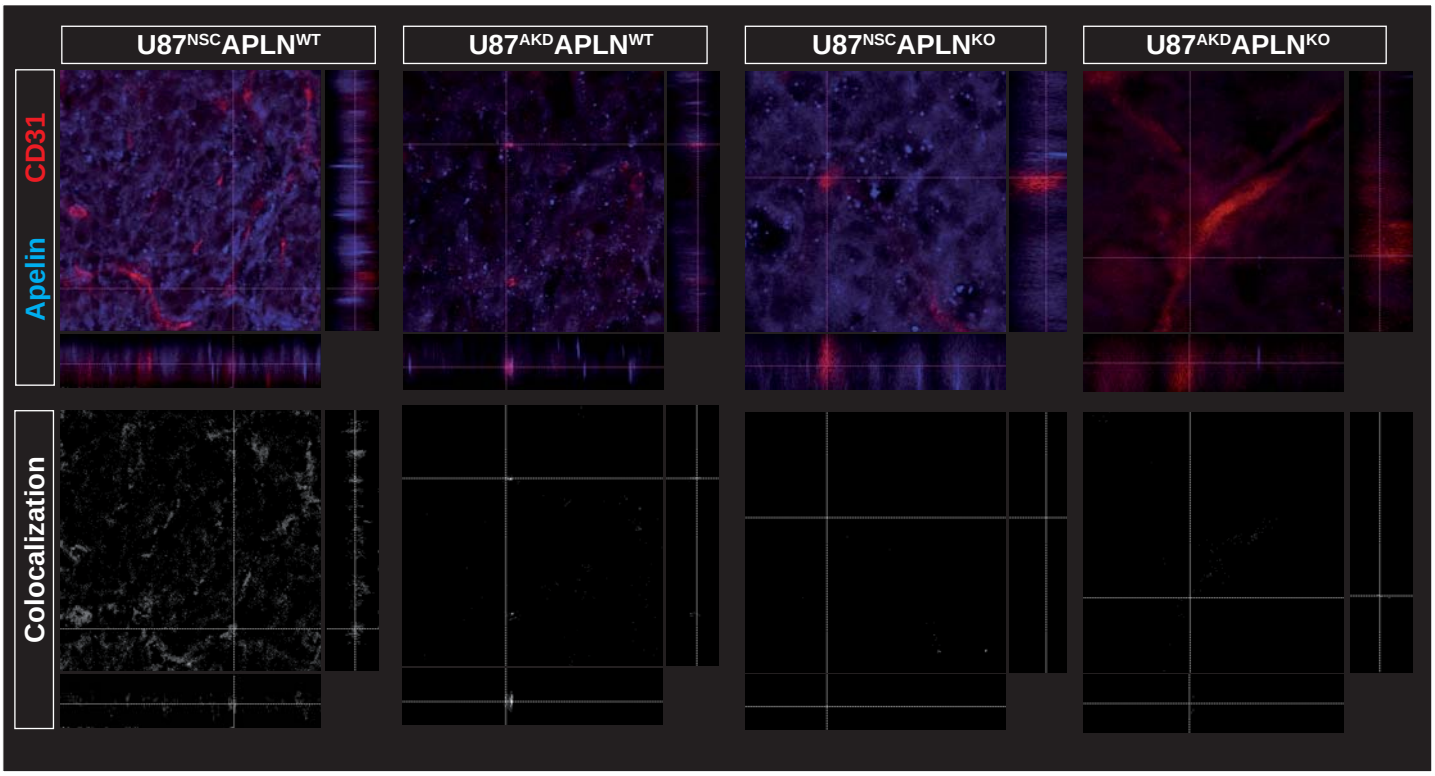
U87NSCAPLNWT
U87AKDAPLNWT
U87NSCAPLNKO
U87AKDAPLNKO
Apelin
CD31
Colocalization

Fig. S3

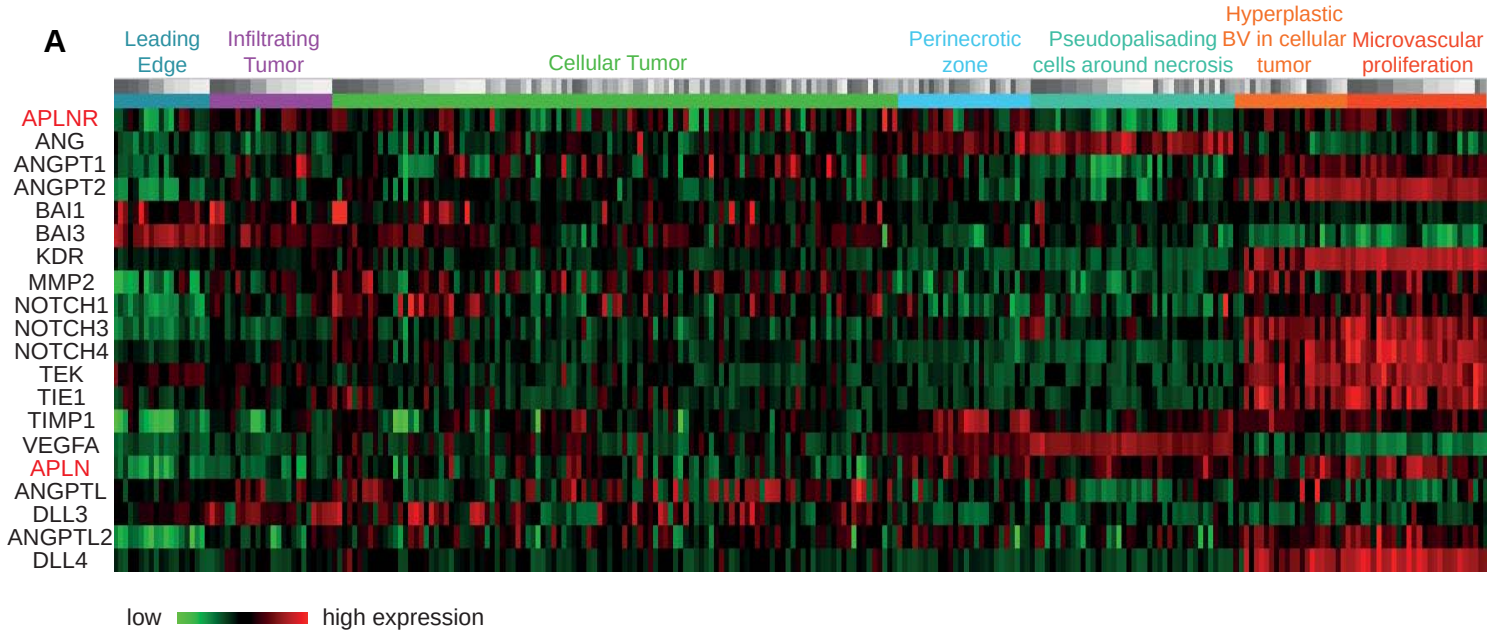
A
Leading Edge
Infiltrating Tumor
Cellular Tumor
Perinecrotic zone
Pseudopalisading cells around necrosis
Hyperplastic BV in cellular tumor
Microvascular proliferation
APLNR
ANG
ANGPT1
ANGPT2
BAI1
BAI3
KDR
MMP2
NOTCH1
NOTCH3
NOTCH4
TEK
TIE1
TIMP1
VEGFA
APLN
ANGPTL
DLL3
ANGPTL2
DLL4
low
high expression

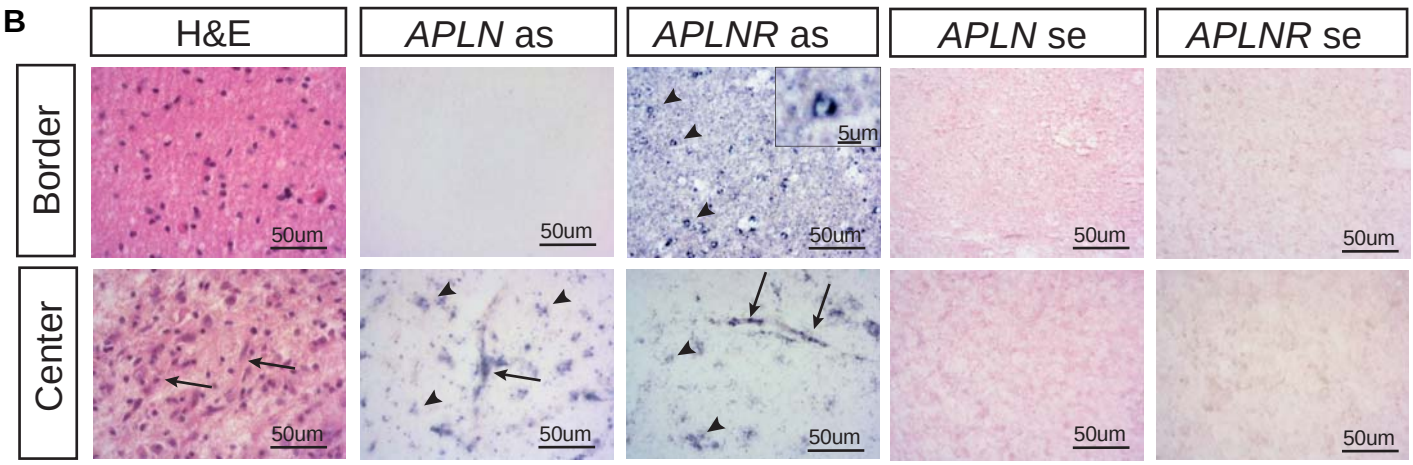
B
H&E
APLN as
APLNR as
APLN se
APLNR se
Border
Center
50um
5um

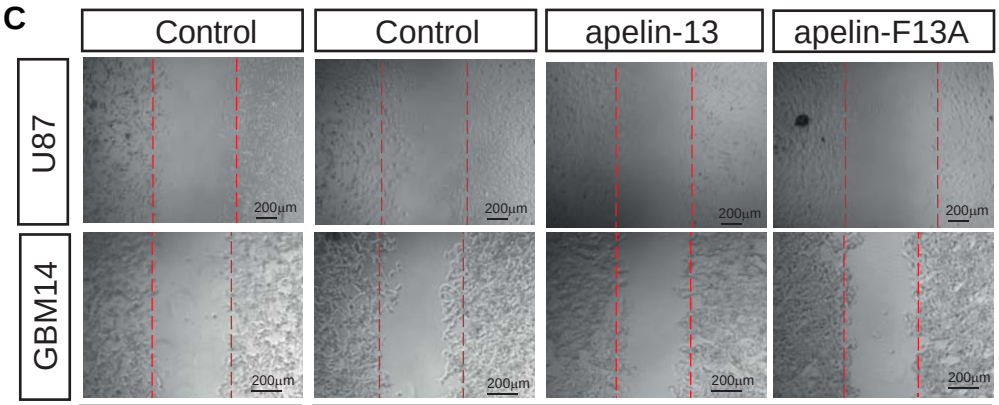
C
Control
Control
apelin-13
apelin-F13A
U87
GBM14
200μm
NSC
AKD

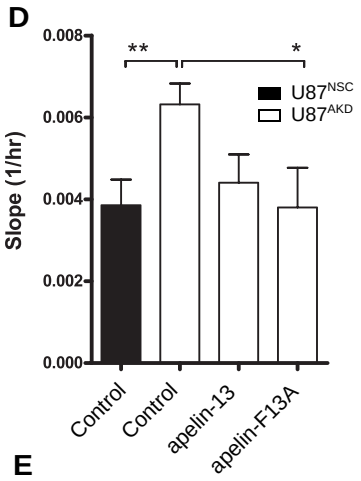
D
Slope (1/hr)
U87NSC
U87AKD
Control
Control
apelin-13
apelin-F13A

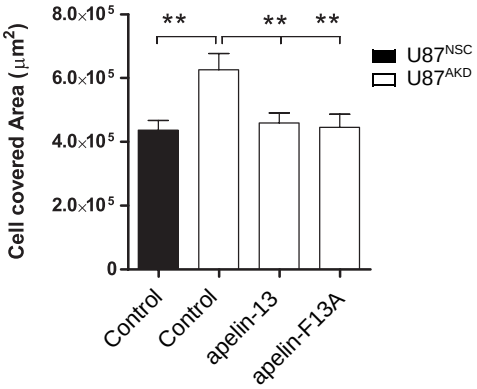
Cell covered Area (μm2)
U87NSC
U87AKD
Control
Control
apelin-13
apelin-F13A

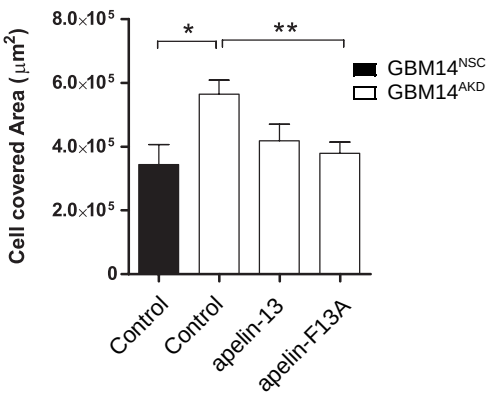
Cell covered Area (μm2)
GBM14NSC
GBM14AKD
Control
Control
apelin-13
apelin-F13A

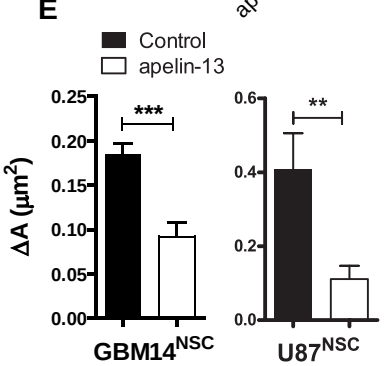
E
Control
apelin-13
ΔA (μm2)
GBM14NSC
U87NSC

Fig. S4

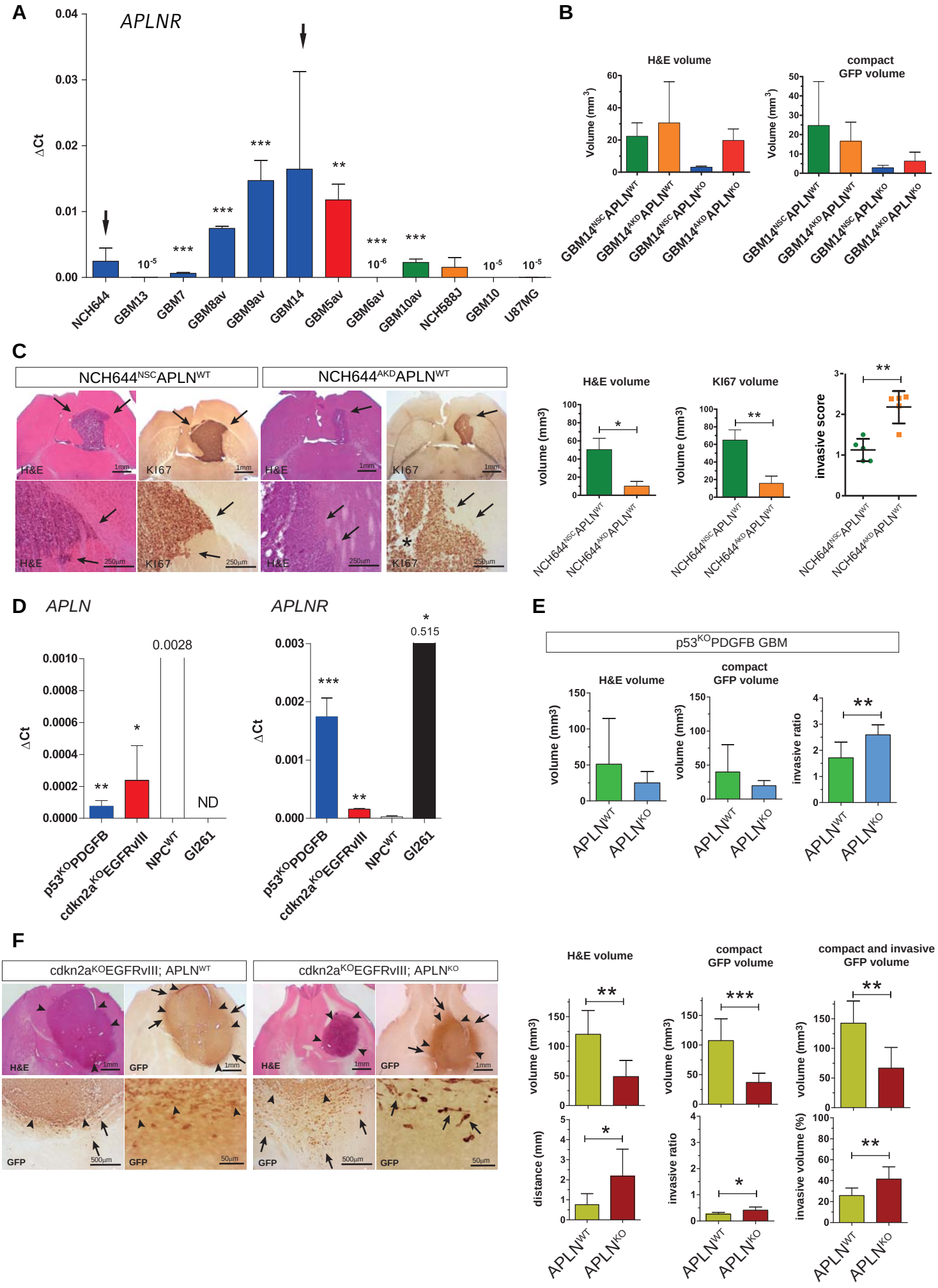
A
APLNR
ΔCt
NCH644
GBM13
GBM7
GBM8av
GBM9av
GBM14
GBM5av
GBM6av
GBM10av
NCH588J
GBM10
U87MG
B
H&E volume
compact GFP volume
Volume (mm3)
GBM14NSCAPLNWT
GBM14AKDAPLNWT
GBM14NSCAPLNKO
GBM14AKDAPLNKO
C
NCH644NSCAPLNWT
NCH644AKDAPLNWT
H&E
KI67
H&E volume
KI67 volume
volume (mm3)
invasive score
D
APLN
APLNR
ΔCt
p53KOPDGFB
cdkn2aKOEGFRvIII
NPCWT
GI261
ND
E
p53KOPDGFB GBM
H&E volume
compact GFP volume
invasive ratio
APLNWT
APLNKO
F
cdkn2aKOEGFRvIII; APLNWT
cdkn2aKOEGFRvIII; APLNKO
H&E
GFP
compact GFP volume
compact and invasive GFP volume
distance (mm)
invasive volume (%)

Fig S4

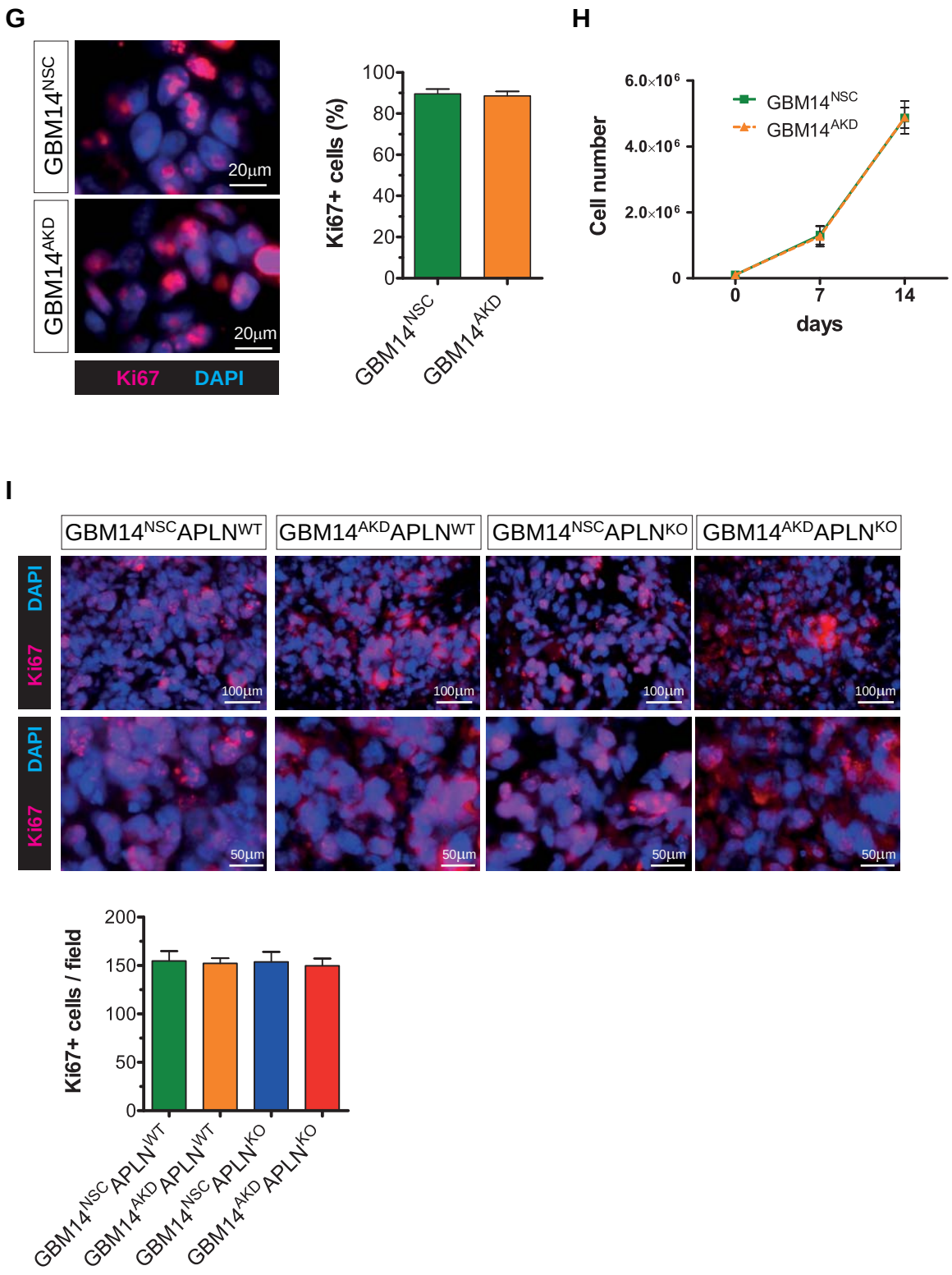
G
GBM14NSC
GBM14AKD
20μm
20μm
Ki67 DAPI
Ki67+ cells (%)
100
80
60
40
20
0
GBM14NSC
GBM14AKD
H
Cell number
6.0×10⁶
4.0×10⁶
2.0×10⁶
0
GBM14NSC
GBM14AKD
0
7
14
days
I
GBM14NSCAPLNWT
GBM14AKDAPLNWT
GBM14NSCAPLNKO
GBM14AKDAPLNKO
DAPI
Ki67
100μm
50μm
Ki67+ cells / field
200
150
100
50
0
GBM14NSCAPLNWT
GBM14AKDAPLNWT
GBM14NSCAPLNKO
GBM14AKDAPLNKO

Fig S4

J

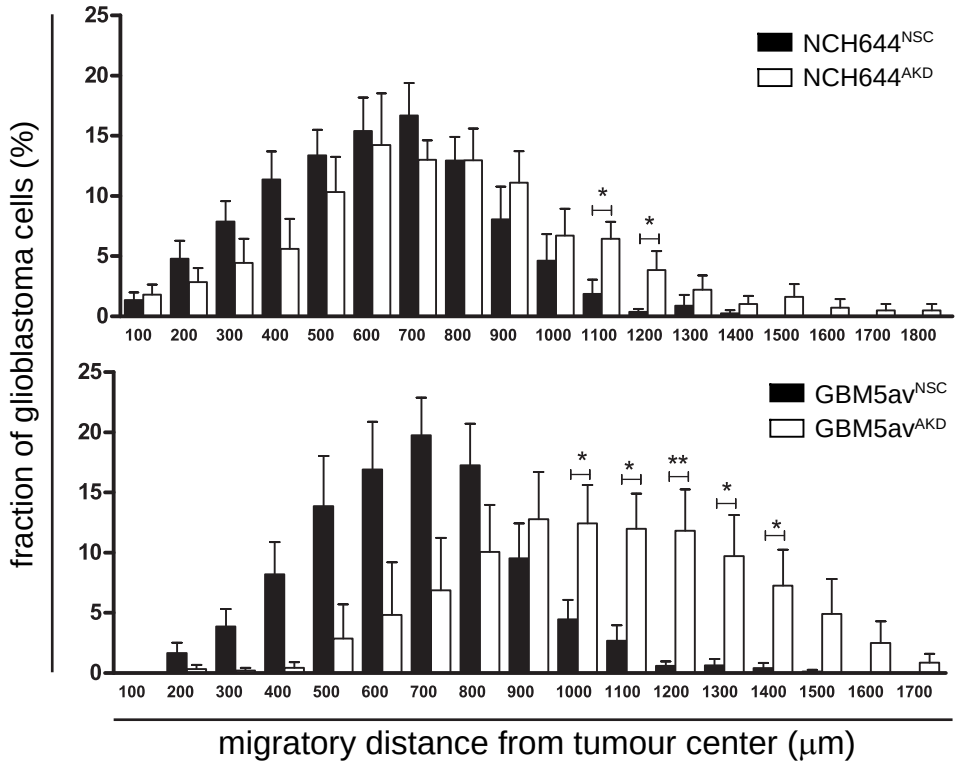
NCH644NSC
NCH644AKD
GBM5avNSC
GBM5avAKD
fraction of glioblastoma cells (%)
migratory distance from tumour center (μm)

K

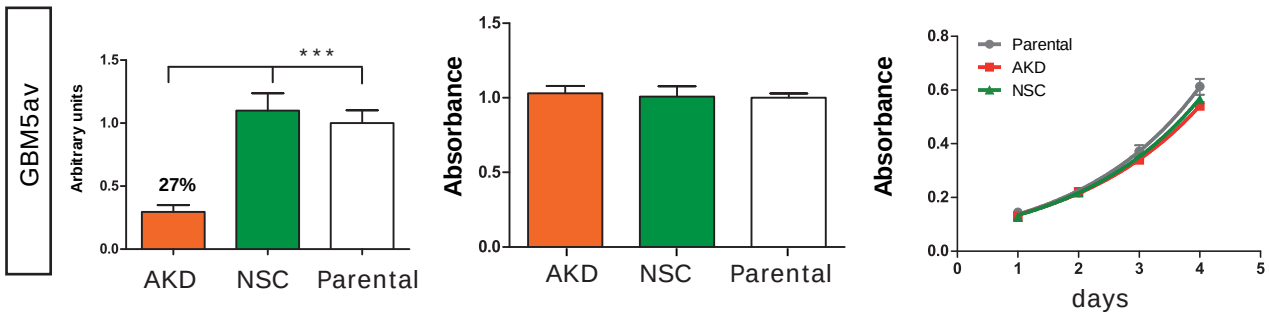
GBM5av
Arbitrary units
27%
AKD
NSC
Parental
Absorbance
Parental
AKD
NSC
days

Fig. S5

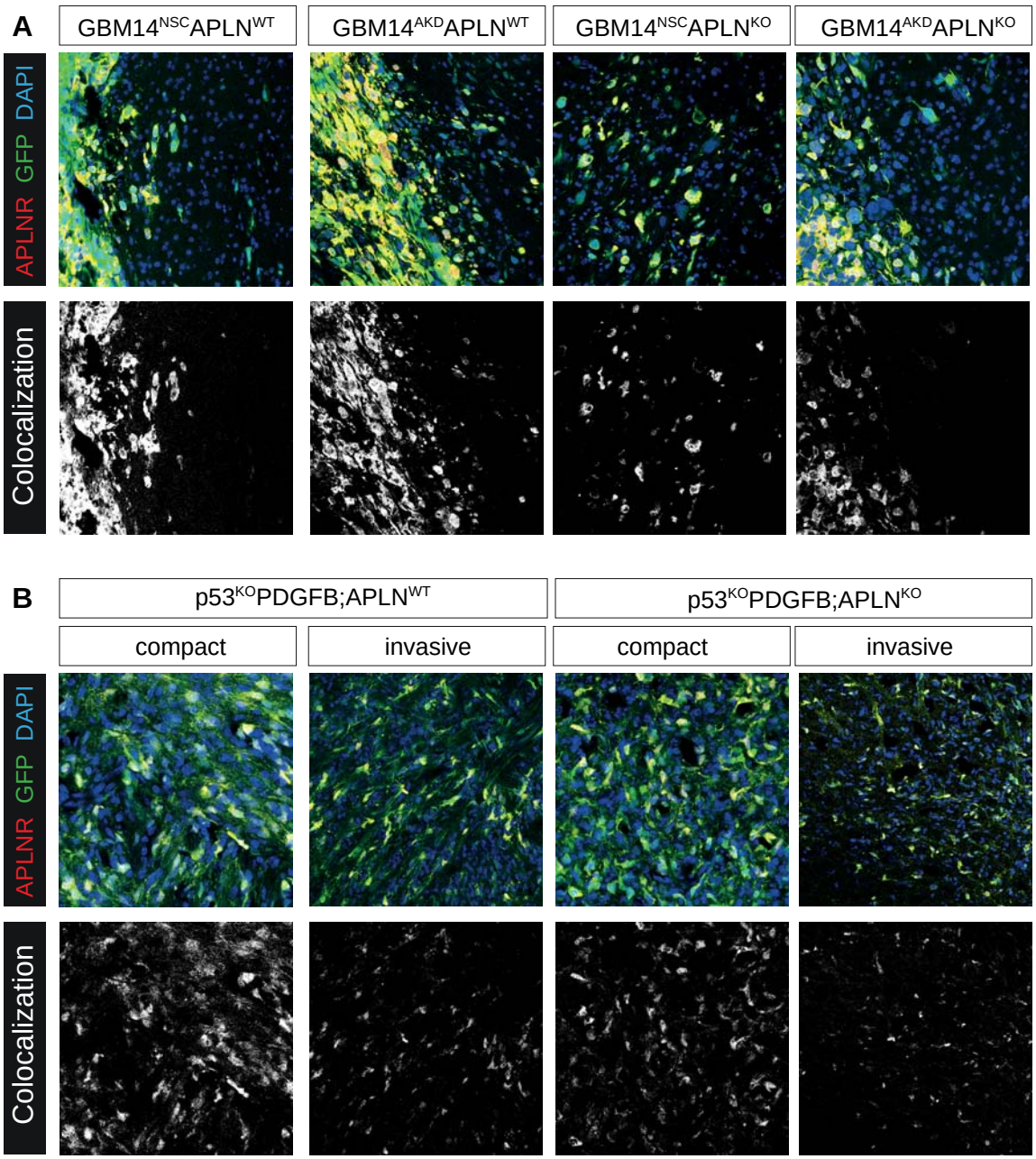
A
GBM14NSCAPLNWT
GBM14AKDAPLNWT
GBM14NSCAPLNKO
GBM14AKDAPLNKO
APLNR GFP DAPI
Colocalization
B
p53KOPDGFB;APLNWT
p53KOPDGFB;APLNKO
compact
invasive
compact
invasive
APLNR GFP DAPI
Colocalization

Fig. S5

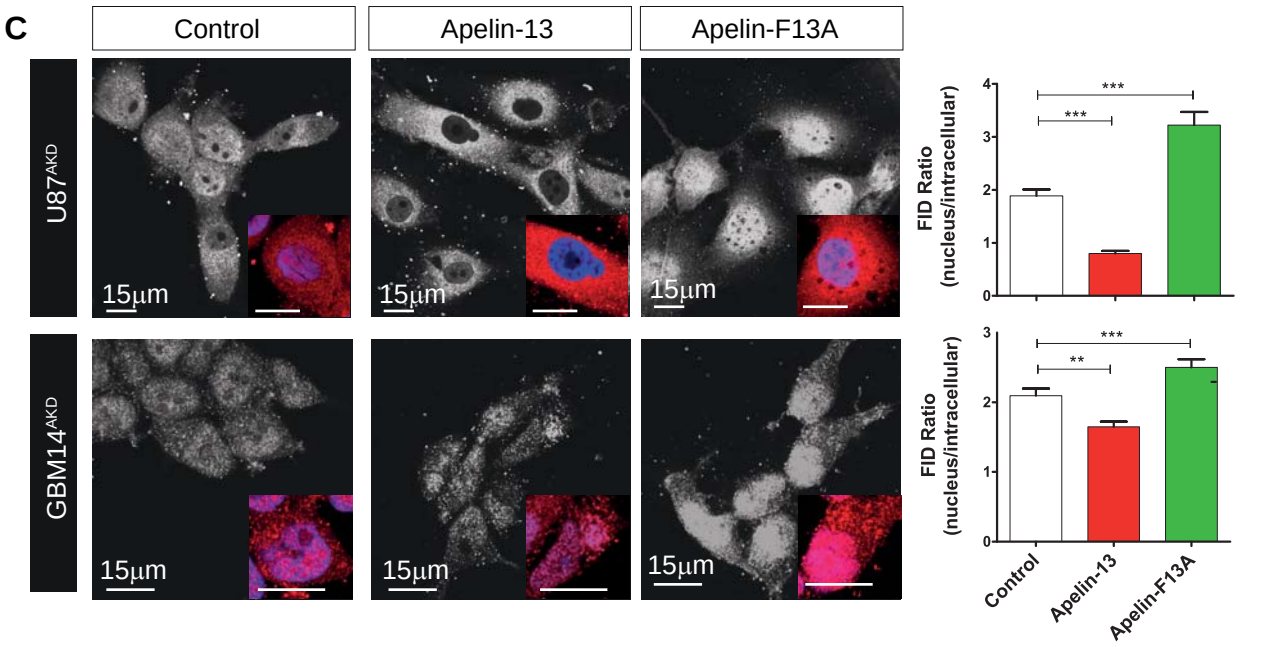
C
Control
Apelin-13
Apelin-F13A
U87AKD
GBM14AKD
15µm
FID Ratio (nucleus/intracellular)
***
**
Control
Apelin-13
Apelin-F13A

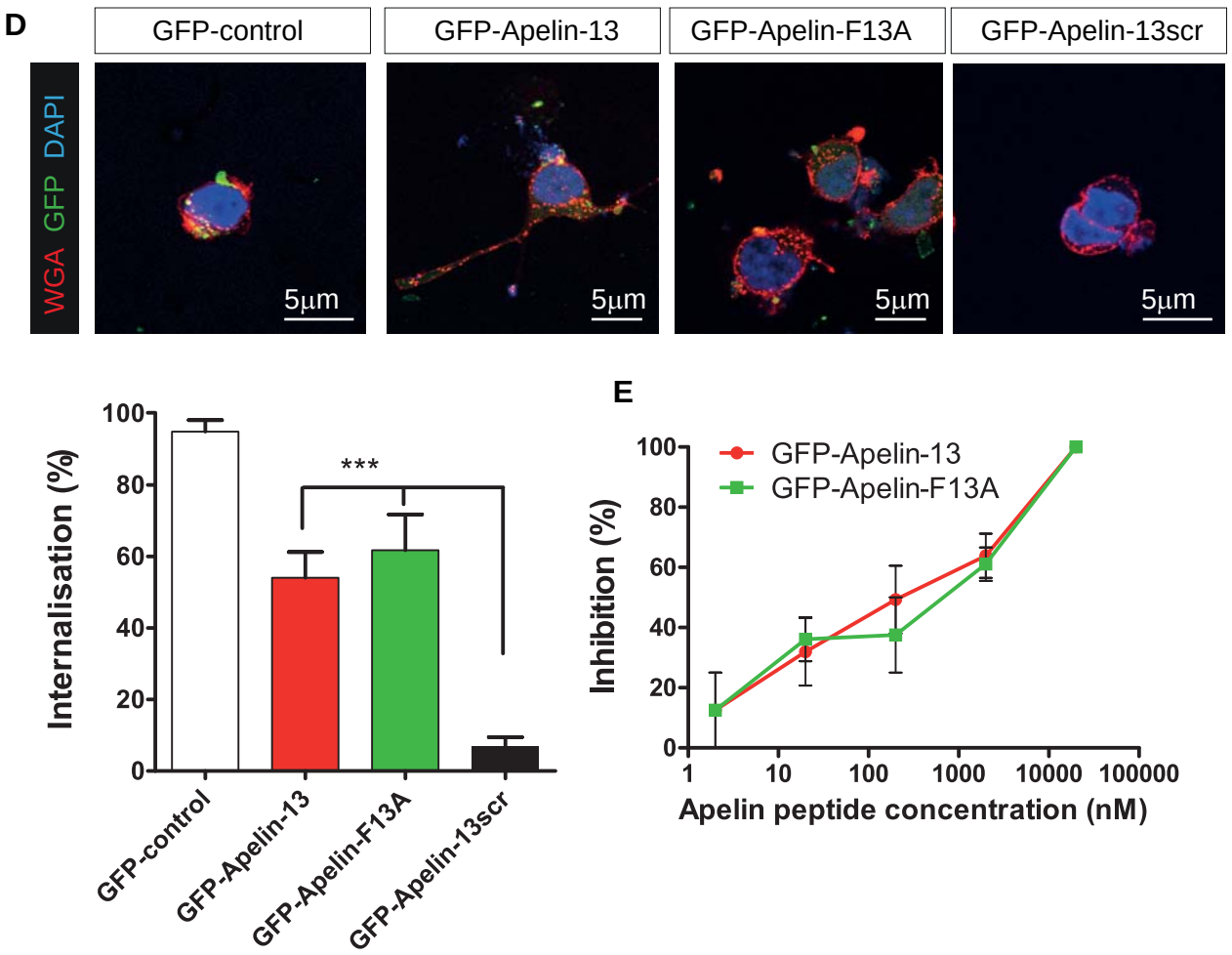
D
GFP-control
GFP-Apelin-13
GFP-Apelin-F13A
GFP-Apelin-13scr
WGA GFP DAPI
5µm
Internalisation (%)
***
GFP-control
GFP-Apelin-13
GFP-Apelin-F13A
GFP-Apelin-13scr
E
GFP-Apelin-13
GFP-Apelin-F13A
Inhibition (%)
Apelin peptide concentration (nM)

Fig. S5

F

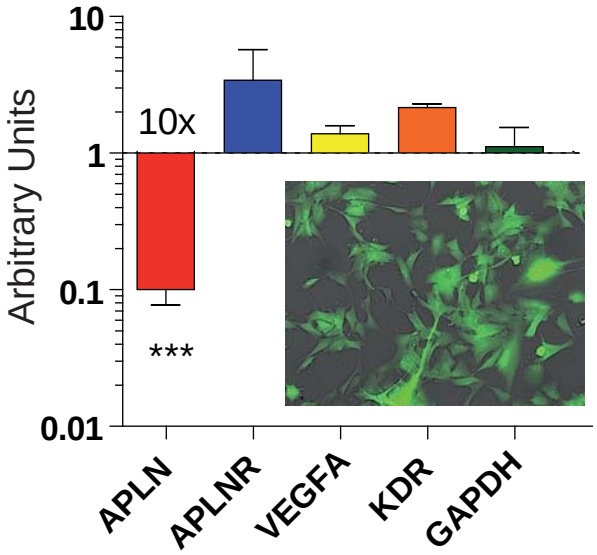

Title: APLN/APLNR-targeting improves anti-angiogenic efficiency and blunts pro-invasive side effects of VEGFA/VEGFR2-blockade in glioblastoma

Running title: APLNR/VEGFA co-targeting inhibits glioblastoma angiogenesis and invasion

Giorgia Mastrella[1*], Mengzhuo Hou[1*], Min Li[1*], Veit Stöcklein[2], , Nina Zdouc[1], Marie N. M. Volmar[1], Hrvoje Miletic[3,4], Sören Reinhard[5], Christel Herold-Mende[6], Susanne Kleber[7], Katharina Eisenhut[1], Gaetano Gargiulo[8], Michael Synowitz[9], Angelo L. Vescovi[10], Patrick Harter[11], Josef M. Penninger[12], Ernst Wagner[5], Michel Mittelbronn[13], Rolf Bjerkvig[4], Dolores Hambardzumyan[14], Ulrich Schüller[15], Jörg-Christian Tonn[2], Josefine Radke[16] , Rainer Glass[1,17] and Roland E. Kälin[18,1,+]

Affiliations:

[1]Neurosurgical Research, Department of Neurosurgery, University Hospital, LMU Munich, Germany;

[18]Walter Brendel Center of Experimental Medicine, Faculty of Medicine, LMU Munich, Germany;

+corresponding author. Tel: +49 89 4400 731 48, Fax:+49 89 4400 777 89, roland.kaelin@med.lmu.de

Supplementary data:

Supplemental Table S1. *APLN* co-expressed genes are enriched for angiogenesis in human glioblastoma of the proneural and classical subtypes

Supplementary Figure S1.

Apelin expression is correlated with angiogenesis in human glioblastoma of the proneural and classical subtypes and is reduced by anti-angiogenic therapy with bevacizumab. **A,** Dot blot representation of *APLN* co-regulated gene clusters. *APLN*-coregulated genes from the adult glioblastoma TCGA data set were obtained by the GlioVis platform and separated according to glioblastoma subtype. The most enriched gene ontology groups with the highest gene count and p-values based on *APLN* co-expression are primarily involved in angiogenesis and blood vessel morphology in the proneural and classical subtype. In the mesenchymal subtype, *APLN* expression is correlated with more general biological functions such as GPCR signaling, regulation of protein transport, and secretion. **B,** H&E overview of *p53*^{KO}PDGFB glioblastomas treated with anti-VEGFR2 antibody (DC101; Ely Lilly) or aCSF. Both groups (n= 7 or 10) grew large proneural glioblastomas. **C, D** Apelin expression is reduced in biopsies of a glioblastoma taken from patient treated with bevacizumab. **C,** A biopsy was taken before bevacizumab treatment and after tumor recurrence, and fresh frozen tissues were subjected to qPCR. Although apelin expression was elevated in tumor tissue compared with tumor-free brain tissue, apelin expression was significantly reduced in tumor samples obtained after treatment. Apelin expression was measured in at least two samples per condition and normalized for GAPDH. **D**, Apelin expression levels analysed by RNAseq from patients shown in Fig. 1D, E before and after bevacizumab treatment decreased to levels not detectable post-treatment. While the hypoxia markers VEGFA, HIF1a and VHL were unchanged, angiogenesis markers like MMP2 and DLL3 were reduced. Increase of gene expression was detectable for certain genes like RNH1 and ANPT4. Values are reported as the mean ± SEM and Student's *t* test was used to determine statistical significance. *p<0.05, **p<0.005, ***p<0.0005.

Supplementary Figure S2.

Glioblastoma cell- and host-derived apelin controls tumor angiogenesis. **A**, Apelin and APLNR are upregulated in the tumor microenvironment upon the angiogenic switch in a serial implantation model. Lentiviral overexpression of dominant negative EGFR (EGFR-CD533) in patient-derived glioblastoma (patient 8) induces angiogenic growth of the tumor (1). The expression of rat apelin, APLNR and KDR increase following the angiogenic switch from invasive to angiogenic xenografts. Two invasive and two angiogenic xenografts were used. The low apelin and APLNR RNA levels could only be detected in one of the invasive control glioblastoma. **B**, The apelin levels vary considerably between different murine transgenic GSC cultures carrying driver mutations that are representative for different human glioblastoma subtypes. Apelin expression levels in all mouse GSCs was quantified by qPCR, which showed variable expression levels in proneural-like (blue) and classical-like (red) glioblastoma subtypes compared with wiltdtype neural precursor cells NPC^{WT}. Arrows indicate GSCs selected for *in vivo* experiments. Apelin mRNA was not detected in $APLN^{KO}$ mice (ND, not detected). **C,** glioblastoma from $cdkn2a^{KO}$EGFRvIII GSCs were grown in wildtype or $APLN^{KO}$ mice and vessel density was assessed by vWF immunostaining. The VLD and VL of $cdkn2a^{KO}$EGFRvIII glioblastoma were greater in wildtype mice (n = 7) and were significantly reduced in $APLN^{KO}$ mice (n = 8). **D,** Apelin expression was determined by qPCR using patient-derived GSCs from WHO grade IV glioblastoma of the proneural (blue), classical (red), mesenchymal (green) or recurrent (orange) subtypes. GSCs with variable apelin expression levels were selected for further experiments (arrows). Samples were subjected to qPCR and compared with U87MG cells in more than three independent experiments. **E** and **F,** Stable *APLN* knockdown does not affect glioblastoma cell behaviour *in vitro*. Lentiviral transduction of GBM14 (**E**) and NCH644 (**F**) parental cells reached 100%,

as indicated by lentiviral GFP (see inset in Supplementary Fig. S5). Transduction leads to shRNAmir-mediated stable *APLN* depletion by 90% and 86% (as analyzed by qPCR) in the respective *APLN*^{KD} cells and is specific (see Supplementary Fig. S5). Cell viability and *in vitro* proliferation of all GSCs was not affected. Data were obtained from more than three independent experiments. Values are reported as the mean ± SD and Student's *t* test was used to determine statistical significance. *p<0.05, **p<0.005, ***p<0.0005 versus parental cells. **G**, Apelin controls tumor angiogenesis in glioblastoma. Patient-derived GSCs were implanted into immunodeficient mice. Immunostaining for CD31 was performed and the microvasculature in the GFP-positive tumor area was analyzed by stereomorphology. The VLD and VL were significantly reduced in NCH44^{AKD} glioblastoma as compared with NCH44^{NSC} glioblastoma grown in wildtype mice (n = 6 and 8, respectively). Values are reported as the mean ± SEM and Student's *t* test was used to determine statistical significance. *p<0.05, **p<0.005, ***p<0.0005. **H**, apelin is expressed in tumor vessels of *APLN*^{WT} but not *APLN*^{KO} mice. Confocal image stacks of 28 days post implantation U87 xenografts co-immunostained for CD31 positive vessels and apelin were taken. Colocalization image is obtained by RG2B Colocalzation plugin for ImageJ. Apelin protein can be observed throughout the tumor (blue) but is decreased in xenografts in U87^{AKD} tumor cells compared to U87^{NSC}. CD31 positive vessels and apelin immunostaining is colocalised in xenografts obtained from U87^{NSC} and U87^{AKD} cells in APLN^{WT} mice but not in APLN^{KO} mice. Note that in U87^{NSC}APLN^{KO} tumors apelin immunostaining is not detected. All pictures were obtained at the confocal microscope with HyD2 detector with identical laser settings.

Supplementary Figure S3.

APLNR expression is upregulated in the infiltrating tumor zone in glioblastoma. **A**, IVY Glioblastoma Atlas Project RNAseq dataset comparison of angiogenesis-related genes in relation to *APLN* and *APLNR*. *APLN* is co-expressed with endothelial markers (*KDR*, *TEK*, and *TIE1*) in the region of microvascular proliferation, and with angiogenic factors like *VEGFA* and *ANGPT1* in the avascular hypoxic tumor region. By contrast, *APLNR* is co-expressed with vascular markers (*KDR*, *TEK*, and *TIE1*) in microvascular regions of the tumor and in the tumor periphery, where infiltrating tumor cells also express genes involved in cell invasion (*MMP2* expression is high; *TIMP1,* an enzymatic inhibitor of *MMP2,* is low; *BAI1/3* is high). The gradient from green over black to red represents the RNAseq expression level of the gene from low towards normal towards high expression. Data source: http://glioblastoma.alleninstitute.org/rnaseq/searches?%7B%22exact_match%22%3Afalse%2C%22search_term%22%3A%22vegf%22%2C%22search_type%22%3A%22gene%22%2C%22features%22%3A%5B%5D%2C%22tumors%22%3A%5B%5D%2C%22page_num%22%3A0%7D

B, *In situ* hybridization of apelin and APLNR mRNA was performed on glioblastoma sections from the tumor center or border, and compared with H&E staining. In the tumor center, both apelin and APLNR can be detected in vascular proliferations (arrows). In addition, APLNR is visible in tumor cells (arrowheads, and magnified inset) at the center and border, while apelin expression is only present in tumor cells located in the center (arrowheads; as: antisense probe; se: sense probe). **C**, **D**, U87MG and GBM14 cells were tested in migration assays. **C**, in a wound healing assay $U87^{AKD}$ and $GBM14^{AKD}$ cells were compared to $U87^{NSC}$ and $GBM14^{NSC}$ control cells. Both cell types showed a significant increase in cell covered array upon apelin knockdown. The addition of apelin-13 or apelin-F13A lead to decreased invasion with

the effect of apelin-F13A being significant in both cell types. Data are obtained from three to 5 independent experiments performed in triplicates. Values are reported as the mean ± SEM and Student's t test was used to determine statistical significance. *p<0.05, **p<0.005, ***p<0.0005. **D**, In a real-time xCelligence chemotaxis assay, both $U87^{AKD}$ and $GBM14^{AKD}$ cells, showed increased migration in response to fetal calf serum containing medium compared to $U87^{NSC}$ or $GBM14^{NSC}$ controls, respectively. Addition of apelin-13 or apelin-F13A peptides reduced migration to the level observed in the respective NSC control cells. Note that the effect conferred by apelin-F13A was significant. Data are obtained from three independent experiments. Values are reported as the mean ± SD and Student's *t* test was used to determine statistical significance. *p<0.05, **p<0.005, ***p<0.0005. **E**, Application of 200 nM of apelin-13 attenuated *in vitro* cell invasion of $GBM14^{NSC}$ and $U87^{NSC}$ significantly. Data are obtained from at least 13 different spheres from three independent experiments per condition analysed at day 7 and reported as the mean ± SEM and Student's t test was used to determine statistical significance. *p<0.05, **p<0.005, ***p<0.0005...

Supplementary Figure S4.

Anti-invasive role of apelin in orthotopic models of proneural glioblastoma. . **A,** APLNR expression varies between glioblastoma cells of different genetic subtypes qPCR of APLNR on patient-derived GSCs from WHO grade IV glioblastoma of proneural (blue), classical (red), mesenchymal (green), or recurrent (orange) subtypes. Arrows indicate the cells used for implantation. Data from more than three independent experiments are shown. Values are reported as the mean ± SD and Student's *t* test was used to determine statistical significance. *p<0.05, **p<0.005, ***p<0.0005 versus U87MG. **B,** GBM14 xenografts were analyzed by H&E and GFP staining. Compact volume was measured on GFP- or H&E-stained sections in addition to the overall GFP volume shown in Fig. 4A, **C,** $NCH644^{NSC}$ (n = 6) or $NCH644^{AKD}$ GSCs (n = 8) were grown in immunodeficient wildtype mice. Depletion of apelin expression in NCH644 cells attenuates tumor growth. Tumor volume was reduced when $NCH644^{AKD}$ xenografts were implanted into wildtype mice. To score invasiveness, tumor cells were visualized by KI67 immunostaining for proliferative tumor cells, and showed that $NCH644^{AKD}$ cells implanted in wildtype mice intermingle with healthy brain cells (asterisk), indicating the greater invasiveness of $NCH644^{AKD}$ cells. Because single invasive cells (arrows) are less frequently observed in NCH644 than in GBM14 xenografts, we assessed tumor invasiveness in a semi-quantitative manner, by scoring tumor sections from 0 to 3, where 0 is no histological sign of cell invasion from the tumor mass, 1 describes a larger, connected group of invading glioblastoma cells, 2 indicates smaller scattered groups of invading glioblastoma cells, and 3 indicates single scattered highly invasive glioblastoma cells, as seen in GBM14 tumors in Fig. 4A. The invasive score increased from 1.2 in $NCH644^{NSC}$ implanted into wildtype mice to 2.2 in $NCH644^{AKD}$ implanted into wildtype mice. **D,** Expression levels of apelin and APLNR mRNA were analyzed by qPCR in murine

GSCs and GL261 glioma cells, and were compared to isolated wildtype neural precursor cells NPC^{WT}. Apelin expression was low in *p53*^{KO}PDGFB GSCs and absent in GL261 cells. Apelin expression was relatively high in *cdkn2a*^{KO}EGFRvIII GSCs and highest in NPC^{WT}. By contrast, APLNR expression was highest in GL261 cells, high in *p53*^{KO}PDGFB GSCs, and lowest in *cdkn2a*^{KO}EGFRvIII GSCs and NPC^{WT}. Data are from more than three independent experiments. Values are reported as the mean ± SD and Student's *t* test was used to determine statistical significance. *p<0.05, **p<0.005, ***p<0.0005. **E**, *p53*^{KO}PDGFB GSCs as a model of proneural-like glioblastoma were implanted into in wildtype or *APLN*^{KO} mice and analyzed by H&E and GFP staining. The ratio of overall GFP tumor volume (shown in Fig. 4B) to compact volume (GFP or H&E) was determined. Although the tumor volume was unchanged in *APLN*^{KO} mice (n = 8) compared with that in wildtype mice (n = 7), the invasiveness assessed by invasive ratio was increased in *APLN*^{KO} mice. **F**, *cdkn2a*^{KO}EGFRvIII GSCs were implanted into wildtype or *APLN*^{KO} mice and H&E and GFP staining was performed to assess overall, compact, and invasive tumor volumes as well as the migration distance of single cells from the tumor mass. Arrowheads indicate the compact border and arrows indicate single invasive cells in all panels. The ratio of overall GFP tumor volume to compact volume (GFP or H&E) was determined and the invasive volume was calculated as the invasive volume as a percent of overall GFP volume. The distance of cells that had migrated away from the tumor increased from 0.8 in wildtype mice to 2.2 in *APLN*^{KO} mice, while the invasiveness ratio increased from 0.3 in wildtype mice to 0.4 in *APLN*^{KO}, and the invasive tumor volume as a percent of overall GFP volume increased from 26% in wildtype mice to 42% in *APLN*^{KO} mice. The overall glioblastoma volume (compact and invasive) decreased significantly, by 53%, from 143 mm^3 in wildtype mice to 68 mm^3 in *APLN*^{KO} mice. Results are shown for eight wildtype and seven *APLN*^{KO} mice.

G, GBM14 cell cultures were analysed by immunocytochemistry for Ki67 positivity. Cells were highly proliferative *in vitro* with 89.6% in GBM14^{NSC} control cells and 88.6% GBM14^{AKD} showing no significant difference. Percent of Ki67 positive DAPI stained nuclei were quantified at 40 × magnification from three independent experiments in triplicates. **H**, GBM14 spheroid cell growth was analysed by counting single cells every 7 days. No significant difference was observed between GBM14^{NSC} control and GBM14^{AKD} cells in 3 independent experiments. **I**, GBM14 tumors grown for weeks were used to analyse the *in vivo* proliferative index by Ki67 immunofluorescence. In all 3 experimental groups with *APLN*^{KD} and/or *APLN*^{KO} xenograft no significant difference in Ki67 positive tumour cell number was observed compared to control tumor with GBM14^{NSC} cells implanted in *APLN*^{WT} mice. Cell were counted at 40 × magnification in 4 different tumor fields on 2 different tumour levels per animal with n = 3 per group. **J**, Invasion of glioblastoma cells within organotypic brain slice cultures was measured representing the two glioblastoma subtypes, proneural (GBM14) and classical (GBM5av). The number of cells migrating a certain distance away from the injection site were determined as previously described (2,3). The migration distance at day 5 (GBM14) or day 7 GBM5av show that a significantly higher percentage of apelin depleted GBM^{AKD} cells in both glioblastoma subtypes reached higher migration distance compared to control GBM^{NSC} cells with migration radii > 900 μm. Experiments were performed in three independent experiments in duplicates. All above values are reported as the mean ± SEM and Student's *t* test was used to determine statistical significance. *p<0.05, **p<0.005, ***p<0.0005. **K**, Stable *APLN* knockdown does not affect GBM5av cell behaviour *in vitro*. Lentiviral transduction of parental cells leads to shRNAmir-mediated stable *APLN* depletion by 73% (as analyzed by qPCR) in the *APLN*^{KD} cells. Cell viability and *in vitro* proliferation was not affected. Data were obtained from more than three independent

experiments. Values are reported as the mean ± SD and Student's *t* test was used to determine statistical significance. *p<0.05, **p<0.005, ***p<0.0005 versus parental cells.

Supplementary Figure S5.

A, **B**, APLNR expression in invasive glioblastoma cells. Confocal images of 42 days post implantation patient derived GBM14 xenografts (**A**) or 21 days post implantation of murine p53KOPDGFB glioblastoma (**B**) co-immunostained for GFP-expressing tumor cells (green) and APLNR (red) were taken. Colocalization figures are obtained by RG2B Colocalization plugin for ImageJ. APLNR staining can be detected in nearly all invasive glioblastoma cells. **A**, manipulation of apelin expression in glioblastoma cells by depletion or in tumor microenvironment of the knockout mouse does not change APLNR expression in tumor cells. **B**, APLNR is expressed in most tumor cells independent of the apelin expression ($APLN^{WT}$ or $APLN^{KO}$ mouse) and their localization in the compact tumor or the invasive tumor front. **C**, APLNR internalization assay. $U87^{AKD}$ and $GBM14^{AKD}$ cells were treated with apelin peptides for 30 min and APLNR internalization was analysed by immunofluorescence. Confocal images were taken and analyzed for fluorescent intensity density (FID) calculating a ratio of the nuclear to cytoplasmic levels. Addition of peptides lead to incrased FID in cytoplasm for both petpides while the FID ratio show the significant redistribution of APLNR from nuclear to cytoplasmic region for apelin-13 and from cytoplasmic to nuclear localization for apelin-F13A. Data are obtained from three independent experiments. Values are reported from as the mean ± SEM and Student's t test was used to determine statistical significance. *$p<0.05$, **$p<0.005$, ***$p<0.0005$ **D,** Specific internalisation of apelin peptides by GBM14 cells. Confocal images of cell treated with 1 μM GFP-peptide were taken and GFP signal was compared to nuclear (DAPI) and membrane staining (weath germ agglutinin; WGA). Internalisation of GFP-peptides was assessed by counting the percent of cells with GFP positive vesicles in four independent experiments. GFP-apelin-13 and GFP-apelin-F13A were taken up specifically by more than 50% of the cells while

scrambled apelin-13scr was not. GFP-positive uptake control was taken up by all cells. **E,** Dose-response curve of the inhibition of peptide internalisation. GBM14 cells were pre-treated with escalating amounts of unlabelled apelin-13 or apelin-F13A peptide for 30 mins before GFP-linked apelin-13 or apelin-F13A (200 nM) were applied, respectively. Inhibition of internalisation by increasing concentrations (2, 20, 200, 2000 and 20000 nM) demonstrates the specificity of GFP-Apelin peptide internalisation. GFP-Scale bar, 15 mm; Student's t-test, *** $p \leq 0{,}005$. **F**, Apelin shRNAmir specifically depletes apelin expression. Lentiviral transduction of U87MG parental cells achieved penetration of 100%, as indicated by lentiviral GFP (see inset). Transduction leads to efficient knockdown by *APLN* shRNAmir- (10×) in $APLN^{KD}$ cells as compared with cells transduced with non-silencing control (NSC)-shRNAmir, while the expression levels of control genes was unaffected by *APLN* knockdown. Data are obtained from more than three independent experiments. Values are reported as the mean ± SD and Student's *t* test was used to determine statistical significance. *p<0.05, **p<0.005, ***p<0.0005.

Supplemental Methods:

Fluorescent immunocytochemistry

Cells were seeded at a concentration of 50,000 cells/well in an 8 well-plate (FALCON Culture Slides, REF354108, REF354118) previously coated with poly-D-lysine 50 µg/ml followed by laminin 5 µg/ml, and then incubated in DMEM containing 1x MEM non-essential amino acids (Cat. 11140-035), 5% penicillin-streptomycin and 10% FBS (Cat. 102270-106; all ThermoFisher Scientific) for 24 hours. Then culture medium was removed, and cells were washed with 1x PBS, fixed with 4% PFA at room temperature for 10 min, and washed with 1x PBS for three times. After permeabilization with the blocking solution (1x PBS containing 5% donkey serum and 0.3% Triton-X) for 1 hour at room temperature, cells were incubated overnight at 4°C with rabbit anti-MKi67 (1:200, Cat. ab16667 Abcam, Cambridge, UK) On the second day, cells were washed with 1x PBS and incubated for 2 hours at room temperature with the secondary antibodies donkey anti-rabbit AF594 (1:500, Cat. 711-585-152, all Jackson Immuno-Research). All antibodies were diluted in blocking solution. The coverslips were mounted with Dako Fluorescent Mounting Medium and pictures were taken by Axiovert25 microscope with Axiocam MRm and Axiovision Rel 4.8 software (Carl Zeiss).

Wound healing assay

U87 or GBM14 cells were seeded in 24-well plates at a density of 3 or 5 × 105 cells/well, respectively. After incubation for 24 hours, a scratch wound was created using a 1,000 µl (U87) or 200µl (GBM14) micropipette tip and cellular debris was removed. Then 200 nM apelin-13 or apelin-F13A was added. Pictures were taken with an Axiovert25 microscope with Axiocam MRm and Axiovision Rel 4.8 software

(Carl Zeiss) and zero and after 10 h (U87) or 24 h (GBM14). The cell covered area was mesured by ImageJ software.

Chemotaxis assay:

In vivo migration assay was performed using the xCelligence RTCA DP system (ACEA Biosciences San Diego, CA, USA)(4) following the manufacturers protocol. Brief, 16 well Cell Invasion & Migration-Plate (CIM-Plate 16) were used. The lower reservoir was filled with DMEM only or supplemented with either FCS, 200nM or apelin-13 peptides (pyroglutamylated-Apelin-13; Cat. H-4568; or (Ala13)apelin-13; Cat. H-6308; all Bachem, Bubendorf, Switzerland). This assembly was incubated for 1 hour at 37°C, 5% CO2 and control impendence was measured. U87 cells (2 × 104 cells) were seeded and impendence was measured every 15 minutes for 36 h. Slope (1/h) represents migration through the chamber.

Gene expression analysis of bevacizumab treated glioblastoma samples

RNAseq of patient matched FFPE-biopsies (Edinger Institute, Frankfurt am Main) before and after bevacizumab therapy was performed by Massive Analysis of cDNA Ends (MACE; GenXpro, Frankfurt am Main) and results for individual genes are shown as reads per kilobase per million (RPKM). Values are reported as the mean ± SEM and Student's t test was used to determine statistical significance. *p<0.05, **p<0.005, ***p<0.0005.

Preparation of ex vivo glioma in organotypic brain slice cultures:

Organotypic brain slice cultures were prepared as described previously (2,3). In brief, OBSCs were made from 6 day old mouse pups under sterile conditions. After

decapitation, the brains were removed. Whole brain hemispheres were cut into 350 µm thick slices using a with a vibratome (Leica VT1200S; Leica Co., Heidelberg, Germany) and transferred to 0.4 µm to a Transwell insert (PICM03050, Millipore) in 6-well plate containing 1 ml of culture medium (25% Hanks balanced salt solution, 44.75% Minimum Essential Medium, 25% heat inactivated horse serum, 200 mM glutamine, 6.5 mg/ml glucose) per well. The slice cultures were kept at 35oC in a humidified atmosphere (5% CO2). After 24 h, 5,000 GFP-positive glioblastoma cells (NCH644, GBM14, GBM5av) within a 0,5µl culture mediium were inoculated into the slices using a 1µl syringe mounted to a micromanipulator. The tip of the syringe was placed at the same defined region on the slice surface. The fluorescent glioma cells were inoculated below the corpus callosum into the globus pallidus. Using the micromanipulator an injection canal was formed. The cell suspension was slowly injected over 30s. Directly after injection the glioma cells remained at the inoculation site, which can therefore mark the point of origin for all further movements of these cells. Fluorescence microscopy images were produced the following days to measure the area of the different tumors produced day 0 (immediately after injection) at day 5 and day 7 by Axiovert25 microscope with Axiocam MRm and Axiovision Rel 4.8 software (Carl Zeiss). Images were analysed as described in (2,3)using Fiji.

APLNR internalisation assay

Cell were seeded at a concentration of 50000 cells/well in a 24 well plate, on round coverslips previously coated with poly-D-lysin 50 µm/ml (U87 cells) or poly-d-lysin 50 µm/ml followed by laminin 50 µm/ml (GBM14 cells). Cell were seeded in full DMEM or DMEM without supplements, and DMEM F12 without supplements, respectively. The treatment was performed by adding apelin-13 at or apelin-F13A 200 nM for 30 mins. After fixation with 4% PFA cells were incubated for 20 min with 1:200 wheat

germ agglutinin (WGA-AF594) to label intracellular membranes. After blocking for 1 h at room temperature in 1 × PBS containing 5% donkey serum and 0,3% Triton-X cells were incubated overnight at 4°C with rabbit anti-APLNR 1:100. On the second day, cells were washed with 1 × PBS and incubated for 3 h at room temperature with donkey anti-rabbit biotinylated 1:250, then for 1h at room temperature with the tertiary antibody Alexa Fluor® 488, 594, or 647 conjugated streptavidin. For nuclear staining To-Pro™-3 Iodide 1:1000 or DAPI 1:1000 was used.. All antibodies were diluted in blocking solution. The coverslips were mounted with Dako Fluorescent Mounting Medium and pictures were taken at the confocal microscope at Leica SP5 inverted confocal with the LAS AF software. . Confocal image z-stacks were taken and fluorescent intensity density (FID) was quantified by ImageJ at a z-plane crossing the nucleus to obtain a ratio of the nuclear normalized on the average of three cytoplasmic regions of interest (ROI). Confocal pictures were taken at equal laser intensity. Data are obtained from more than 20 cells analysed from three independent experiments.

Specific GFP-apelin internalisation

The internalisation was performed on GBM14 GSCs. The cells were plated at a density of 10.000 cells/well on a glass coverslip previously coated with poly-D-lysin 50 µg/ml followed by laminin 50 µg/ml. The day after, the medium was replaced with 200 µl of fresh medium and the N-terminally GFP-conjugated Apelin-13, Apelin-F13A, Apelin-13scr (containing the scrambled amino acid sequence of Apelin-13) or GFP-linked oligomer 728 were added to the cells for 120 min at 37 °C. For the competition experiment, 1 µM unlabelled apelin-13 or apelin-F13A was added to the GBM14 cells 30 mins prior to the addition 200 nM GFP-apelin-13 or GFP-apelin-F13A, respectively. After that, cells were fixed for 30 mins with 4% PFA and

incubated for 10 mins at room temperature with WGA-594 1:200 and DAPI 1:1000 diluted in 1 × PBS washed and mounted on a glass slide with Dako Fluorescent Mounting Medium. The pictures were taken at the Leica SP8X WLL upright confocal microscope or at the Leica SP5 inverted confocal microscope, with the LAS X software, and analysed with ImageJ. For the quantification of the GFP-positive cells, 6 pictures per condition were used, and for each picture the data were measured as number of GFP-positive cells on the total number of cells.

Literature:

1. Talasila KM, Soentgerath A, Euskirchen P, Rosland GV, Wang J, Huszthy PC, *et al.* EGFR wild-type amplification and activation promote invasion and development of glioblastoma independent of angiogenesis. Acta Neuropathol **2013**;125:683-98
2. Markovic DS, Glass R, Synowitz M, Rooijen N, Kettenmann H. Microglia stimulate the invasiveness of glioma cells by increasing the activity of metalloprotease-2. J Neuropathol Exp Neurol **2005**;64:754-62
3. Markovic DS, Vinnakota K, Chirasani S, Synowitz M, Raguet H, Stock K, *et al.* Gliomas induce and exploit microglial MT1-MMP expression for tumor expansion. Proc Natl Acad Sci U S A **2009**;106:12530-5
4. Martinez-Serra J, Gutierrez A, Munoz-Capo S, Navarro-Palou M, Ros T, Amat JC, *et al.* xCELLigence system for real-time label-free monitoring of growth and viability of cell lines from hematological malignancies. Onco Targets Ther **2014**;7:985-94